MODELING AND ANALYSIS OF SUBSYSTEMS OF A DC POWER DISTRIBUTION SYSTEM IN AIRLIFTERS IN POWER SHARING MODE

MAJOR THESIS

Submitted by

SWEETY KUMARI

(11/PSY/2010)

Under the Supervision of

Sh. J. N. RAI

In partial fulfillment of the requirements for the award of the degree of

MASTER IN TECHNOLOGY

IN

POWER SYSTEM

DEPARTMENT OF ELECTRICAL AND ELECTRONICS ENGINEERING

DELHI TECHNOLOGICAL UNIVERSITY

July 2012

DEPARTMENT OF ELECTRICAL AND ELECTRONICS ENGINEERING

DELHI TECHNOLOGICAL UNIVERSITY

Delhi

02-07-2012

CERTIFICATE

This is to certify that the project entitled **MODELING AND ANALYSIS OF SUBSYSTEMS OF A DC POWER DISTRIBUTION SYSTEM IN AIRLIFTERS IN POWER SHARING MODE** is a record of the bonafide work done by **SWEETY KUMARI(11/PSY/2010)**, in partial fulfillment of the requirements for the award of the Degree of Master in Technology in Power System of Delhi Technological University, Delhi, during the academic year 2011-2012 under my supervision and guidance. It is also certify that this dissertation has not been submitted elsewhere for any other degree.

Sh. J. N. RAI

Associate Professor

Department of Electrical Engineering

Delhi Technological University

Acknowledgment

I would like to express my gratitude and indebted to my project supervisor Sh. J. N. Rai for his constant supervision, affectionate encouragement and motivation through the course of the project. I wish to acknowledge his contribution in solving the numerous problems that arose during the development of the project. The project would not have achieved the level of success that it has, without his ceaseless support.

It gives me immense pleasure to express my heartfelt gratitude to my HOD Dr. Narender Kumar for providing excellent lab facilities to me. I would also like to thank all lab assistants and lab technicians who helped while I worked on the project.

Sweety kumari
(11/PSY/2010)

Abstract

A DC power distribution system (PDS) of a transport aircraft was modeled and analyzed using MATLAB/Simulink software. The multi-level modeling concept was used as a modeling approach, which assumes modeling subsystem of the PDS at three different levels of complexity. The subsystem models were implemented in Simulink and combined into the whole PDS model according to certain interconnection rules. Effective modeling of different scenarios of operation was achieved by mixing subsystem models of different levels in one PDS model. The PDS model was used to examine the system stability and the DC bus power quality under bidirectional power flow conditions. Small-signal analysis techniques were employed to study stability issues resulting from subsystem interactions. Certain PDS configurations and operational scenarios leading to instability were identified. An analysis of energy transfer in the PDS showed that a large energy storage capacitor in the input filter of a flight control actuator is effective for reduction of the DC bus voltage disturbances produced by regenerative action of the actuator. However, energy storage capacitors do not provide energy savings in the PDS and do not increase its overall efficiency.

Contents

List of Figures

Chapter 1

Introduction

Recently, the aircraft industry has achieved a tremendous progress either in civil or military sectors, for example some currently commercial airliners operate with weights over 3,00,000 kg and have the ability to fly up to 16,000km in non-stop journey at speed of 1000 km/h . The non-propulsive aircrafts systems are typically driven by a combination of different secondary power types such as hydraulic, pneumatic, electrical and mechanical power. These powers are extracted from the aircraft main engine by different disciplines. For example, mechanical power is obtained from the engine by a driven shaft and distributed to a gearbox to drive lubrication pumps, fuel pumps, hydraulic pumps and electrical generators . Pneumatic power is extracted by a bleeding compressor and used to drive turbine motors for the engine start systems, wing anti-icing and Environmental Control Systems (ECS), while electrical power and hydraulic power are distributed throughout the aircraft for driving subsystems such as flight control actuators, landing gear brakes, utility actuators, avionics, lighting, galleys, and weapon system in case of military aircraft. This combination has been always debated, because these systems are becoming rather complicated, and their interactions reduce the efficiency of the whole system. For example, a easily handled. Furthermore, the market prospects for reducing the cost of simple leak in pneumatic or hydraulic system results in a grounded aircraft and inconvenient ownership and the future legislation regarding the climate change require a radical change to the entire aircraft, since it is not sufficient to optimize the current aircraft sub-systems and components individually to achieve these goals.

The trend is to use the electrical power for extracting and distributing the non-propulsive powers. This trend is defined as MEA. The MEA has been questioned for several decades since W.W. II . Nevertheless, due to the lack of electric power generation capabilities and volume requirements of the required power conditioning equipments, the focus has been drifted into the conventional

power types. The recent breakthroughs in the field of power electronic systems, fault-tolerant electric machines, electro-hydrostatic actuators, electromechanical actuators, and fault-tolerant electrical power systems have renewed the interest in the MEA. The adoption of MEA in the future aircraft either in civil or military sectors results in tremendous benefits such as:

1. Removing hydraulic systems improves the aircraft reliability, vulnerability, and reduces complexity, redundancy, weight, installation and running cost.
2. Employing electrical starting for the aero-engine through the engine starter/generator eliminates the engine tower shaft and gears, power take-off shaft, accessory gearboxes, and reduces engine starting power especially in the cold conditions.
3. Using the Advanced Magnetic Bearing (AMB) system, which could be integrated into the internal starter/generator for both the main engine and auxiliary power units, allows for oil-free, gear-free engine.
4. Using a fan shaft generator that allows emergency power extraction under windmill conditions, removes the conventional inefficient single-shot ram air turbine, which increases the aircraft reliability, and survivability under engine-failure conditions.
5. Replacing the engine-bleed system by electric motor-driven pumps reduces the complexity and the installation cost.

In general, adopting MEA revolutionizes the aerospace industry completely, and significant improvements in terms of aircraft-empty weight, reconfigure ability, fuel consumption, overall cost, maintainability, supportability, and system reliability, can be achieved. On the other side, the MEA concept requires increased demands on the aircraft electric power system in areas of power generation and handling, reliability, and fault tolerance, which mandates innovations in power generation, processing, distribution and management systems.

1.1. Electric Power Generation in More Electric Aircraft (MEA)

The MEA represents recently the major driver for increasing the generation of the electric power. Moreover, the MEA directs the research into new generation options. These schemes are summarized in the following.

1. The constant frequency (CF) options are the most common. However, the need for unreliable gearbox to match between the engine speed and the generator requirements of fixed speed, makes the CF expensive and cumbersome. The CF is alternatively termed Integrated Drive Generator (IDG).

2. Variable Speed Constant Frequency (VSCF) DC link system is now the preferred option for the most new military aircraft application and some commercial aircraft. Currently, the range of VSCF DC link system has been widened due to the recent advancements in field of high power electronic switches. VSCF DC link option is generally characterized by simplicity and reliability.

3. Variable Speed Constant Frequency (VSCF) Cyclo converters convert directly the variable frequency AC input power into AC power with fixed frequency and amplitude. The power generation efficiency of the cycloconverters increase as lagging power factor decrease, which would be beneficial if this technique is applied to motor loads with significant lagging power factors .

4. Variable Frequency (VF), typified frequency wild, is the most recent electric power generation contender. The promising features of VF are the small size, weight, volume, and cost as compared with other aircraft electrical power generation options. Also VF offers a very cost-effective source of power for the galley loads, which presents a major proportion in aircraft electric system loads.

However VF may pose significant risk at higher power levels, particularly with high power motor loads; furthermore, the cost of motor controllers required due to the variation in the supply frequency, need to be taken into consideration when assessing the VF three-stage wound field synchronous generator. This machine is highly reliable and inherently safe, as the field excitation can be removed, which de-energizes the machine.

Therefore, the rating of the three-stage synchronous generator has increased over the years reaching to 150KVA on the Airbus A380. However, the anticipated increased electrical power generation requirements on the MEA suggests that the high power generators may be attached directly to the engine, mounted on the engine shaft and used for the engine start in Integral Starter/Generator (IS/G) scheme. The harsh operating conditions and the high ambient temperatures push most commonly materials close or beyond their limits, therefore innovations in materials, processes and thermal management systems are required. Induction, switched reluctance, and permanent magnet machine types have been considered for application in MEA due to their rugged features. However, the induction generator requires complex power electronics and is considered unlikely to have the power
density of the other machines.

The Switched Reluctance (SR) machine has a very simple robust structure, and can operate over a wide speed range. The power electronics is comparatively simple. Moreover, the machine is inherently fault-tolerant .

The fault-tolerant Permanent Magnet (PM) generator is considered to be one of the most attractive options for the MEA. It has a high kW/mass ratio and a good efficiency throughout a wide speed range. Additionally, the reliability, ruggedness, and ease of cooling are also positive features .

1.2. Electric Power Processing in More Electric Aircraft (MEA)

There are many occasions within the aircraft electrical system where it is required to convert the electrical power from one level/form to another level/form. Thus the aircraft electrical system has plenty of power electronic circuits such as AC/DC, DC/DC, DC/AC and matrix converters. The general requirements, which these circuits should satisfy, are:

1. The system should have light weight and small size.

2. The system should be fault-tolerant, which implies its ability to continue functioning under abnormal conditions without much loss in the output power or degradation of the performance.
3. The system should be efficient and have the ability for operation in harsh conditions such as high temperature and low maintenance.

Innovations in the area of power electronic components are required to enable realization of MEA. Wide-Band Gap (WBG) High-Temperature Electronics (HTE) is an example of these developments. The devices manufactured from WBG-HTE are capable of operating at both higher temperatures (600 0C) and higher efficiencies then to Si-based devices (-55 0C to 125 0C). The anticipated benefits of using WBG-HTE are:

1. Reduction in flight control system and improved reliability
2. Reduction/Elimination of ECS required to cool power management and distribution and flight control electronics
3. Reduction in engine control system weight and increased reliability using a distributed processing architecture
4. Improved reliability and maintainability of stores management system avionics

The big challenge for the power electronic circuits in the aircraft is the size of the passive components, as the current components usually have large size, especially for the high power level expected in the MEA. However, the on-going research in the design and fabrication of the passive components for MEA gives some optimistic results. For example, some advanced polymer insulation materials such as Eymyd, L-30N, and Upilex S have the ability to operate over a wide temperature range (-269 0C to 300 0C). Also these materials can withstand the environmental conditions such as humidity, ultraviolet radiation, basic solution and solvent at high altitudes. Another example is the ceramic capacitors, which offers remarkable advantages in volumetric density compared to other capacitor technology.

The “More Electric Initiative” is becoming a leading design concept for future aircrafts. It assumes using electrical energy instead of hydraulic, pneumatic, and mechanical means to power

virtually all aircraft subsystems including flight control actuation, environmental control system, and utility functions. The concept offers advantages of reduced overall aircraft weight, reduced need for ground support equipment and maintenance personnel, increased reliability, and reduced susceptibility to battle damage in military applications. Hence, all electrically powered subsystems become parts of an electric power distribution system (PDS), which unites all electrical sources and loads of an aircraft by means of a power distribution bus. A PDS of a more-electric aircraft includes the following elements: internal engine electric starter/generators, integrated power units, solid-state power controllers, electric driven flight actuators, electric-actuated brakes, electric anti-icing system, fault-tolerant solid state electrical distribution system, electric aircraft utility functions, electric-driven environmental and engine control.

A PDS consists of two independent channels, according to the number of starter/generators in the aircraft. An auxiliary/emergency power unit contains an additional auxiliary starter/generator. The generating system includes starter/generators, power control units, and a generator and system control unit. Either three-phase synchronous machines or switched-reluctance machines may be used as starter/generators in a more-electric aircraft. The power control units are used to transform the "wild frequency" AC power produced by the synchronous generators into 270V DC power. This power is supplied to the DC power distribution bus, which consists of several different sections. The generator and system control unit controls the generators, power control units, and the DC busses. An auxiliary power unit and battery system provides power for starting the engines and emergency back-up. Electromechanical (EMA) and electro hydrostatic (EHA) flight actuators are used in a more-electric aircraft instead of traditional hydraulic actuators with a central hydraulic system. The EMA and EHA employ DC brushless motors powered from the 270V DC distribution bus through DC-AC inverters. Other loads of the PDS include environmental control system loads, utility loads, and avionics. Solid-state DC-DC and DC - AC power converters are used to convert 270V DC power to 115/200V, 400Hz AC power for brushless and induction motor loads and 28V DC power for electronic equipment. Up to 75% of total PDS load installed in an aircraft will be the constant power type of load. The following reasons motivated the choice of the 270V DC distribution bus:

- it is a good voltage source for inverters that power motor loads of the aircraft,
- it is easy to provide uninterruptible power on the bus by using a battery back-up,

- regenerative power from electrical actuators can be easily returned to the bus.
-

At the same time, there are a number of technical issues related to the choice of the 270V DC bus. Among those addressed in are the following:

- system stability,
- power quality on the bus,
- regenerative power flow.

Stability is the most important requirement for a PDS. The issue of stability is closely related to the EMI filter design for subsystems powered through switching power converters. Improper designs of the input filter for such subsystems may result in undesirable interactions. Currently, stability of a PDS in a more-electric aircraft for a particular design is proposed to be evaluated through computer modeling. Therefore, the importance of development of computer-aided modeling and analysis tools for a PDS cannot be underestimated. Considerable experience is developed in evaluating stability of subsystem interactions in distributed power systems. Usually, the impedance ratio stability criterion is used to analyze stability of interactions between two interconnecting subsystems. The system simulated included a synchronous generator, a diode bridge rectifier, and a resistive load. A circuit-oriented type of simulation software was used. No stability analysis was performed. It is seen that although some work on modeling, analysis, and simulation of distributed power systems similar to the PDS of a more-electric aircraft has already been done, the issues of stability, DC bus power quality, and regenerative power flow in the PDS of an aircraft have not been addressed comprehensively.

Therefore, the following research objectives are proposed:

1. Develop computer-aided analysis tools for modeling and analysis of a PDS in a more-electric transport aircraft.
2. Create nonlinear models of a PDS for large-signal simulations and small-signal analysis.
3. Present examples of using the modeling and simulation tools for analysis of a PDS:
   - stability analysis of a PDS with an electromechanical actuator,
   - stability analysis of a PDS with constant power load and mixed load,
   - analysis of the DC bus power quality under bidirectional power flow conditions,

- analysis of ways to optimize regenerative energy flow in the PDS in order to increase its overall efficiency.

In order to achieve the research objectives, a representative power distribution system architecture of transport aircraft (Figures 1.1 and 1.2) was developed. The electrical energy sources are two main Starter/Generators (S/G) and a Starter/Generator of an Auxiliary Power Unit (APU). The system loads are two flight control electric actuator systems with electromechanical and electro hydrostatic actuators, Environmental Control System (ECS) motor loads, and utility loads. There is also a battery unit, which can work as either source or load. All the PDS components are connected by a 270V DC bus, which consists of two primary busses and an APU bus. Each subsystem is connected to the power distribution bus through a Bidirectional Power Converter (BDC), which may be DC–DC or Three-Phase–DC type.

The Electric Load Management System provides system level control and protective functions. A prominent feature of this PDS is bidirectional power flow in the DC bus and in many of its subsystems. Normally, the power flows from the sources (generators) to the loads (actuators, ECS, battery, utility loads). However, in certain modes of operation, some loads can work in regenerative mode, thus supplying electric power to the DC distribution bus. For example, a flight control actuator works in regenerative mode when it has to slow down a moving flight control surface, or when the surface is being moved by the air flow. Another example is using the battery as an energy source and the APU starter/generator as a motor to start the APU engine.

Bidirectional power flow in the PDS becomes possible because all power converters connecting subsystems to the DC distribution bus possess bidirectional power flow capability. The regenerative power phenomenon mentioned above has potential advantages since the power regenerated by one subsystem can potentially be used to power the others or be stored in the PDS for future use. However, it also has potential problems because unused regenerative power may create voltage spikes on the DC bus, which may exceed the limits set by the standard. This effect may happen because a load with sufficient power consumption may not be available on the bus at the time of regeneration. Figure 1.3 shows the limits of the DC bus voltage transients set by MIL-STD-704E, which specifies power quality characteristics of the DC bus. These transients

may affect normal operation of the equipment connected to the bus or even damage it. In order to store the regenerative energy, it is necessary to provide additional energy storage components in the PDS.

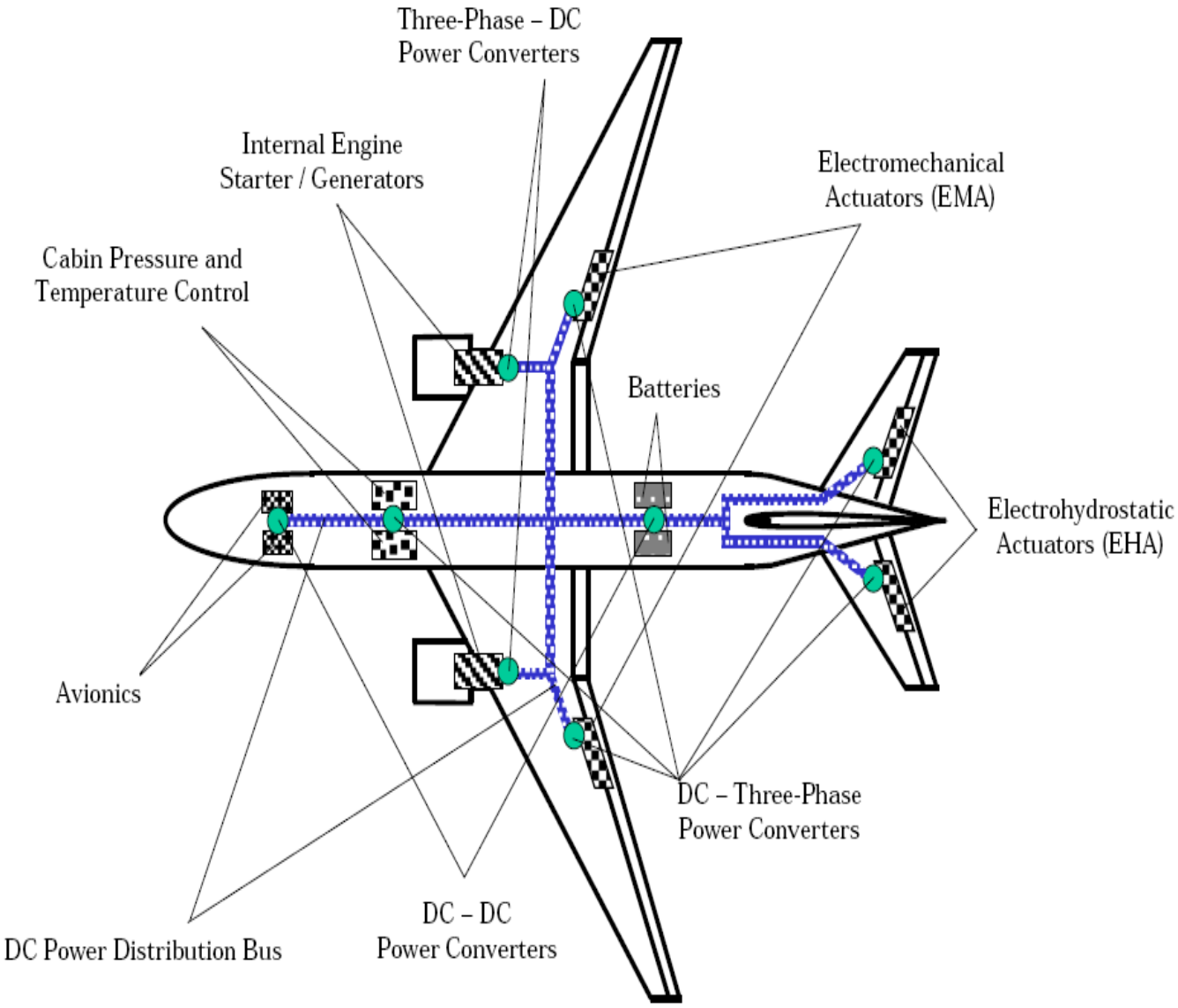

Figure 1.1 Power distribution system of a transport aircraft.

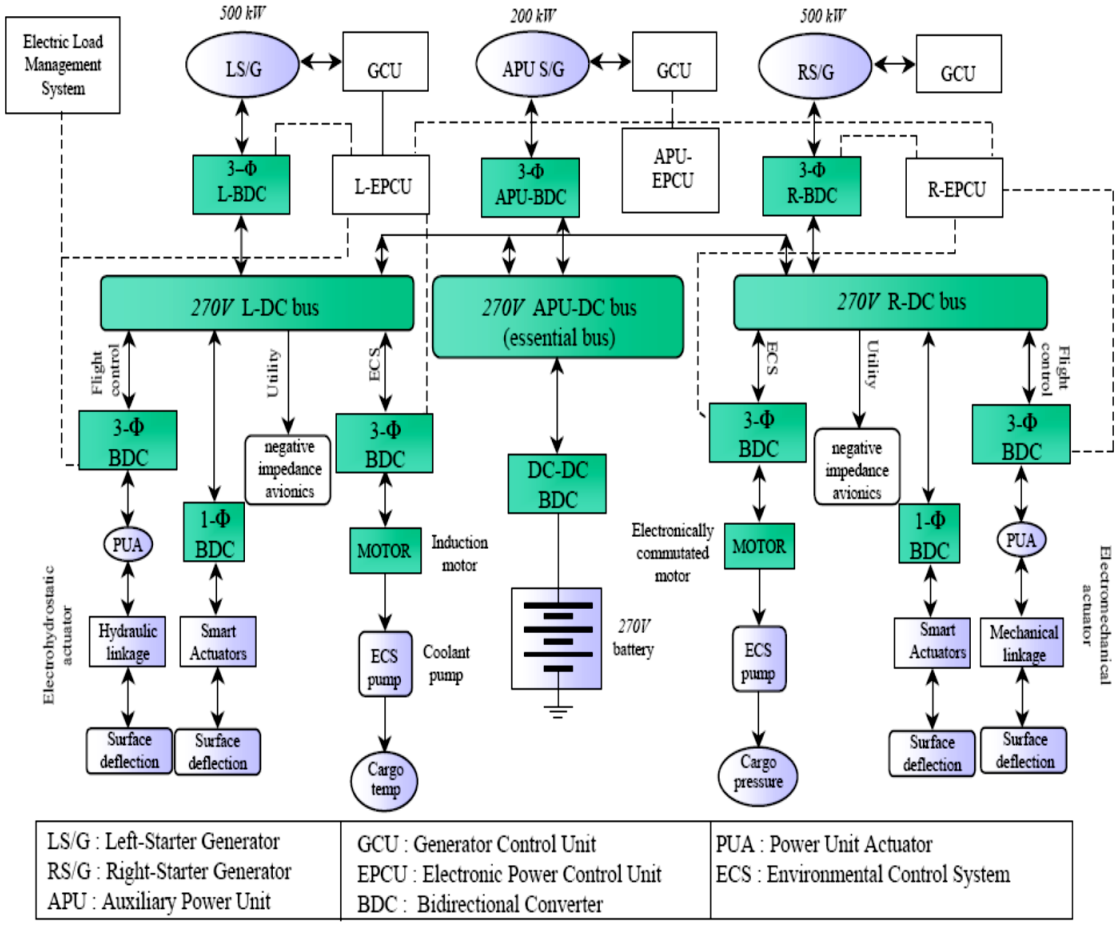

Figure 1.2 Power distribution system architecture.

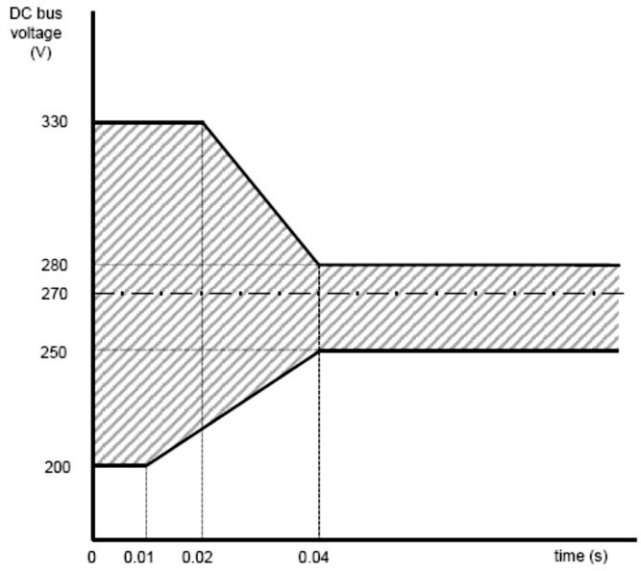

Figure 1.3 DC bus voltage specifications according to MIL-STD-704E.

Since the battery alone charges too slowly to accept transient power spikes generated in certain modes of operation, a significant number of capacitors in the PDS will be needed to fully utilize the regenerative power. Unlike the current PDS designs based on using components that have minimal interactions, the PDS under investigation consists of highly coupled subsystems closely interacting with each other. This approach brings potential benefits, which include an opportunity for optimization of the whole system that will allow resources of one subsystem such as regenerative energy to be shared with the others. The result would be reduction of the overall weight and cost of the aircraft and increase of the efficiency of its power distribution function.

One possible problem of the PDS with highly coupled subsystems might be a loss of the system stability because of undesirable subsystem interactions. Another possible problem is deterioration of power quality as a result of transient voltage disturbances on the DC bus, especially in regenerative mode of operation. The subsystems constituting the whole PDS must be designed keeping in mind issues of compatibility with the other subsystems.

Avoiding undesirable interactions can be achieved by choosing appropriate designs and modes of operation. Therefore, the key to successful subsystem integration into the whole PDS is developing an understanding of possible subsystem interactions.

The objective of this research is to develop nonlinear models of subsystem interactions, especially in the context of bidirectional power flow, to create efficient computational tools for computer-aided analysis of the PDS, and to provide examples of using these tools for robust and energy efficient PDS designs that would take advantage of highly coupled subsystems while avoiding undesirable consequences of subsystem interactions.

Chapter 2

Literature Review

[1]Moir, Ian; Seabridge, Allan.3rd ed. Chichester (West Sussex): Wiley, 2008.: In these new aircrafts the electrical power distribution systems (PDS) are the key element, principally due to the new requirements of demanded power and the required functionality. Therefore the new electrical systems have evolved towards new distribution architectures based on distributed systems, where traditional voltages levels at 28 VDC and 115 VAC, have been replaced by levels of 270 VDC, ±270 VDC and 230 VAC. Because of these new PDS, more electric aircrafts require a greater number of electronic equipments, such as converters, rectifiers, inverters and solid state protections, that allow to fulfil the needs arising from these new architectures. One of the key elements of these new PDS is the introduction of the solid state power controllers (SSPC) as elements of wiring protection and control of the electrical loads. These devices allow to replace the magneto-thermal and relays that are used in the conventional SDP, since these conventional devices present operational problems in the new PDS, due mainly to the changes in the voltage levels. Furthermore, the development of the new functionality and capabilities of the SSPC are related to: the configuration of the new PDS architectures, the elements that interact, their location within the architecture and the loads to which they connect.

[2]Rosero, J.A.; Ortega, J.A.; Aldabas, E.; Romeral, L. Aerospace and Electronic Systems Magazine, IEEE Volume 22, Issue 3, March 2007: The latest advances in electric and electronic aircraft technologies from the point of view of an "all-electric" aircraft are presented herein. Specifically, we describe the concept of a "more electric aircraft" (MEA), which involves removing the need for on-engine hydraulic power generation and bleed air off-takes, and the increasing use of power electronics in the starter/generation system of the main engine. Removal of the engine hydraulic pumps requires fully-operative electrical power actuators and mastery of the flight control architecture. The paper presents a general overview of the electrical power generation system and electric drives for the MEA, with special regard to the flight controls.

Some discussion regarding the interconnection of nodes and safety of buses and protocols in distributed systems is also presented

[3] Lester F. Faleiro, Proc. 25th International Congress of the Aeronautical Sciences ICAS 2006: In the new designs of military aircraft (cargo and fighters) there is a clear trend towards increasing demand of electrical power. This fact is mainly due to the replacement of mechanical, pneumatic and hydraulic equipments by partially or completely electrical systems. The purpose of this article is to present and describe the technological project HV270DC. In this project, one Electrical Power Distribution System (EPDS), applicable to the all electric aircrafts, has been developed. Tests with different loads of 270 VDC have been done, with objective to detect possible problems of whole systems stability. During the consecutive closures of the contactors of 270 VDC, the ripple of the voltage in the bus bars of principal distribution was measured. This ripple can cause instability of the system and provoke problems in the downstream equipments operation.

[4]David Blanding, Proc. 25th International Congress of the Aeronautical Sciences ICAS 2006: Military and commercial aircraft designers are leading a quiet revolution in the aviation industry. Their goal is an all-electric aircraft that will be controlled by small high speed motors instead of heavy maintenance intensive hydraulic, pneumatic and mechanical systems. This revolutionary usage of electrical power technologies promise military and commercial airframers greater aircraft reliability and a significantly smaller logistical tail to support tomorrow's air and space force. Hence, the More Electric Aircraft (MEA) is becoming a reality. Electric actuation is an evolving technology with high payoffs in terms of vehicle safety, reduced cost, reduced maintenance, and reduction in overall vehicle weight. Electromechanical actuators are a cost-effective alternative because there is one energy conversion versus two in a hydraulic system. Because of absence of hydraulic fluid, electromechanical actuators will be the preferred solution for most MEA aerospace platforms. Advances in electric motor and power electronics are making the technology both affordable and cost effective as well as providing a greater opportunity for expanded subsystem integration.

[5]M. Howse, Power Engineer, vol. 17, pp. 35-37, 2003: The More-Electric Aircraft (MEA) underlines the utilization of the electrical power to power the non-propulsive aircraft systems. Adopting the MEA achieves numerous advantages such as optimizing the aircraft performance and decreasing operating and maintenance costs. Moreover, the MEA reduces the emission of the air pollutant gases from the aircraft, which can contribute in solving the problem of climate change. However, the MEA put some challenge on the aircraft electrical system either in the amount of the required or the processing and management of this power. Replacing the conventional non-propulsive aircraft power, mechanical, hydraulic and pneumatic with single electric power is known as MEA, and considered as the future trendsetter. The MEA improves the aircraft reliability, affordability, fuel consumption. Moreover, MEA reduces cost of ownership, operation and maintenance cost. However, the implementation of MEA requires innovation in the areas of power generation, distribution and management.

[6]M. David Kankam 36th Intersociety Energy Conversion Engineering Conference; Savannah, Georgia, July 29–August 2, 2001: The insertion of power electronics in aerospace technologies is becoming widespread. The application of semiconductor devices and electronic converters, as summarized in this paper, includes the International Space Station, satellite power system, and motor drives in 'more electric' technology applied to aircraft, starter/generators and reusable launch vehicles. Flywheels, servo systems embodying electromechanical actuation, and spacecraft on-board electric propulsion are discussed. Continued inroad by power electronics depends on resolving incompatibility of using variable frequency for 400 Hz-operated aircraft equipment. Dual-use electronic modules should reduce system development cost.

[7]G. L. Fronista and G. Bradbury, Proceedings of the 32nd Intersociety Energy Conversion Engineering Conference, 1997: The More Electric Aircraft Initiative (MEI) embraces the concept of utilizing electrical power for driving aircraft subsystems. Power electronics and motor drives are essential elements of the MEI. Advancements in power semiconductor devices, capacitors, and integrated circuits for control has enabled high density, reliable power electronic and motor drive systems for the MEI. Wright Laboratory and Sundstrand Aerospace have been working on the development of an electromechanical actuator to be compatible with the requirements of a spoiler for a typical transport aircraft. The focus of

this development effort is in the motor drive, meaning the controller, inverter and motor utilized to control the actuator. Efforts are underway to increase the power density of the motor drive to achieve 1 kW/lb, with an efficiency of greater than 80%. This paper discusses the design criteria and some of the trade-offs that were accomplished during this development. This work includes the use of a novel soft switched inverter driving a five-phase switched reluctance motor. A digital signal processing (DSP) chip is utilized for responsive controls and field programmable gate arrays (FPGA) to reduce size and increase control electronics reliability. A power electronics module is developed which is comprised of insulated gate bipolar transistor (IGBT) inverter switches, diodes, a current sensor and gate drives. The thermal management system utilizes a reflux heat exchanger with integral phase change material that will enable the motor drive to operate in the environment of the actuator.

[8]M. L. Maldonado, N. M. Shah, K. J. Cleek, P. S. Walia, G. Korba, Proceedings of the 31st Intersociety Energy Conversion Engineering Conference, 1996: This paper presents the simulation and transient analysis of conventional and advanced aircraft electric power systems with harmonics mitigation. Complete modeling of aircraft electric power systems is proposed. The conventional aircraft electrical power system is analyzed considering equivalent passive AC and DC loads under transient and steady-state operating conditions. The electric power source is simulated to ensure constant frequency and voltage which meet the aircraft electrical standards for all loading cases. To mitigate the harmonics generated by the converters, passive input filters are designed to keep THD values within the standard limits. Furthermore, the advanced aircraft electrical system is simulated and analyzed under the same electric power source and loads. The results are compared to those of the conventional aircraft electric power system.

[9]K.C. Reinhardt, M. A. Marciniak, Proceedings of the 31st Intersociety Energy Conversion Engineering Conference, 1996: Developments in solid-state electronics have provided the United States Air Force with the most sophisticated and capable avionics systems in the world. Steady advancements in solid-state devices and integrated circuits have enabled modern electronic warfare, navigation, and flight and propulsion control electronics. Wide-bandgap (WBG) electronic devices are capable of operating at high temperature and high efficiencies, thus reducing the amount of heat dissipated by the electronics, thus enabling a

reduction in, or elimination of, existing heavy, single-redundant distributed aircraft electronics cooling systems. Consequently, WBG high-temperature electronics (HTE) are expected to play an enabling and vital role in the design of the future concept More Electric Aircraft (MEA). The system-level benefits of employing WBG-HTE in the MEA include a reduction in flight control system weight and improved reliability; a reduction in size and weight, or elimination of, the environmental control system (ECS) required to cool management and distribution (PMAD) and flight electronics; a reduction in engine control system weight and increased reliability using a distributed processing architecture; and the improved reliability and maintainability of stores management system (SMS) avionics. The paper address important aircraft subsystem WBG electronics applications, the temperature range in which electronics will be expected to operate if they are to be un-cooled, and a description of WBG-HTE components desired for use in future MEA electronic systems.

[10]T. L. Skvarenina, S. Pekarek, O. Wasynczuk, P. C. Krause, Proceedings of the Intersociety Energy Conversion Engineering Conference, 1996: A detailed system model for a More-Electric Aircraft power system equipped with a wound-rotor synchronous generator is presented. The simulation employs a new approach that automatically generates a state-space model of power components and the complete system. In this approach, the composite system state equations are established algorithmically given the standard node incidence matrix and elementary branch data (e.g. resistances, inductances, back emf's). The resulting state equations can be solved using a variety of numerical techniques or commercially available computer simulation programs. Example computer studies are presented and verified with experimental tests

[11]M. E. Elbuluk, M. D. Kankam, Proceedings of the IEEE 1995 National Aerospace and Electronics Conference, NAECON'95: The PDS model was used to examine the system stability and the DC bus power quality under bidirectional power flow conditions. Small-signal analysis techniques were employed to study stability issues resulting from subsystem interactions. The DC bus stability diagram was proposed for predicting stability of the PDS with different types of loads without performing an actual stability test based on regular stability analysis tools. Certain PDS configurations and operational scenarios leading to instability were

identified. An analysis of energy transfer in the PDS showed that a large energy storage capacitor in the input filter of a flight control actuator is effective for reduction of the DC bus voltage disturbances produced by regenerative action of the actuator. However, energy storage capacitors do not provide energy savings in the PDS and do not increase its overall efficiency.

[12]J. A. Weimer, Proceedings of the 30th Intersociety Energy Conversion Engineering Conference, 1995: This paper presents the simulation and transient analysis of conventional and advanced aircraftelectricpower systems with harmonics mitigation. Complete modeling of aircraftelectricpower systems is proposed. The conventional aircraft electrical power system is analyzed considering equivalent passive AC and DC loads under transient and steady-state operating conditions. The electricpower source is simulated to ensure constant frequency and voltage which meet the aircraft electrical standards for all loading cases. To mitigate the harmonics generated by the converters, passive input filters are designed to keep THD values within the standard limits. Furthermore, the advanced aircraft electrical system is simulated and analyzed under the same electricpower source and loads. The results are compared to those of the conventional aircraftelectricpower system.

[13]S. Hiti, D. Borojevic, IEEE 1994 IAS Annual Meeting Proceedings: The paper presents new small-signal modeling of uniformly-sampled three-phase PWM modulators. The models reveal that the uniformly-sampled modulators, which are commonly used in three-phase power conversion, introduce delays and additional coupling between the power converter control inputs, as well as time-variation of the power converters' small-signal dynamics. Experimental results are given.

[14] W. A. Tabisz, M. M. Jovanovic, F. C. Lee, Proceedings of the Applied Power Electronics Conference, 1992: The current stage of development of distributed power systems is presented. Various DC-bus and AC-bus distributed power system architectures are discussed. System integration issues related to paralleling and cascading of DC/DC converters are explained. Benefits and challenges of distributed power systems in various applications are summarized.

[15]B. H. Cho and B. Choi, Proceedings of the Virginia Power Electronics Conference, 1991:Multistage distributed power systems are analyzed, focusing on the dynamic interactions between two cascaded converter stages. An unterminated modeling and design approach is proposed to design a converter driving other converters downstream. Results of the analysis were verified by both frequency- and time-domain simulations

Chapter 3

Model Development for Power Distribution System Components

3.1 Modeling of Subsystem Elements

As we have seen in the previous section, elementary blocks typical for switching power converters are PWM switches and RLC networks (usually low-pass filters). These elements are two-ports; therefore, the interconnection rules for voltages and currents should be observed. It will be shown below how to use modeling capabilities of Simulink to build models for these elements.

As an example of an RLC network, we will consider a low-pass LC filter (Figure 3.1), which is a generic component of many types of power converters. The circuit is described by equations:

$$\begin{aligned} L\frac{di_{in}}{dt} &= v_{in} - v_o - i_{in}R_l \\ C\frac{dv_c}{dt} &= i_{in} - i_o \\ v_o &= v_c + R_c(i_{in} - i_o) \end{aligned} \qquad (3.1)$$

The “Integrator” block of the built-in Simulink library is used to integrate the state variables of the network while the input and output variables are picked up according to the interconnection rules. The resulting Simulink model is shown in Figure 3.2.

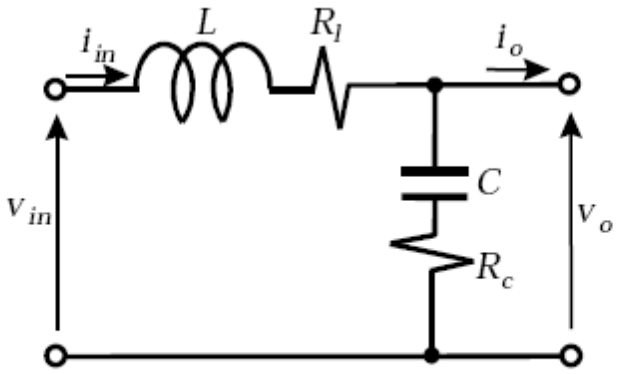

Figure 3.1 Low-pass L-C filter.

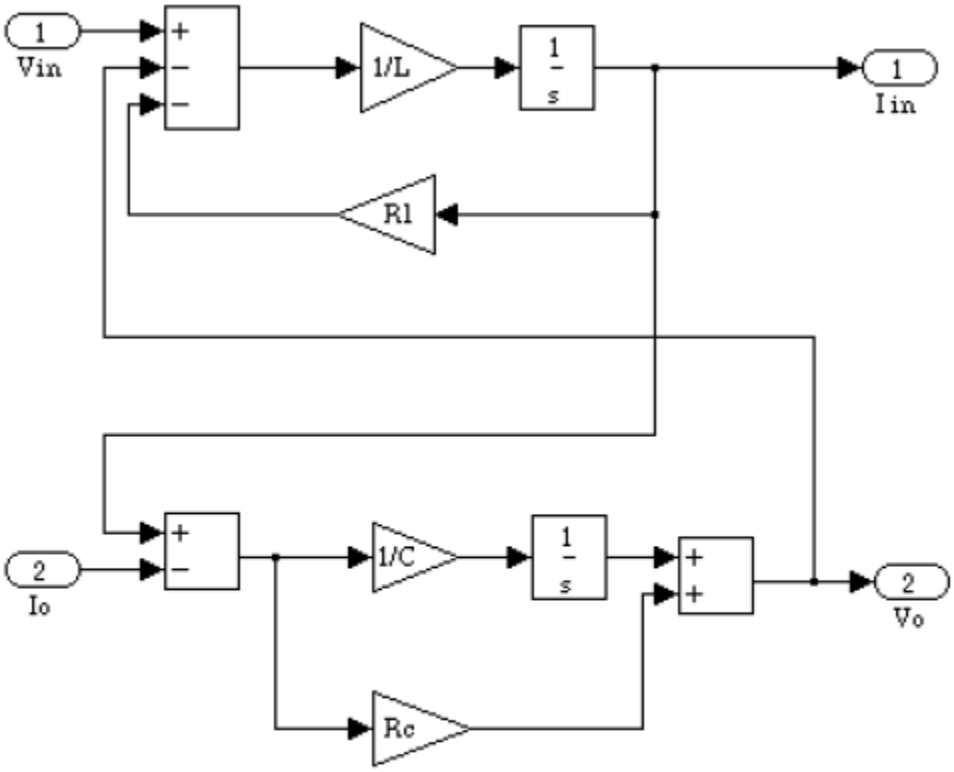

Figure 3.2 Simulink model of the L-C filter.

Another way of building a model for this network is using the "State-space" Simulink block as shown in Figure 3.3 because this filter is a linear system. In order to use this block, it is

necessary to identify state-space matrices for the network by writing its equations in state-space form:

$$\frac{d}{dt}\begin{bmatrix} i_{in} \\ v_c \end{bmatrix} = \begin{bmatrix} -\dfrac{R_c + R_l}{L} & -\dfrac{1}{L} \\ \dfrac{1}{C} & 0 \end{bmatrix}\begin{bmatrix} i_{in} \\ v_c \end{bmatrix} + \begin{bmatrix} \dfrac{1}{L} & -\dfrac{R_c}{L} \\ 0 & -\dfrac{1}{C} \end{bmatrix}\begin{bmatrix} v_{in} \\ i_o \end{bmatrix} \qquad (3.2)$$

$$\begin{bmatrix} i_{in} \\ v_o \end{bmatrix} = \begin{bmatrix} 1 & 0 \\ R_c & 1 \end{bmatrix}\begin{bmatrix} i_{in} \\ v_c \end{bmatrix} + \begin{bmatrix} 0 & 0 \\ 0 & R_c \end{bmatrix}\begin{bmatrix} v_{in} \\ i_o \end{bmatrix}$$

The models in Figures 3.2 and 3.3 are equivalent. The model in Figure 3.2 represents a general approach for model building based on the system equations, which is generally used in this research. The other approach is applicable only to linear systems represented in state-space form. It can be convenient for modeling of high-order systems with a large number of parameters, for which using the previous approach may be too cumbersome. Also, it may be more computationally efficient since it reduces the number of algebraic operations in the process of simulation.

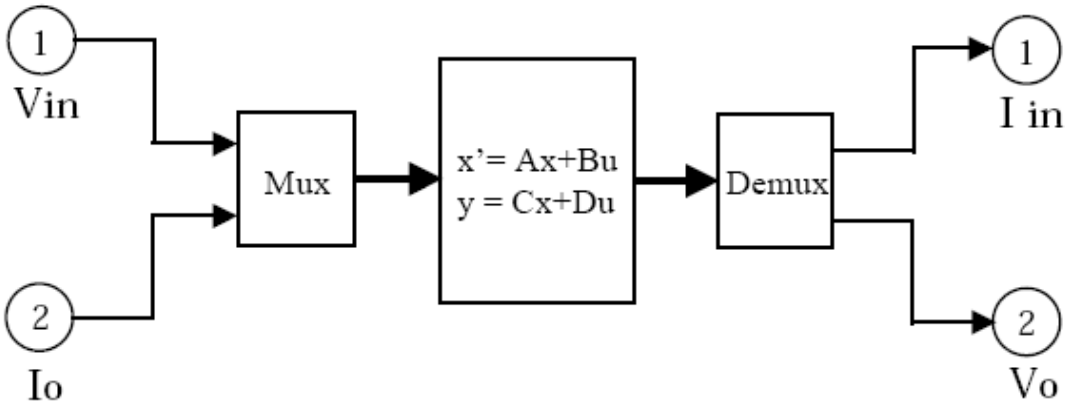

Figure 3.3 Alternative Simulink model of the L-C filter based on state-space representation.

The models for the L-C filter developed above are detailed, average, and linearized at the same time because no switching or nonlinearities are present in the network. The models for the PWM switch that will be considered next are different at detailed and average levels.

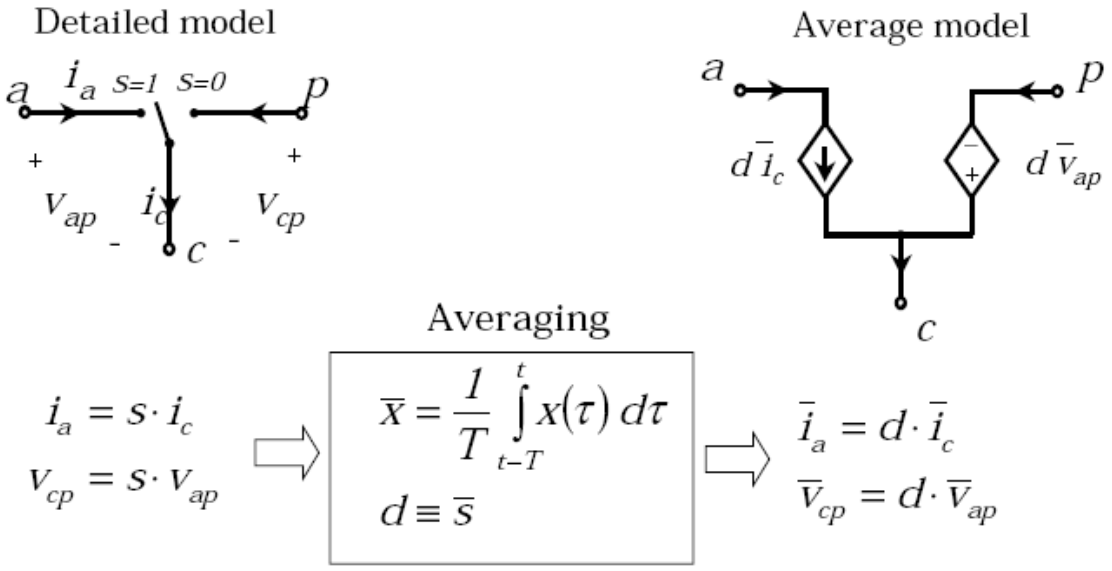

Figure 3.4 Development of detailed and average models for the PWM switch.

The PWM switch configuration used in the buck converter (Figure 2.3) is a two-port switching network with three terminals: active, passive, and common. The switching action of the PWM switch is described by the switching function *s*, which accepts the values of 0 and 1 as shown in Figure 3.4. The terminal behavior of the PWM switch, therefore, is described by the following equations upon which the detailed model of the switch is based:

$$\begin{aligned} i_a &= s \cdot i_c \\ v_{cp} &= s \cdot v_{ap} \end{aligned} \qquad (3.3)$$

The switching voltage and current waveforms produced by the PWM switch are averaged by the low-pass filtering action of the input and output filters of the converter as they are seen at the load and source terminals. This filtering action presents a physical basis for using an average model of the switch, which neglects its switching action while preserving quantitative relationships between average values of voltages and currents at its terminals. Mathematically, averaging of a periodical function *x(t)* is defined as

$$\bar{x} = \frac{1}{T}\int_{t-T}^{t} x(\tau)\,d\tau, \qquad (3.4)$$

where T is the period of the function $x(t)$.

The operation of averaging, being applied to the discrete switching function $s(t)$ with a discrete value of duty cycle d for each switching period, results in a continuous duty cycle function $d(t)$ and the following equations for the PWM switch, which constitute its average model (Figure 3.4):

$$\begin{aligned} \bar{i}_a &= d \cdot \bar{i}_c \\ \bar{v}_{cp} &= d \cdot \bar{v}_{ap} \end{aligned} \qquad (3.5)$$

The Simulink implementations of the detailed and average PWM switch models are shown in Figure 3.5. Besides the terminal voltages and currents, the models have an additional input – the duty cycle command. The detailed model then turns this command into the output voltage and current switching waveforms by comparing it with a ramp generator signal, in a manner very similar to the operation of real PWM modulator circuits. The average Simulink model is based on the average model equations (3.5). Note that the interconnection rules for voltages and currents are observed.

A Simulink model for the buck converter in Figure 2.4 may employ either detailed or average model for the PWM switch developed above. Both models preserve low-frequency dynamics of the system, but without the switching ripple in the state variables' waveforms if the average model is used. Figure 3.6 illustrates this idea. It shows simulated output filter capacitor voltage and inductor current transients of the buck converter obtained with both detailed and average models of the PWM switch. It is seen that the current response obtained with the average model reflects all the details of the current response obtained with the detailed model except the switching ripple. This is also true for the output voltage waveforms. The switching ripple of the output voltage is so small that both curves look almost identical on the plot. Although the average model does not show the switching ripple, it provides much faster simulation and an

additional opportunity for small-signal analysis and control design using MATLAB's Control System Toolbox A nonlinear system such as the buck converter described above can be linearized at an equilibrium point, and a number of transfer functions can be obtained. For example, Figure 3.7 shows the input impedance transfer function of the buck converter in open loop configuration obtained by using the Control System Toolbox.

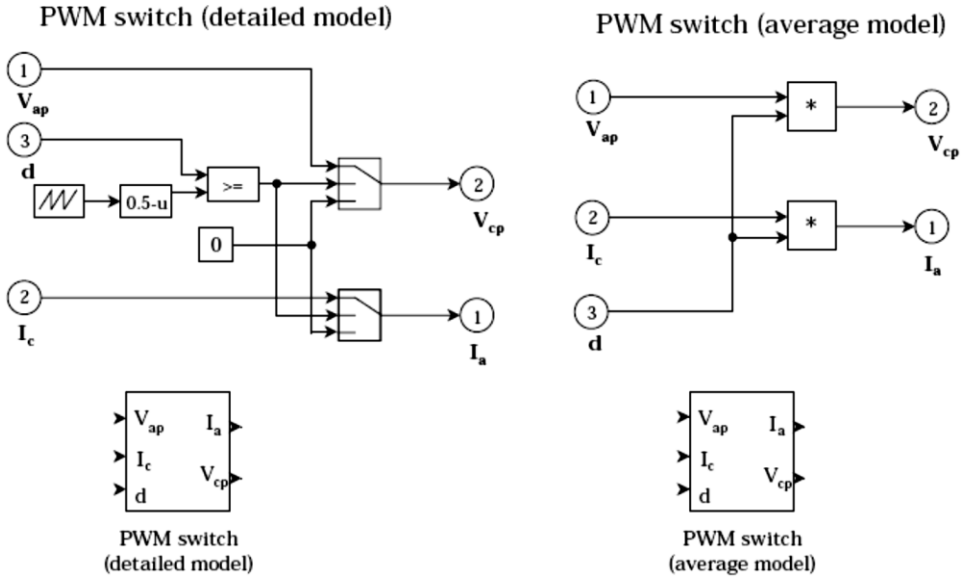

Figure 3.5 Detailed and average Simulink models for the PWM switch.

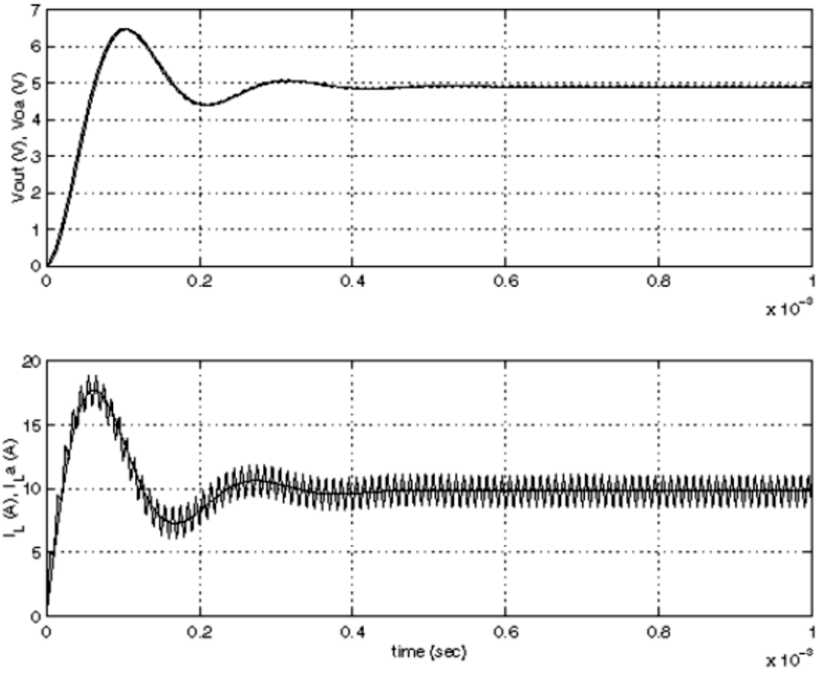

Figure 3.6 Buck converter example of simulation with detailed and average models for the PWM switch.

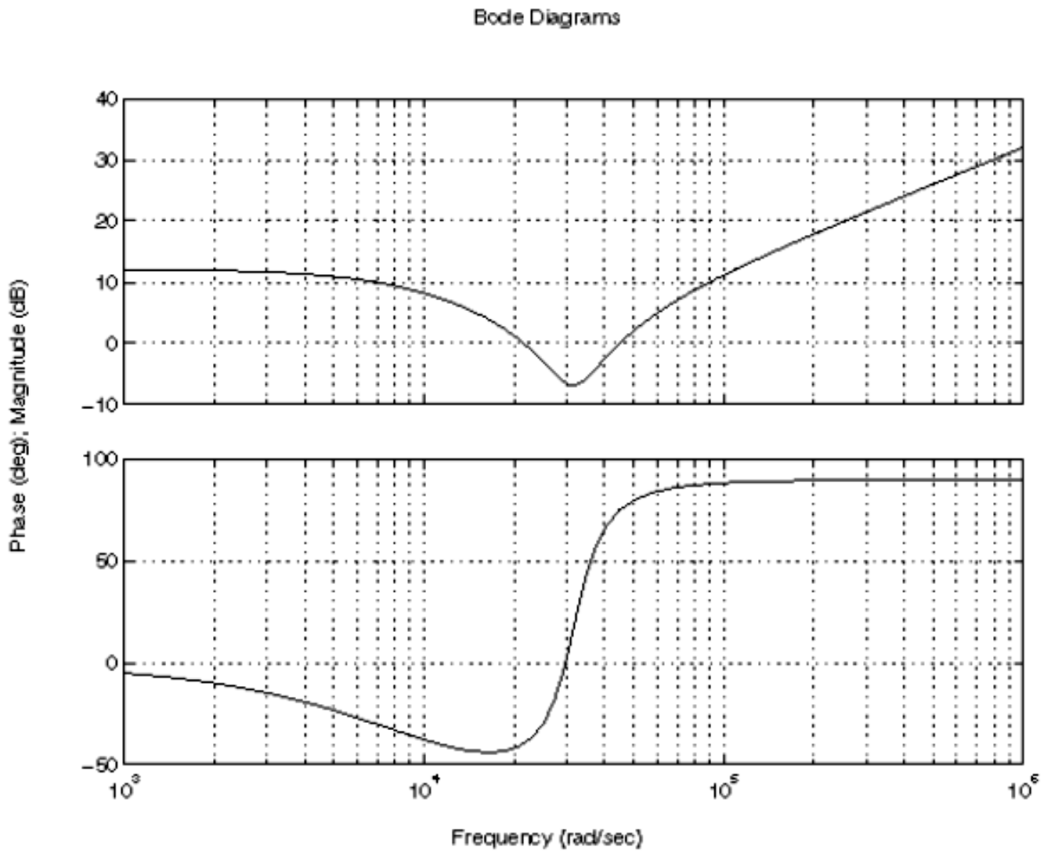

Figure 3.7 Buck converter open loop input impedance.

3.2 Modeling of DC-DC Switching Power Converters

3.2.1 DC-DC Buck Converter Modeling

The buck converter topology was already discussed above (Figure 2.3). A complete Simulink model of a buck converter is shown in Figure 3.8. The model features input and output LC filters and an average model of the PWM switch. The converter model can use a different input filters topology with a proper Simulink model. The model has an improved two-pole, two-zero feedback compensator, which provides voltage mode control to the converter. The feedback controller includes the integrator anti-windup feature and provides soft start with the reference voltage rising from zero at the power-up.

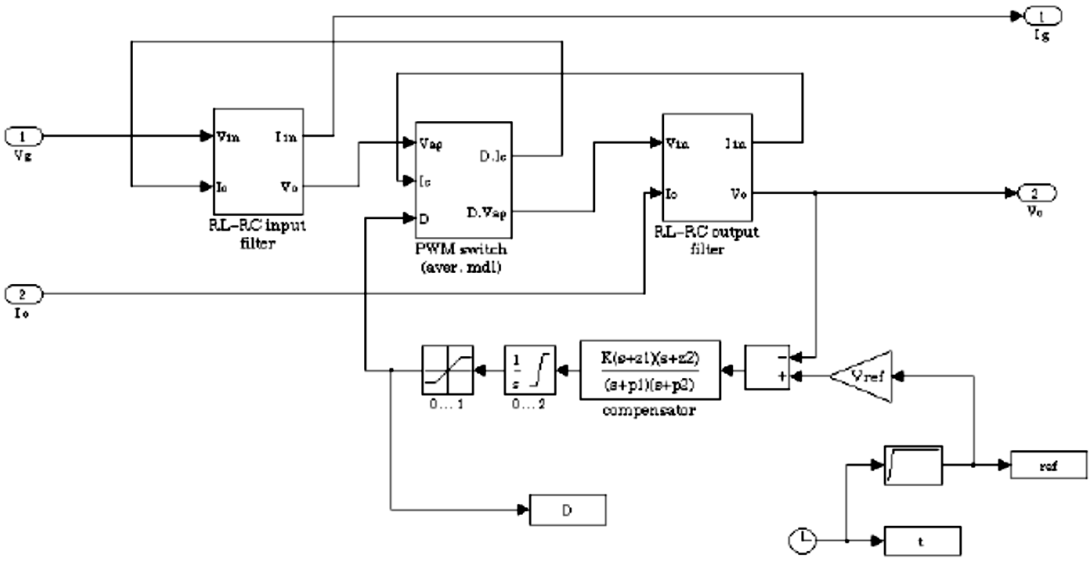

Figure 3.8 Bidirectional buck converter Simulink model.

The model supports bidirectional power flow, i.e. it is valid for power stage topologies that allow reverse output current. The model can be used in the aircraft power distribution system simulations to power low-voltage DC applications such as avionics from 270V DC bus. The model can also be used for bidirectional DC-DC full-bridge buck converter topologies, provided that the lower limit of duty cycle in the feedback loop is set to –1.

3.2.2 DC-DC Boost Converter Modeling

The boost converter has an output filter split by the PWM switch (Figure 3.9); therefore, the power stage model cannot be obtained by interconnecting the existing PWM switch and L-C filter models. A separate Simulink model (Figure 3.11) for the power stage of the boost converter (Figure 3.10) is developed based on the circuit equations:

$$
\begin{aligned}
L\frac{di_g}{dt} &= v_g - v_o(1-d) - i_g R_l \\
C\frac{dv_c}{dt} &= i_g(1-d) - i_o \\
v_o &= v_c + R_c(i_g(1-d) - i_o)
\end{aligned}
\tag{3.6}
$$

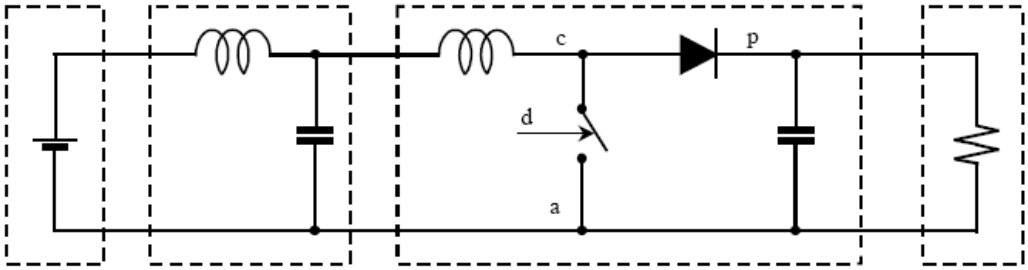

Figure 3.9 Boost converter topology.

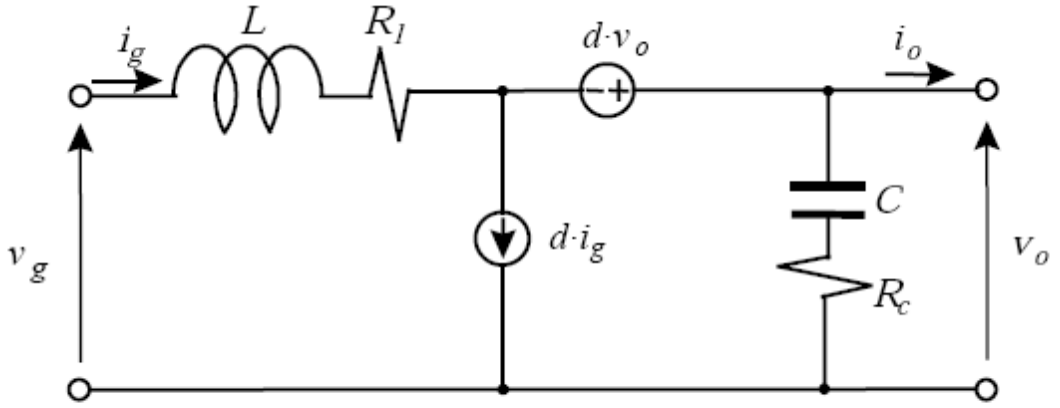

Figure 3.10 Equivalent circuit of the boost converter power stage.

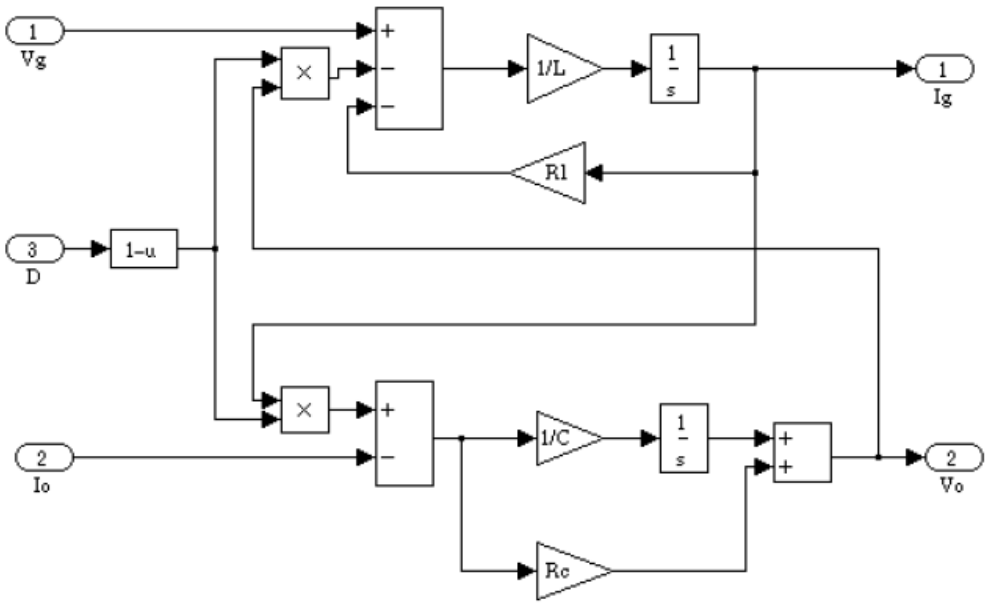

Figure 3.11 Simulink average model for the boost converter power stage.

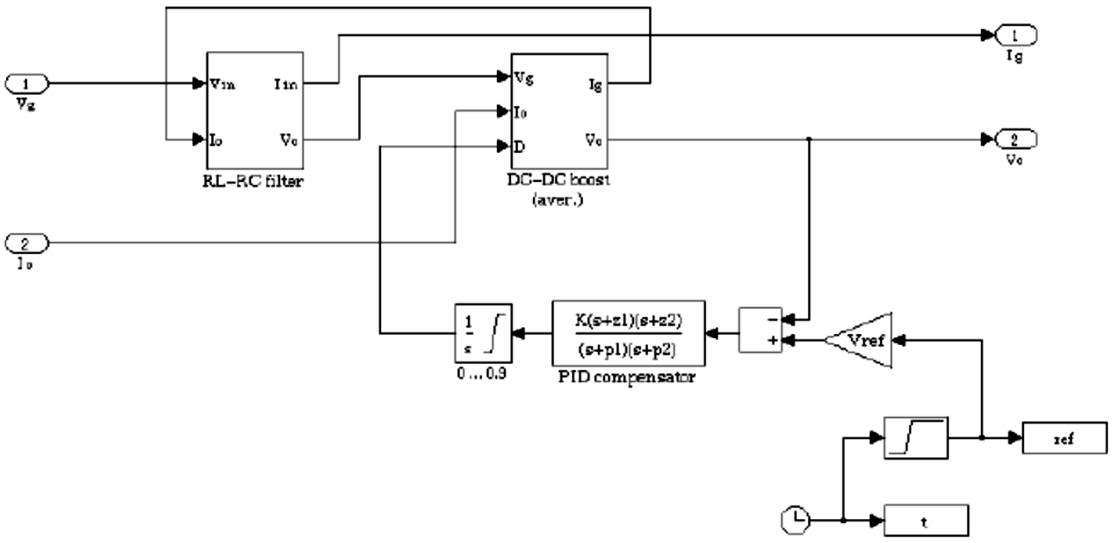

Figure 3.12 Bidirectional closed-loop Simulink model for the boost converter.

A complete model of the boost converter with voltage feedback loop is shown in Figure 3.12. It is

composed of the average model of the boost converter power stage, the input filter model, and the feedback controller. The model has a soft start feature. The compensator with anti-windup is very similar to the one used in the buck converter. Of course, the compensator zeros, poles, and gain should be designed individually for a particular converter.

3.3 Modeling of Three-Phase Subsystems

3.3.1 Three-Phase Subsystem Modeling Approach

Three-phase subsystems of the PDS considered in this research include three-phase synchronous motors/generators and three-phase bidirectional converters. We will take a close look at modeling and simulation techniques for a three-phase synchronous starter/generator loaded by a three-phase-to-dc boost rectifier. The models should reflect bidirectional power flow in the subsystems (both generating and motoring) found under different scenarios. Direct modeling of three-phase systems by writing their circuit equations in the three phase reference frame is undesirable for several reasons. For a synchronous machine, this would result in equations with time-varying parameters because the self-inductances and mutual inductances of the machine windings depend on the rotor position. For the boost rectifier, even after averaging of the switching ripple, a three-phase model would not allow using the linearization and feedback control design techniques because the steady state waveforms of the system variables are sinusoids, and no operating point could be specified. Simulation of sinusoidal waveforms would require a very small integration step even in steady state operation, which would create computational problems (long simulation time and insufficient memory for storing the simulation history in the workspace). These problems may be overcome by modeling the subsystems in the synchronously rotating reference frame commonly known as *dq* coordinates. The synchronous generator and the boost rectifier must be modeled in separate *dq* reference frames according to their modeling approaches. The relationship between a set of *dq* variables and the corresponding set of three-phase *abc* variables is provided by the transformation matrix *T*. Since the three-phase systems studied in this research are balanced, no 0-axis components are present, which allowed using a simplified version of *dq*-transformation:

$$\begin{bmatrix} X_d \\ X_q \end{bmatrix} = T \begin{bmatrix} X_a \\ X_b \\ X_c \end{bmatrix}, \tag{3.7}$$

$$T = \frac{2}{3} \begin{bmatrix} \cos\omega t & \cos(\omega t - \frac{2\pi}{3}) & \cos(\omega t + \frac{2\pi}{3}) \\ -\sin\omega t & -\sin(\omega t - \frac{2\pi}{3}) & -\sin(\omega t + \frac{2\pi}{3}) \end{bmatrix}. \tag{3.8}$$

The inverse transformation from *dq* to *abc* variables is defined as

$$\begin{bmatrix} X_a \\ X_b \\ X_c \end{bmatrix} = T' \begin{bmatrix} X_d \\ X_q \end{bmatrix}, \tag{3.9}$$

$$T' = \begin{bmatrix} \cos\omega t & -\sin\omega t \\ \cos(\omega t - \frac{2\pi}{3}) & -\sin(\omega t - \frac{2\pi}{3}) \\ \cos(\omega t + \frac{2\pi}{3}) & -\sin(\omega t + \frac{2\pi}{3}) \end{bmatrix}. \tag{3.10}$$

To provide a means for *abc-dq* and *dq-abc* transformation of variables during simulation process, two Simulink blocks "ABC-to-DQ" (Figure 3.13) and "DQ-to-ABC" (Figure 3.14) are developed. These blocks must be used with a very small integration step because they contain sinusoidal signal sources. For systems modeled completely in *dq* coordinates without using sinusoidal sources, much larger integration steps may be allowed, which would unleash the full power of robust variable-step integration routines. After the simulation is done, the results in *dq* variables may be converted to *abc* variables using the inverse transformation matrix *T'*.

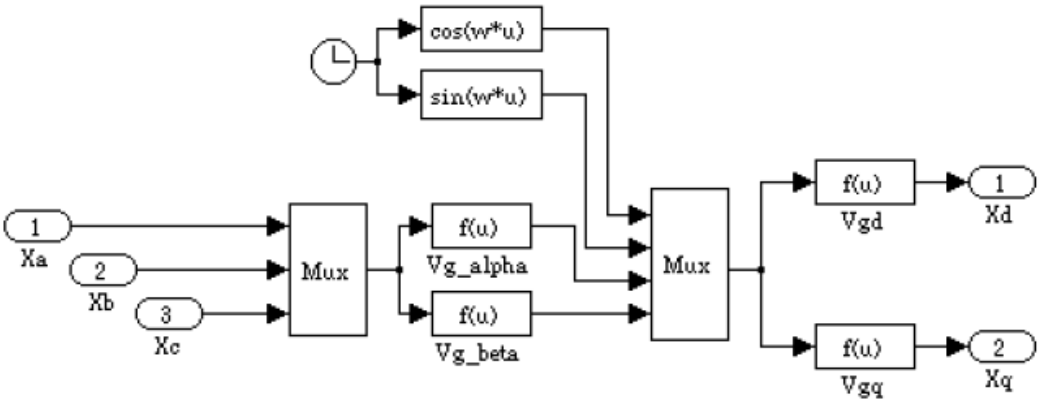

Figure 3.13 ABC-to-DQ transformation Simulink block.

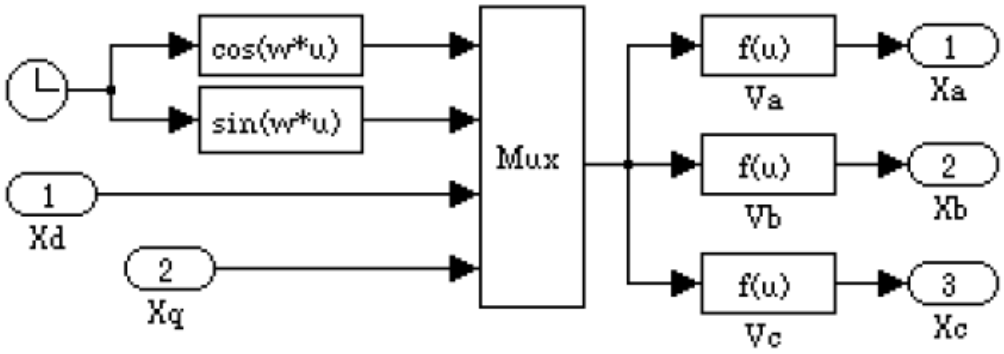

Figure 3.14 DQ-to-ABC transformation Simulink block.

3.3.2 Three-Phase Synchronous Generator Modeling

An equivalent circuit of a synchronous generator with a balanced load is presented in Figure 3.15. As mentioned above, modeling of a synchronous machine in *dq* coordinate frame avoids the problem of time-variance of the winding inductances. It converts the ac system variables into equivalent dc variables, which relate to the magnitude of the sinusoids in the steady state operation and in transients. In addition, the *dq* transformation actually reduces the order of the system (a three-phase system becomes a two-phase system). The machine is described by the following equations corresponding to the equivalent circuit:

$$
\begin{aligned}
v_d &= (i_{sd} - i_d)R_a \\
v_q &= (i_{sq} - i_q)R_a \\
0 &= R_a i_d - (R_a + R_s)i_{sd} + \omega(L_{ls} + L_{mq})i_{sq} - \omega L_{mq} i_{kq} - (L_{ls} + L_{md})\frac{di_{sd}}{dt} + L_m d\frac{di_{fd}}{dt} + L_{md}\frac{di_{kd}}{dt} \\
0 &= R_a i_q - (R_a + R_s)i_{sq} - \omega(L_{ls} + L_{md})i_{sd} + \omega L_{md} i_{fd} + \omega L_{md} i_{kd} - (L_{ls} + L_{mq})\frac{di_{sq}}{dt} + L_{mq}\frac{di_{kq}}{dt} \qquad (3.11) \\
v_{fd} &= R_{fd} i_{fd} - L_{md}\frac{di_{sd}}{dt} + (L_{lfd} + L_{md})\frac{di_{fd}}{dt} + L_{md}\frac{di_{kd}}{dt} \\
0 &= R_{kd} i_{kd} - L_{md}\frac{di_{sd}}{dt} + (L_{lkd} + L_{md})\frac{di_{kd}}{dt} + L_{md}\frac{di_{fd}}{dt} \\
0 &= R_{kq} - L_{mq}\frac{di_{sq}}{dt} + (L_{lkq} + L_{mq})\frac{di_{kq}}{dt}
\end{aligned}
$$

where

R_s - armature phase resistance,

w□ - rotor speed,

v_d - armature *d* axis terminal voltage,

v_q - armature *q* axis terminal voltage,

i_d - armature *d* axis terminal current,

i_q - armature *q* axis terminal current,

i_{sd} - *d* axis phase current,

i_{sq} - *q* axis phase current,

v_{fd} - field winding terminal voltage (reflected to the stator),

i_{fd} - field winding terminal current (reflected to the stator),

i_{kd} - *d* axis damper winding current (reflected to the stator),

i_{kq} - *q* axis damper winding current (reflected to the stator),

In this model, we assume a constant rotor speed. This is justified for studying dynamic behavior of the PDS since changes in the generator load would not likely affect the aircraft engine speed. If it is necessary to include mechanical dynamics into consideration, a According to the interconnection rules for voltages and currents specified above, a mechanical equation of motion should be added to the equations above. Simulink model for the generator must have a current port as an input and a voltage port as an output. They will be coupled with the boost rectifier's input voltage port and the output current port. The phase currents i_{sd} and i_{sq}, being state variables,

cannot be the input variables at the same time. Therefore, a fictitious terminal resistance *Ra* was added to the model. This resistance has a relatively high value and does not affect other variables. It may also account for magnetic losses in the generator. A Simulink model for this subsystem could be built directly by drawing a block diagram corresponding to the equations (3.11) similarly to the block diagram for the LC filter in Figure 3.2. However, because of complexity of the equations, this approach would be too cumbersome to implement. An alternative approach used in this research uses the "State-space" Simulink block. Equations (3.11) represent a linear system with state variables i_{sd}, i_{sq}, i_{kd}, i_{kq}, i_{fd}, input variables i_d, i_q, v_{fd}, and output variables v_d, v_q. These equations are solved for the state derivatives and represented in state-space form.

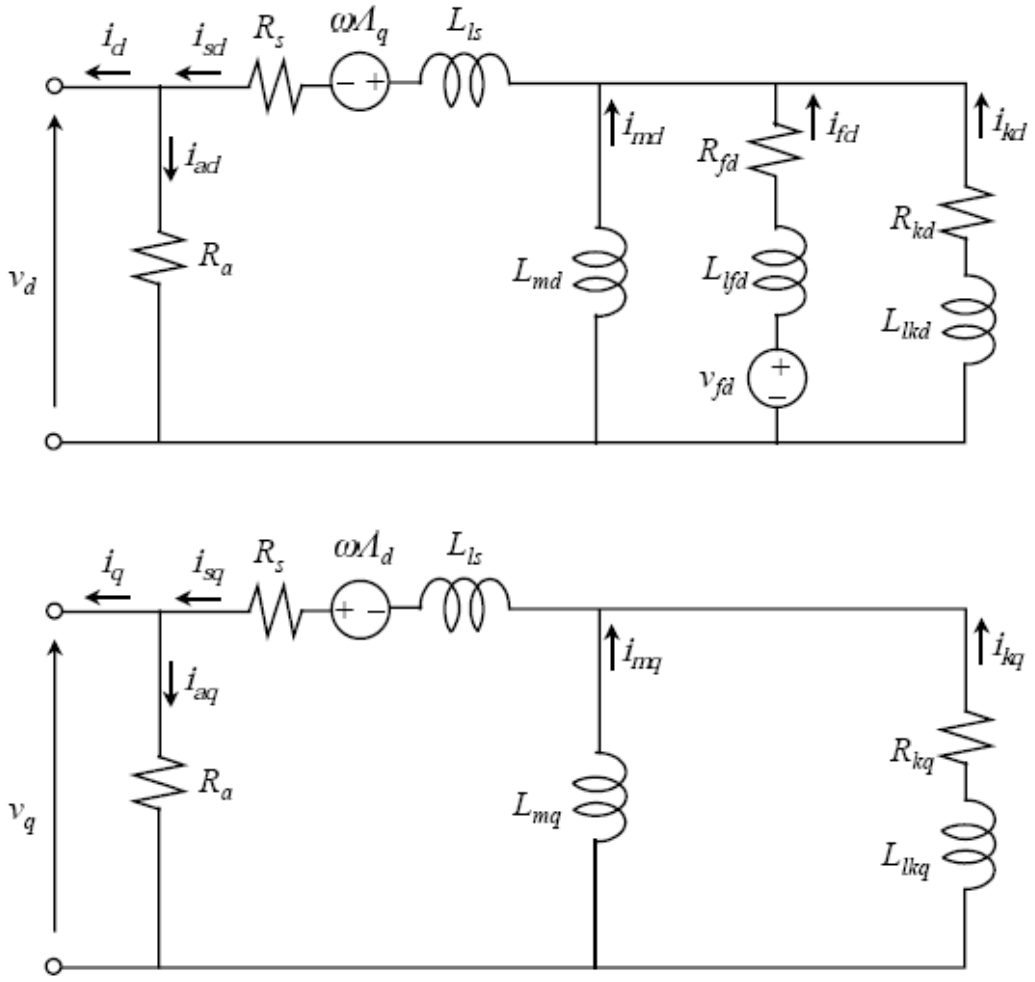

Figure 3.15 Equivalent circuit of a synchronous generator in *dq* coordinates.

State-Space Model for a Synchronous Generator

In order to present the generator equations (3.11) in the standard state-space form, it is necessary to solve them for the state derivatives and collect the input and state variables into matrices. The five equations of (3.11) containing the state derivatives may be represented as follows:

$$\begin{bmatrix} a_{11} & 0 & a_{13} & 0 & a_{15} \\ 0 & a_{22} & 0 & a_{24} & 0 \\ a_{31} & 0 & a_{33} & 0 & a_{35} \\ a_{41} & 0 & a_{43} & 0 & a_{45} \\ 0 & a_{52} & 0 & a_{54} & 0 \end{bmatrix} \begin{bmatrix} x_1 \\ x_2 \\ x_3 \\ x_4 \\ x_5 \end{bmatrix} = \begin{bmatrix} b_1 \\ b_2 \\ b_3 \\ b_4 \\ b_5 \end{bmatrix},$$

where the auxiliary variables are

$$x_1 = \frac{di_{sd}}{dt} \qquad a_{11} = -(L_{ls} + L_{md})$$

$$a_{13} = L_{md}$$

$$x_2 = \frac{di_{sq}}{dt} \qquad a_{15} = L_{md}$$

$$b_1 = -R_a i_d + (R_a + R_s) i_{sd} - \omega(L_{ls} + L_{mq}) i_{sq} + \omega L_{mq} i_{kq}$$

$$x_3 = \frac{di_{kd}}{dt}$$

$$x_4 = \frac{di_{kq}}{dt} \qquad a_{22} = -(L_{ls} + L_{mq})$$

$$a_{24} = L_{mq}$$

$$x_5 = \frac{di_{fd}}{dt} \qquad b_2 = -R_a i_q + (R_a + R_s) i_{sq} + \omega(L_{ls} + L_{md}) i_{sd} - \omega L_{md} i_{fd} - \omega L_{md} i_{kd}$$

$$a_{31} = -L_{md} \qquad a_{41} = -L_{md} \qquad a_{52} = -L_{mq}$$

$$a_{33} = L_{md} \qquad a_{43} = L_{lkd} + L_{md} \qquad a_{54} = L_{lkq} + L_{mq}$$

$$a_{35} = L_{lfd} + L_{md} \qquad a_{45} = L_{md} \qquad b_5 = -R_{kq} i_{kq}$$

$$b_3 = v_{fd} - R_{fd} i_{fd} \qquad b_4 = -R_{kd} i_{kd}$$

Solving the equation symbolically in terms of the circuit parameters would be too cumbersome, and it is unnecessary because the parameters do not change during simulation. The solution is obtained by inverting the matrix of coefficients numerically:

$$X = A^{-1} \cdot B,$$

where

$$X = \begin{bmatrix} x_1 \\ x_2 \\ x_3 \\ x_4 \\ x_5 \end{bmatrix}, \qquad A = \begin{bmatrix} a_{11} & 0 & a_{13} & 0 & a_{15} \\ 0 & a_{22} & 0 & a_{24} & 0 \\ a_{31} & 0 & a_{33} & 0 & a_{35} \\ a_{41} & 0 & a_{43} & 0 & a_{45} \\ 0 & a_{52} & 0 & a_{54} & 0 \end{bmatrix}, \qquad B = \begin{bmatrix} b_1 \\ b_2 \\ b_3 \\ b_4 \\ b_5 \end{bmatrix}.$$

It can be seen that

$$\begin{bmatrix} b_1 \\ b_2 \\ b_3 \\ b_4 \\ b_5 \end{bmatrix} = \begin{bmatrix} R_a + R_s \\ \omega(L_{ls} + L_{md}) \\ 0 \\ 0 \\ 0 \end{bmatrix} \cdot i_{sd} + \begin{bmatrix} -\omega(L_{ls} + L_{mq}) \\ R_a + R_s \\ 0 \\ 0 \\ 0 \end{bmatrix} \cdot i_{sq} + \begin{bmatrix} 0 \\ -\omega L_{mq} \\ 0 \\ -R_{kd} \\ 0 \end{bmatrix} \cdot i_{kd} + \begin{bmatrix} \omega L_{mq} \\ 0 \\ 0 \\ 0 \\ -R_{kq} \end{bmatrix} \cdot i_{kq} + \begin{bmatrix} 0 \\ -\omega L_{md} \\ -R_{fd} \\ 0 \\ 0 \end{bmatrix} \cdot i_{fd} +$$

$$\begin{bmatrix} -R_a \\ 0 \\ 0 \\ 0 \\ 0 \end{bmatrix} \cdot i_d + \begin{bmatrix} 0 \\ -R_a \\ 0 \\ 0 \\ 0 \end{bmatrix} \cdot i_q + \begin{bmatrix} 0 \\ 0 \\ 1 \\ 0 \\ 0 \end{bmatrix} \cdot v_{fd} = B_1 \cdot \begin{bmatrix} i_{sd} \\ i_{sq} \\ i_{kd} \\ i_{kq} \\ i_{fd} \end{bmatrix} + B_2 \cdot \begin{bmatrix} i_d \\ i_q \\ v_{fd} \end{bmatrix},$$

where

$$B_1 = \begin{bmatrix} b_{11} & b_{12} & 0 & b_{14} & 0 \\ b_{21} & b_{22} & b_{23} & 0 & b_{25} \\ 0 & 0 & 0 & 0 & b_{35} \\ 0 & 0 & b_{43} & 0 & 0 \\ 0 & 0 & 0 & b_{54} & 0 \end{bmatrix}, \qquad B_2 = \begin{bmatrix} b_{16} & 0 & 0 \\ 0 & b_{27} & 0 \\ 0 & 0 & b_{38} \\ 0 & 0 & 0 \\ 0 & 0 & 0 \end{bmatrix},$$

$$\begin{aligned} b_{11} &= b_{22} = R_a + R_s \\ b_{21} &= \omega(L_{ls} + L_{md}) \\ b_{12} &= -\omega(L_{ls} + L_{mq}) \\ b_{23} &= -\omega L_{mq} \\ b_{43} &= -R_{kd} \\ b_{14} &= \omega L_{mq} \\ b_{54} &= -R_{kq} \\ b_{16} &= b_{27} = -R_a \\ b_{38} &= 1. \end{aligned}$$

From equations it is seen that

$$\frac{d}{dt}\begin{bmatrix} i_{sd} \\ i_{sq} \\ i_{kd} \\ i_{kq} \\ i_{fd} \end{bmatrix} = A^{-1} \cdot B_1 \cdot \begin{bmatrix} i_{sd} \\ i_{sq} \\ i_{kd} \\ i_{kq} \\ i_{fd} \end{bmatrix} + A^{-1} \cdot B_2 \cdot \begin{bmatrix} i_d \\ i_q \\ v_{fd} \end{bmatrix} = A_g \cdot \begin{bmatrix} i_{sd} \\ i_{sq} \\ i_{kd} \\ i_{kq} \\ i_{fd} \end{bmatrix} + B_g \cdot \begin{bmatrix} i_d \\ i_q \\ v_{fd} \end{bmatrix},$$

which is the state equation of the model. The output equation is obtained from the two equations of (3.11) containing the output variables. The state variables are obtained as well by adding them to the vector of output variables.

$$\begin{bmatrix} v_d \\ v_q \\ i_{sd} \\ i_{sq} \\ i_{kd} \\ i_{kq} \\ i_{fd} \end{bmatrix} = \begin{bmatrix} R_a & 0 & 0 & 0 & 0 \\ 0 & R_a & 0 & 0 & 0 \\ 1 & 0 & 0 & 0 & 0 \\ 0 & 1 & 0 & 0 & 0 \\ 0 & 0 & 1 & 0 & 0 \\ 0 & 0 & 0 & 1 & 0 \\ 0 & 0 & 0 & 0 & 1 \end{bmatrix} \begin{bmatrix} i_{sd} \\ i_{sq} \\ i_{kd} \\ i_{kq} \\ i_{fd} \end{bmatrix} + \begin{bmatrix} -R_a & 0 & 0 \\ 0 & -R_a & 0 \\ 0 & 0 & 0 \\ 0 & 0 & 0 \\ 0 & 0 & 0 \\ 0 & 0 & 0 \\ 0 & 0 & 0 \end{bmatrix} \begin{bmatrix} i_d \\ i_q \\ v_{fd} \end{bmatrix} = C_g \begin{bmatrix} i_{sd} \\ i_{sq} \\ i_{kd} \\ i_{kq} \\ i_{fd} \end{bmatrix} + D_g \begin{bmatrix} i_d \\ i_q \\ v_{fd} \end{bmatrix}$$

Hence equation will be

$$\frac{d}{dt} \begin{bmatrix} i_{sd} \\ i_{sq} \\ i_{kd} \\ i_{kq} \\ i_{fd} \end{bmatrix} = A_g \begin{bmatrix} i_{sd} \\ i_{sq} \\ i_{kd} \\ i_{kq} \\ i_{fd} \end{bmatrix} + B_g \begin{bmatrix} i_d \\ i_q \\ v_{fd} \end{bmatrix} \tag{3.12}$$

$$\begin{bmatrix} v_d \\ v_q \end{bmatrix} = C_g \begin{bmatrix} i_{sd} \\ i_{sq} \\ i_{kd} \\ i_{kq} \\ i_{fd} \end{bmatrix} + D_g \begin{bmatrix} i_d \\ i_q \\ v_{fd} \end{bmatrix},$$

where A_g, B_g, C_g, D_g are the state-space matrices.

It can be seen from Equations (3.11) that the output voltage of the synchronous generator significantly depends on its load current. In order to keep the output voltage at a specified level regardless of load conditions, a voltage feedback loop is introduced into the Simulink model.

The feedback provides the rms value of the output voltage calculated from its *dq* components according to the formula:

$$v_{rms} = \frac{1}{\sqrt{2}}\sqrt{v_d^{\,2} + v_q^{\,2}} \qquad (3.13)$$

The field winding voltage controller, which is modeled here as a simple gain, uses the output voltage error signal. Since the dc distribution bus voltage is precisely regulated by the boost rectifier, the presence of a small steady-state error in the generator output voltage is not a problem.

The complete Simulink model for the synchronous generator is presented in Figure 3.16. A soft-start feature is added to avoid large transients in the beginning of simulation. The transfer function T_{func} with a very high frequency pole is introduced into the feedback path in order to break an algebraic loop in the model, which may cause numerical problems when the model is used in large system simulations. The transfer function does not affect the model operation otherwise.

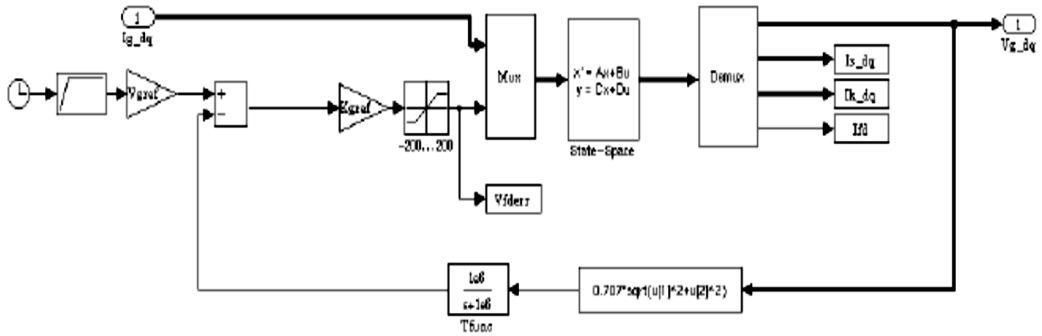

Figure 3.16 Closed-loop Simulink model of the synchronous generator in *dq* coordinates.

3.3.3 Three-Phase Boost Rectifier Modeling

The boost rectifier provides front-end three-phase-to-dc power conversion from the synchronous generator to the dc distribution bus. The rectifier operates with unity power factor and draws

sinusoidal currents from the three-phase source. When the output current reverses its direction, the boost rectifier reverses the power flow through it and operates as a voltage source inverter.

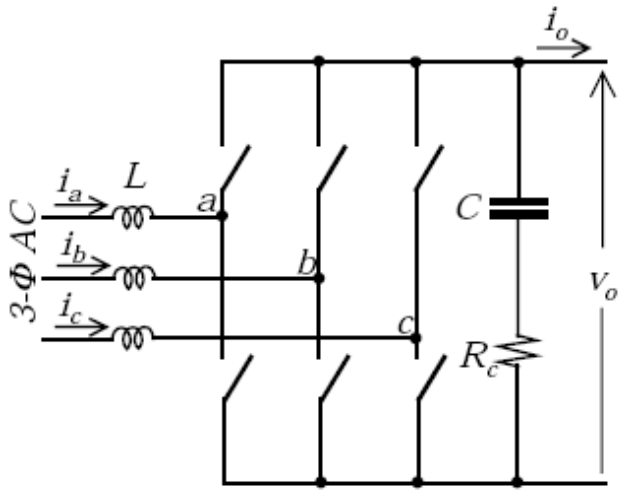

Figure 3.17 Power stage topology of the boost rectifier.

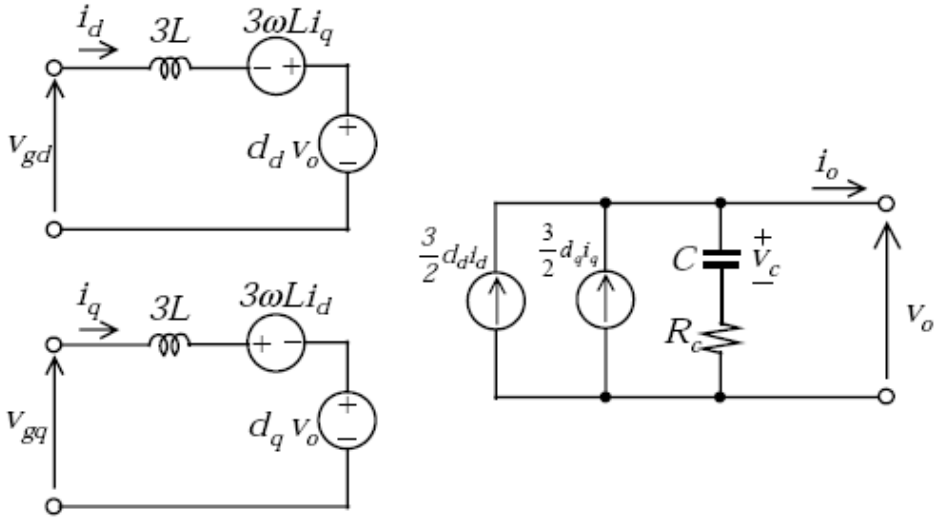

Figure 3.18 Average model of the boost rectifier in *dq* coordinates.

The power stage of the boost rectifier as modeled in this research is shown in Figure 3.17. The output capacitor ESR is taken into consideration in order to reflect the converter dynamics more accurately. By averaging the switching action of the semiconductor switches and applying the *dq*

transformation to the resulting average model, a large signal average model in *dq* coordinates is obtained. The equivalent circuit is shown in Figure 3.18 and described by equations:

$$\begin{aligned}
\frac{di_d}{dt} &= \frac{1}{3L}(v_{gd} + 3\omega L i_q - d_d v_o) \\
\frac{di_q}{dt} &= \frac{1}{3L}(v_{gq} - 3\omega L i_d - d_q v_o) \\
\frac{dv_c}{dt} &= \frac{1}{C}(\frac{3}{2}(d_d i_d + d_q i_q) - i_o) \\
v_o &= v_c + R_c(\frac{3}{2}(d_d i_d + d_q i_q) - i_o),
\end{aligned} \tag{3.14}$$

where

i_d, i_q - input currents in dq coordinates,

v_{gd}, v_{gq} - input voltages in dq coordinates,

i_o - output dc current,

v_o - output dc voltage,

d_d, d_q - duty cycle in dq coordinates,

ω - angular frequency,

L - phase inductance,

C - output capacitance,

R_c - capacitor ESR.

A Simulink model derived from these equations is shown in Figure 3.19. The model accepts *dq* voltages, *dq* duty cycles, and dc output current as input variables and supplies dc voltage and *dq* currents as output variables. The control diagram for the boost rectifier is shown in Figure 3.20. It includes decoupling terms $3wL/V_o$ to eliminate cross-coupling between the d and q channels so that they could be controlled independently. Perfect decoupling is achieved at a specified line frequency and output voltage and is load-independent, which satisfies the conditions of this research.

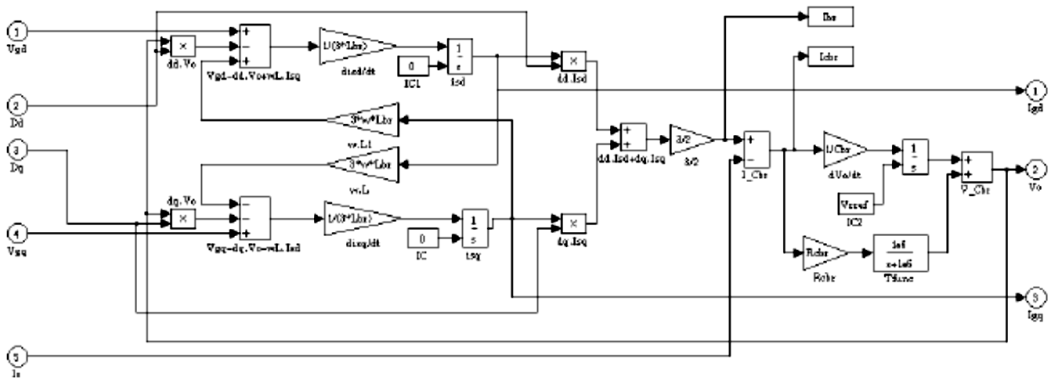

Figure 3.19 Simulink model of the boost rectifier power stage in *dq* coordinates.

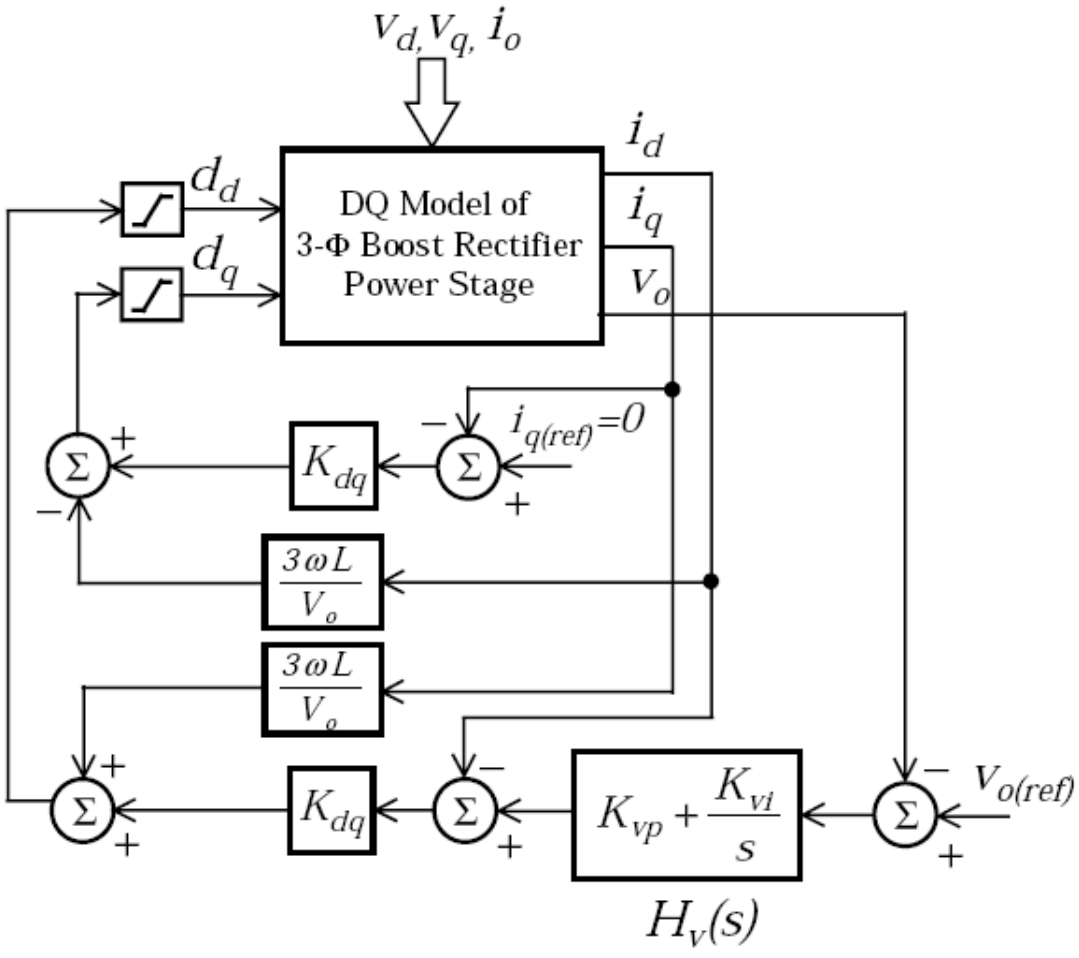

Figure 3.20 Control diagram of the boost rectifier.

The voltage mode feedback control is provided with a feedback voltage loop and two current loops. The current loops control the decoupled channels of the power stage independently by adjusting their duty cycles. They both use proportional controllers with the same gain K_{dq}. The reference signal for the q channel is set to zero since the input currents should be in phase with the input voltages. The reference signal for the d channel is provided by the voltage loop compensator. Closed-loop transfer functions for both current loops are load independent. The voltage loop uses a proportional-integral compensator with a transfer function

$$H_v(s) = K_{vp} + \frac{K_{vi}}{s}, \qquad (3.15)$$

which provides fast response and no steady-state error in the output voltage. Control-to-output transfer function v_o/i_{dref} significantly depends on the load and direction of the power flow; therefore, the voltage loop compensator can be optimized only for a specific load. In order to use this type of control for the whole range of loads under bidirectional power flow conditions as assumed in this research, a compromise in the compensator design was required. The resulting design provided a low closed-loop bandwidth yet stable operation and acceptable transient response under all load conditions.

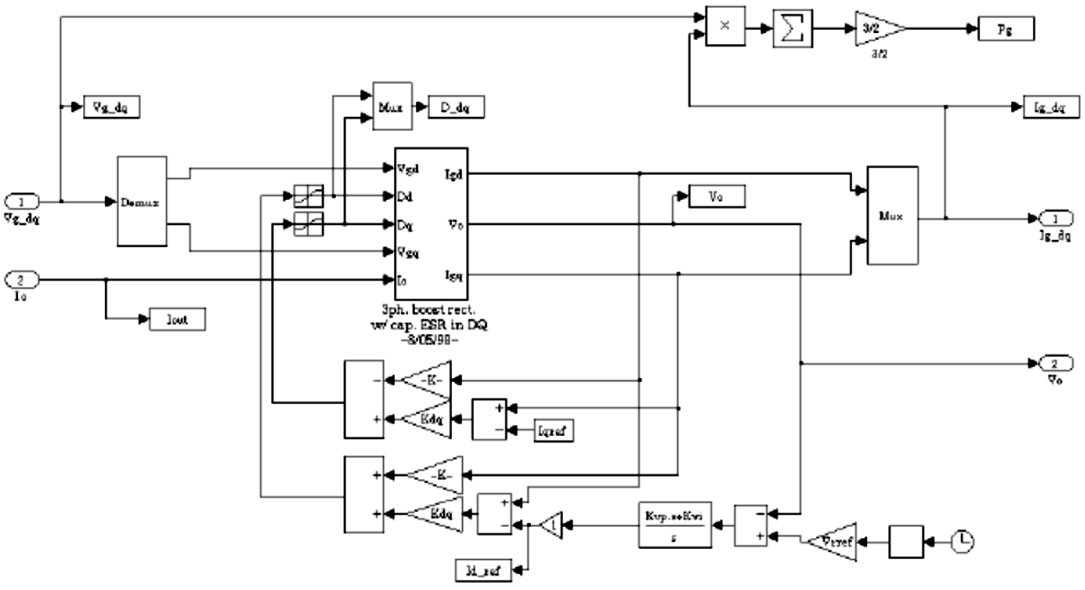

Figure 3.21 Closed-loop Simulink model of the boost rectifier in *dq* coordinates.

The complete closed-loop Simulink model for the boost rectifier is shown in Figure 3.21.
It utilizes the Simulink model of the rectifier power stage as a subsystem.

3.4 Modeling of Flight Actuators

3.4.1 Electromechanical Actuator Modeling

An electromechanical actuator driving an inboard spoiler surface of an aircraft was chosen as an example of a flight actuator being a part of the PDS. A Simulink model of the actuator surface system was developed by Lockheed Martin Control Systems in Johnson City, New York. A system diagram of the electromechanical actuator (EMA) is shown in Figure 3.22. It consist of a dc-dc power converter feeding a dc motor, which moves the inboard spoiler surface through a mechanical transmission consisting of a gearbox and a ball screw mechanism. The dc-dc converter is connected to the dc power distribution bus through an input filter, whose purpose is to prevent the switching ripple of the converter from going to the bus. Finally, a multi loop feedback controller is employed to precisely control the surface movement. A typical EMA architecture of a modern aircraft employs a three-phase brushless motor fed by a dc-to-three phase inverter. However, the model developers came to conclusion that the use of a dc-dc converter and a dc motor model instead will not affect essential features of the subsystem dynamics.

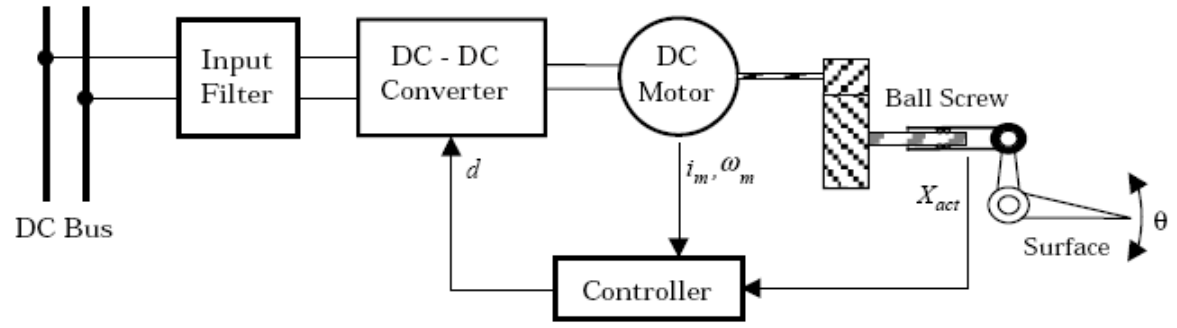

Figure 3.22 Electromechanical actuator system diagram

A Simulink model for the EMA subsystem (Figure 3.23) follows its structure and consists of six functionally complete modules. The input filter is modeled as an LC filter, whose modeling was already discussed above (Figures 3.1 and 3.2). The dc-dc converter module represents a power

stage of the buck converter without an output LC filter because its load (dc motor) provides sufficient filtering effect due to its own inductance.

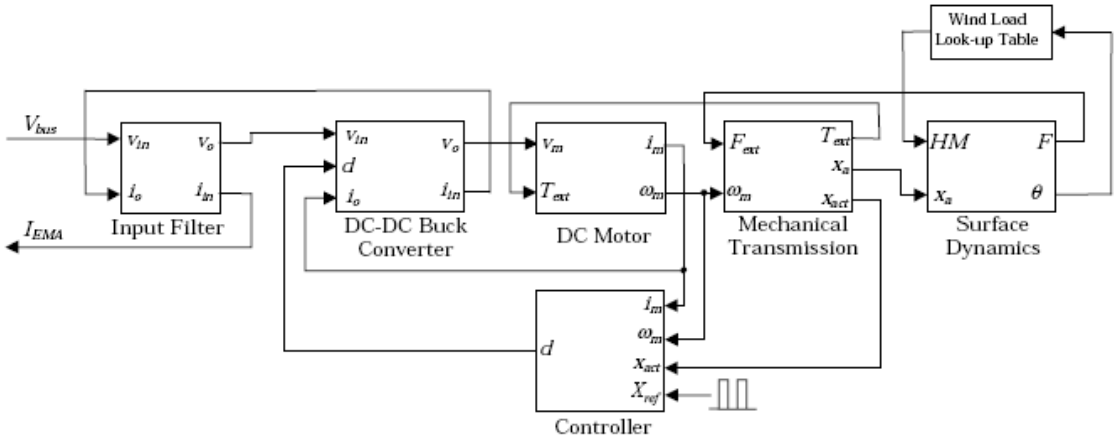

Figure 3.23 Electromechanical actuator Simulink block diagram

Therefore, the average model of the PWM switch shown in Figures 3.4 and 3.5 was used for the dc-dc converter. A Simulink model for a separately excited dc motor is shown in Figure 3.24. The model is derived from the motor equations:

$$v_m = K_e\omega_m + i_m R + L\frac{di_m}{dt}$$

$$K_t i_m - T_{ex} = B_m\omega_m + J\frac{d\omega_m}{dt}$$

where

v_m - armature voltage,

i_m - armature current,

ω_m - armature angular speed,

T_{ex} - external (load) torque applied to the shaft,

L - armature inductance,

R - armature resistance,

J_m - armature inertia,

B_m - viscous friction coefficient,

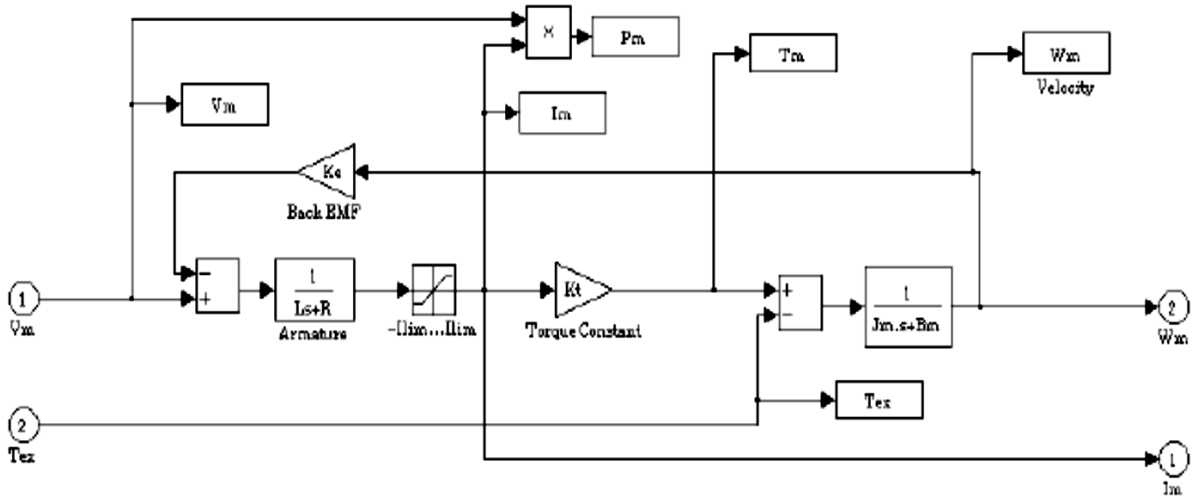

Figure 3.24 Simulink model for a separately excited dc motor

K_e - back-emf constant,

K_t - electromagnetic torque constant.

The mechanical actuator module includes a gearbox and a ball screw mechanism. A Simulink model for the mechanical transmission (Figure 3.25) takes into account inertia, damping, and stiffness of the ball screw mechanism and stiffness of the bearing structure.

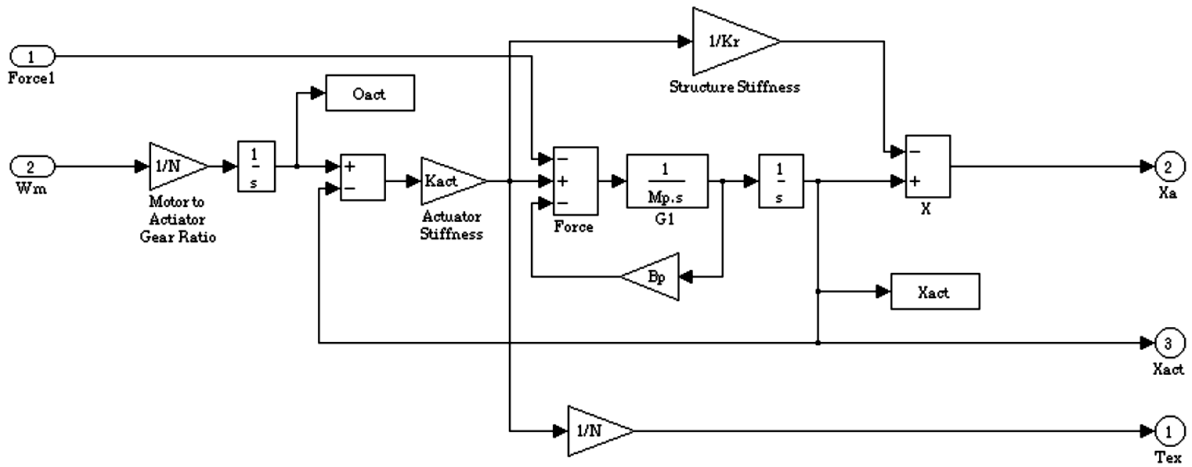

Figure 3.25 Simulink model for the mechanical transmission of the EMA.

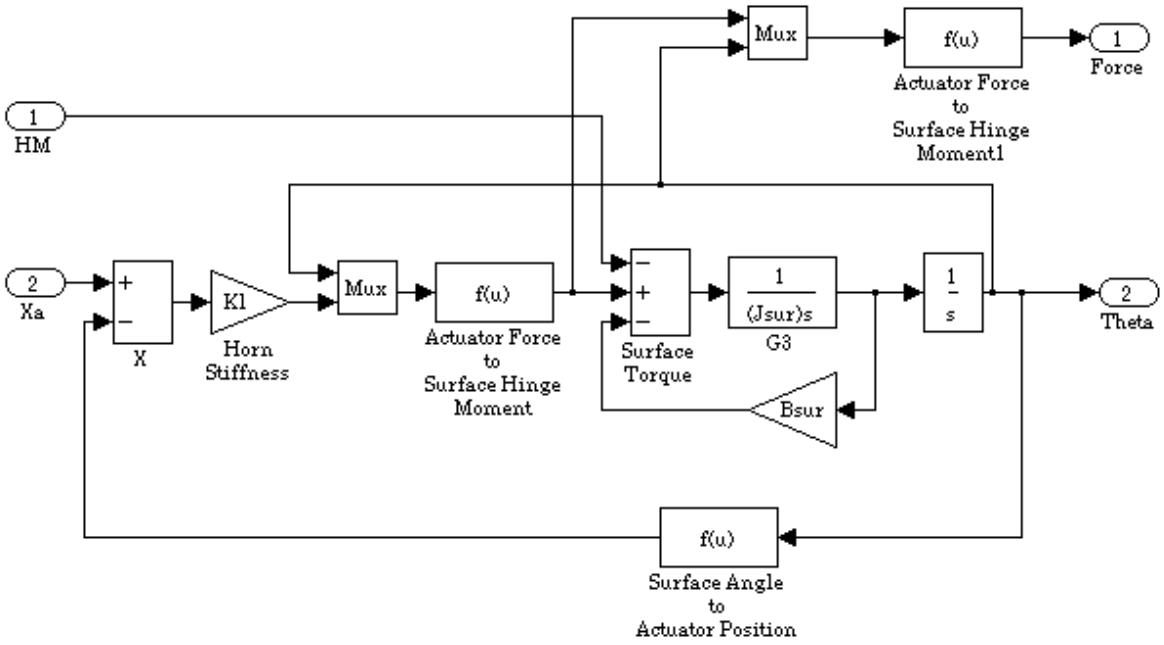

Figure 3.26 Simulink model for the surface dynamics.

A Simulink model for the surface dynamics is shown in Figure 3.26. The model reflects the horn stiffness, surface inertia and damping, and a nonlinear relationship between the mechanical actuator movement and the surface deflection angle. The feedback controller (Figure 3.27) controls duty cycle of the dc-dc converter according to the actuator position command. The controller employs the motor current, motor speed, and the actuator position feedback loops.

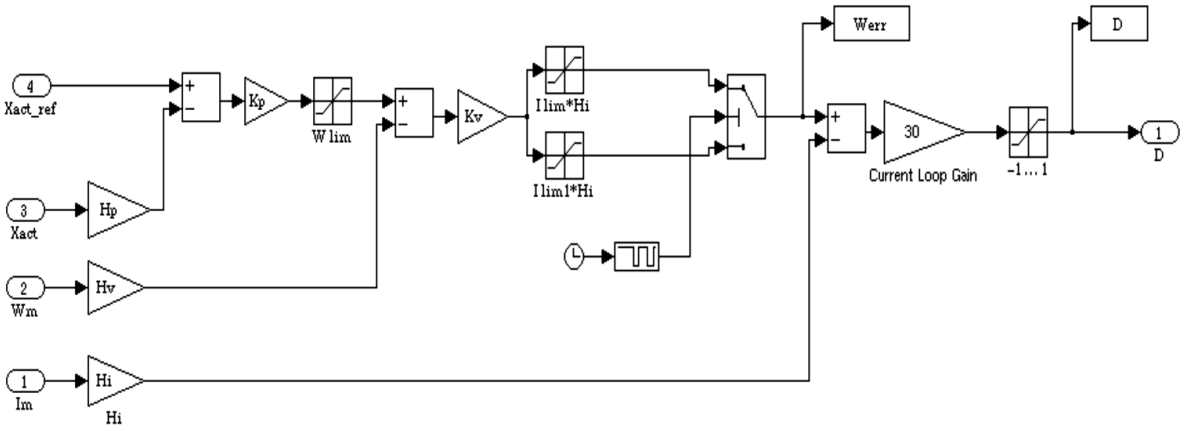

Figure 3.27 Simulink model for the EMA feedback controller.

A part of the EMA model is a Simulink look-up table containing an approximation of the wind load on the spoiler surface as a function of its deflection angle. This table was used in simulations of normal flight conditions. Another possible scenario investigated in this research is testing the system on the ground, which assumes that there is no wind load to the surface.

3.4.2 Electrohydrostatic Actuator Modeling

Another model developed by Lockheed Martin Control Systems as an example of a flight actuator modeling was an electrohydrostatic actuator driving the elevator surface. A system diagram of the actuator is shown in Figure 3.28, and its Simulink model – in Figure 3.29.

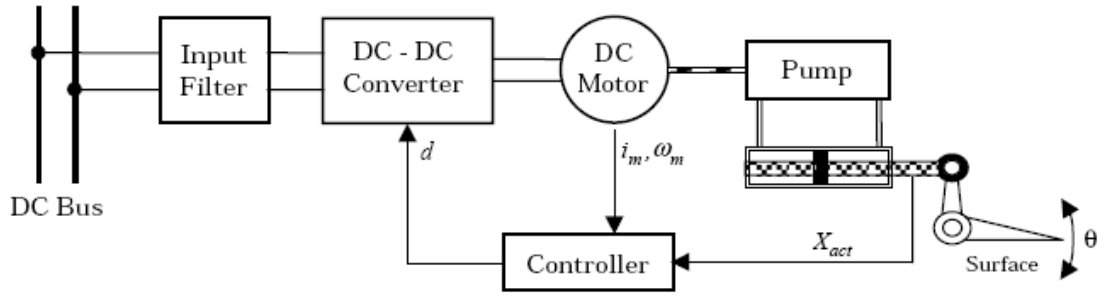

Figure 3.28 Electro hydrostatic actuator system diagram.

The electrohydrostatic actuator (EHA) model is very similar to the EMA model described above. The model employs a hydraulic actuator consisting of a hydraulic pump and a hydro cylinder instead of a mechanical actuator to convert the motor rotation to the surface movement. A Simulink model of the hydraulic actuator is shown in Figure 3.30. It takes into account the pump leakage, the piston inertia and damping, and the bearing structure stiffness. All the other components of the EHA model have the same structure as the corresponding EMA components but different parameter values. The EHA model was used in simulations in the same way as the EMA model.

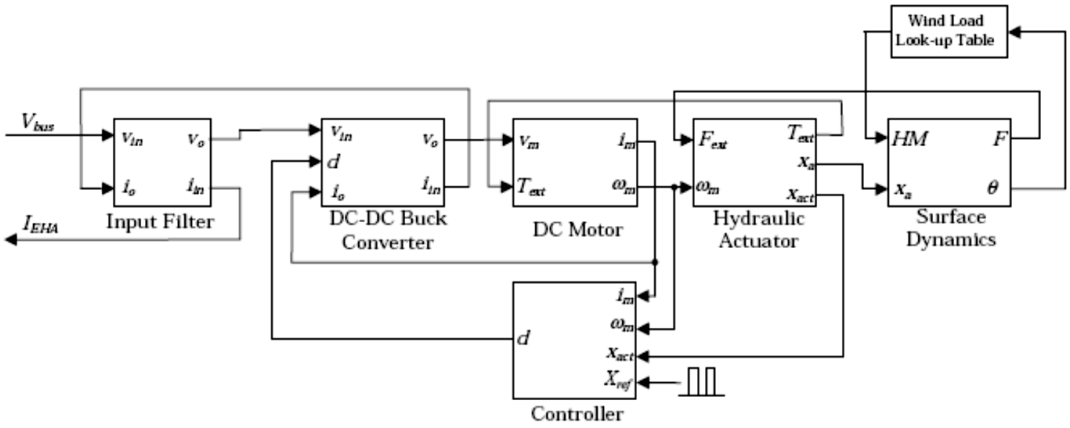

Figure 3.29 Electro hydrostatic actuator Simulink block diagram.

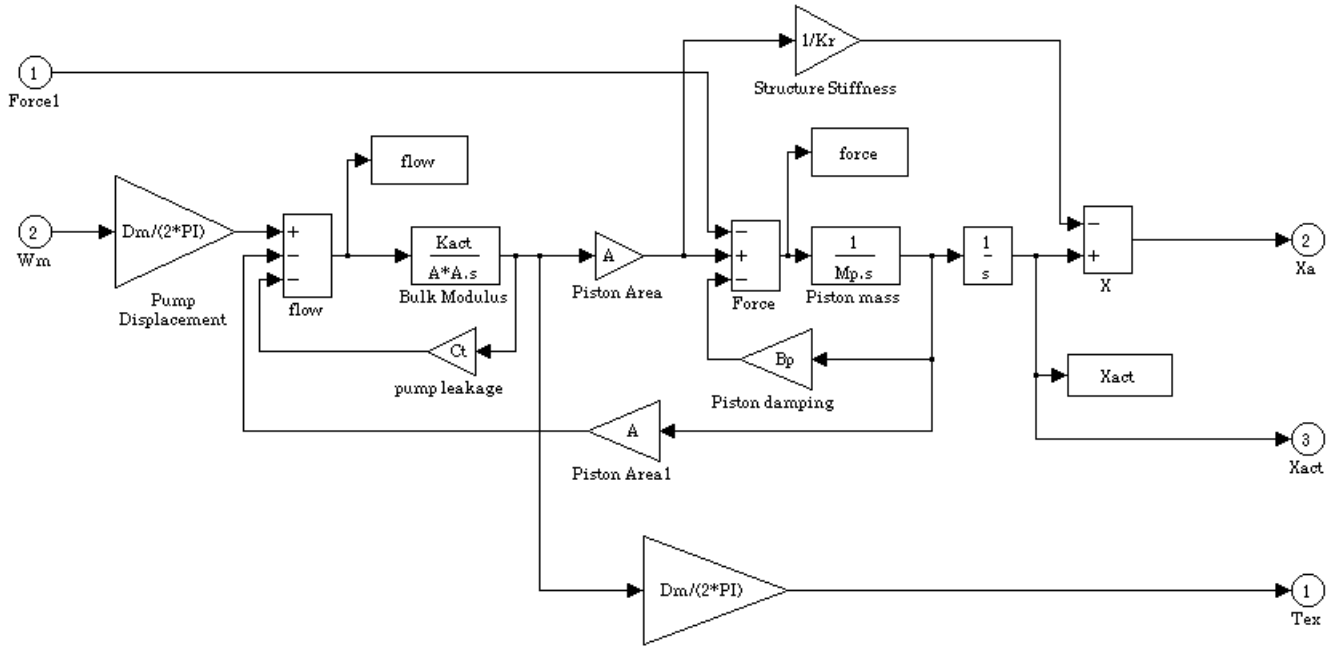

Figure 3.30 Hydraulic actuator Simulink model.

3.5 DC Power Distribution Bus Modeling

The dc bus as viewed in this research consists of wires and cables transmitting dc power between the three-phase-to-dc converters and the loads. These connection elements are characterized by R, L, C parameters distributed along their lengths. Although these parameters are fairly small compared to the corresponding lumped parameters of the subsystems connected to the bus, they do affect the processes in the PDS under certain scenarios of operation and therefore must be taken into account. Since we are not interested in studying propagation of voltages and currents along the bus, there is no need in modeling it as a transmission line. A much more computationally effective bus model may be obtained by modeling any piece of the bus between two adjacent subsystems connected to it as a network with lumped parameters. In order to account for attenuation and phase delay produced by such a piece a simple LC filter model would suffice. The LC filter network (Figure 3.1) and its Simulink model (Figure 3.2) were already discussed above.

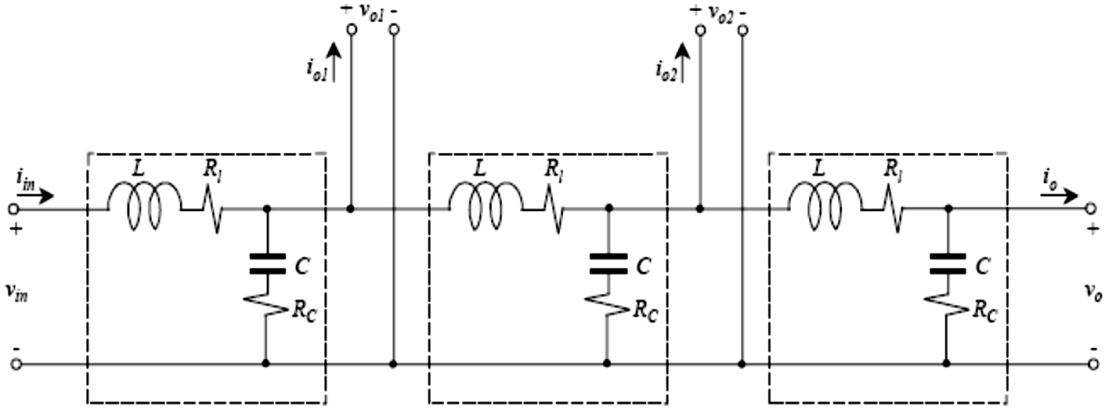

Figure 3.31 Three-section dc bus equivalent circuit.

Figure 3.31 shows a three-section dc distribution bus with two subsystems connected to its ends and two others connected in the middle. Each section is modeled as an LC filter network whose parameters should be determined specifically for each section based on the section length and the distributed parameter values. The leakage conductance between wires is not modeled since it is negligible for aircraft busses. A corresponding Simulink model shown in Figure 3.32 is based on the LC filter models assembled into a subsystem model according to the interconnection rules.

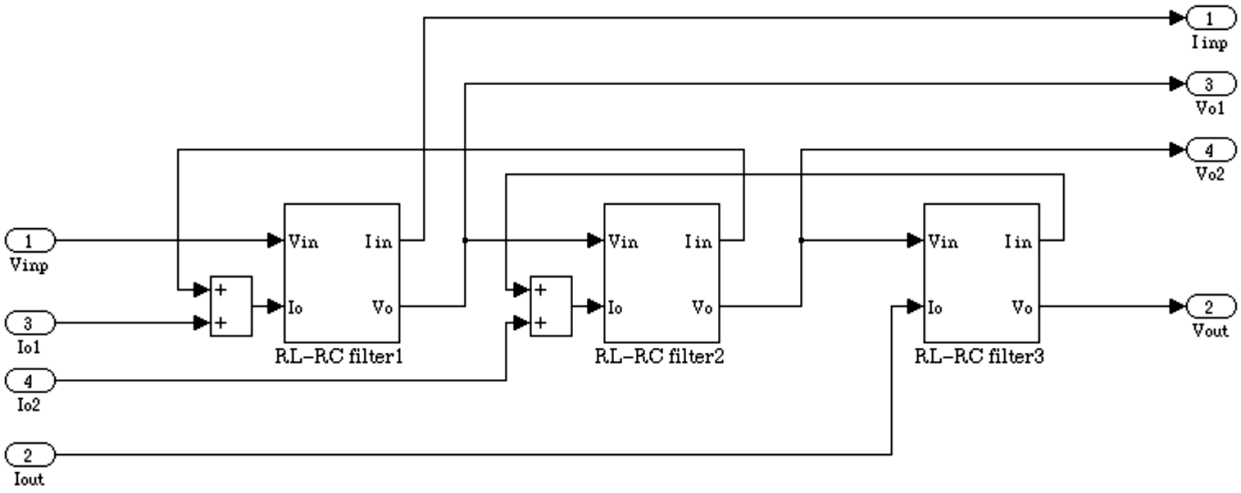

Figure 3.32 Simulink model for a three-section dc bus.

Chapter 4

Analysis of Bidirectional Power Flow in a DC Power Distribution System

4.1 Introduction

A prominent feature of the PDS is bidirectional power flow in its subsystems and the DC distribution bus. As opposite to the normal power flow from the sources to the loads, the reverse power flow occurs when certain loads in the system work in regenerative mode. For example, this mode of operation is typical for flight control actuators, which alternate normal and regenerative modes during their operational cycle. This chapter presents an analysis of the effect of regenerative power flow on the overall system performance characteristics such as DC bus power quality and system efficiency.

The energy coming from a regenerating subsystem tends to raise the DC bus voltage unless this energy is utilized by certain means. When no other load with sufficient power consumption is present at the moment of regeneration, and no measures are taken to utilize the regenerative energy, the bus voltage can easily rise beyond allowable limits specified by MILSTD- 704E. This phenomenon may affect normal operation of the PDS and cause damage to the equipment connected to the bus. An attractive solution would be to store this energy in the battery for future use. Unfortunately, the battery charges too slowly to accept the regenerative energy, which usually comes in short transient spikes of high power. Presently, there are several possible ways to deal with regenerative energy in the system:

- dissipate it in resistors connected to the bus at the time of regeneration,
- let it go back to the engine by using the generator and three-phase-to-dc power converter in regenerative mode,

- use large capacitors in order to store the regenerative energy either in the DC bus, or in the regenerating subsystem,
- use a DC bus conditioner (a power converter that stores the extra energy from the bus in a large capacitor and returns the energy to the bus when loads are available).

Currently, industry uses the first approach with damping resistors dissipating the regenerative energy. Unfortunately, the amount of this energy is so high that the resistors require liquid cooling. This solution complicates the system and reduces the benefits of the "more electric approach" in aircraft design. The use of a bus conditioner seems to be too complicated and expensive at this time; it is left for future consideration. This chapter considers utilizing the regenerative energy in the power source (the engine) with the use of additional capacitors in the DC bus and in the regenerating subsystem in order to alleviate transient voltage spikes caused by regenerative power flow.

4.2 System Configuration for Bidirectional Power Flow Analysis

The system configuration shown in Figure 4.1 was used to study the effects of additional capacitors on the DC bus power quality and the system efficiency under bidirectional power flowconditions. The system consists of a three-phase synchronous generator, three-phase-to-dc boost rectifier, the EMA including an input filter, and a constant resistive load on the DC bus, representing all other system loads except the EMA. The system waveforms during one operating cycle of the EMA are shown in Figure 4.2 (operation without the wind load) and Figure 4.3 (operation with the wind load). The analysis is performed for the time period from 0.5s to 2.5s, which corresponds to the full cycle of the EMA. The period from 0 to 0.5s is a "start-up" period; it is used to bring the simulation model to the initial conditions corresponding to the beginning of the cycle. This period is not included into consideration.

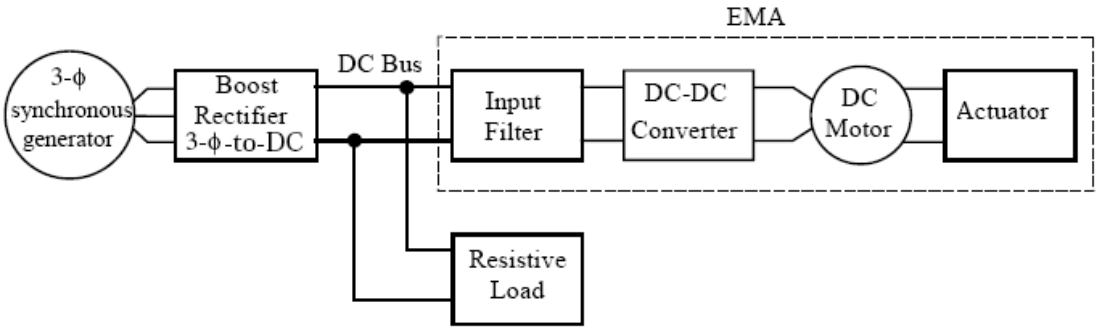

Figure 4.1 System configuration for bidirectional power flow analysis.

Figures 4.2 and 4.3 are typical examples of the system operation with and without the wind load for a certain set of system parameters. The plots show the DC bus voltage and power, the motor current, the flight control surface deflection angle, and the EMA reference signal coming from a higher-level control system. The major phenomena under investigation such as regenerative energy flow and voltage disturbances on the bus occurs at times when the actuator reference signal changes abruptly and the actual position of the actuator reaches its commanded value. This causes the actuator motor to speed up or to slow down, thus consuming or regenerating a certain amount of energy, which causes significant current flow in the system and, as a result, voltage disturbances on the DC bus. Regenerative energy flow always occurs in the system when the actuator reference signal causes the actuator moving parts to slow down, and their mechanical energy is converted into electrical. In addition, the wind load produces regenerative energy when the surface moves in the direction of the air flow. In this case, the wind energy is converted into electrical energy. This energy will have to be consumed from the boost rectifier later during the cycle when the actuator reference signal causes the actuator surface to move against the air flow.

What happens to the regenerative energy in this particular system configuration depends primarily on the value of the resistive load on the DC bus. If the load is large enough such that the power that it draws from the bus exceeds the peak value of the actuator regenerative power, the power drawn from the boost rectifier remains positive at all times. The actuator regenerative power is completely consumed by the resistive load, thus merely decreasing the power drawn

from the boost rectifier. If the peak actuator regenerative power exceeds the load power requirement, the excessive power will be transformed back to the generator by the boost rectifier. This case is shown in Figures 4.2 and 4.3, where the load draws 1kW power from the DC bus. If the rectifier does not possess bidirectional energy flow capability, the excessive amount of energy will be stored in the rectifier output capacitor and the input filter capacitor, which will cause the DC bus voltage to increase. The amount of this increase will be determined by the capacitor's total value and the amount of energy regenerated. When a bidirectional boost rectifier is used, the capacitors do not store the regenerative energy permanently, but only affect the system transients.

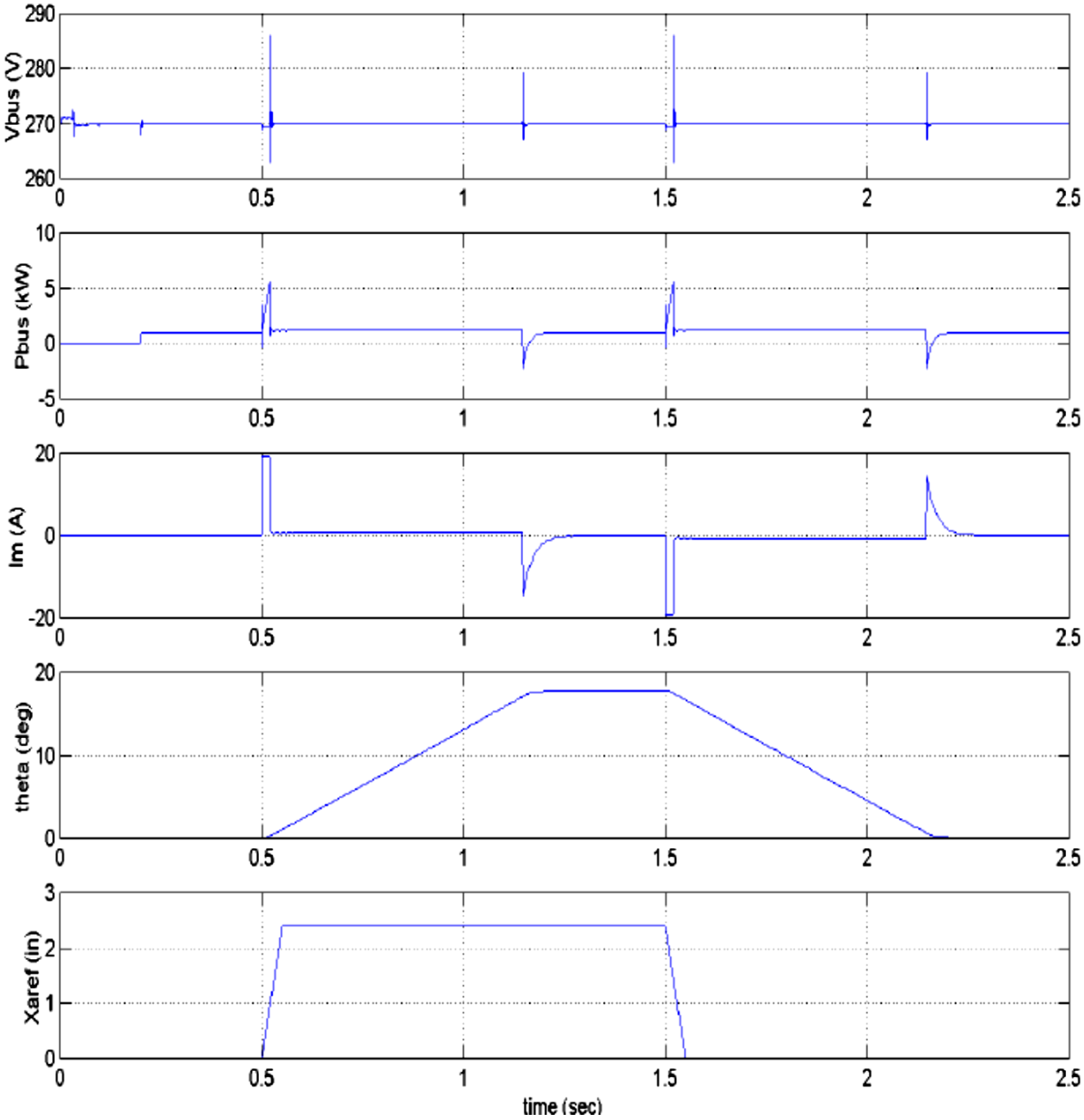

Figure 4.2 System operation without the wind load.

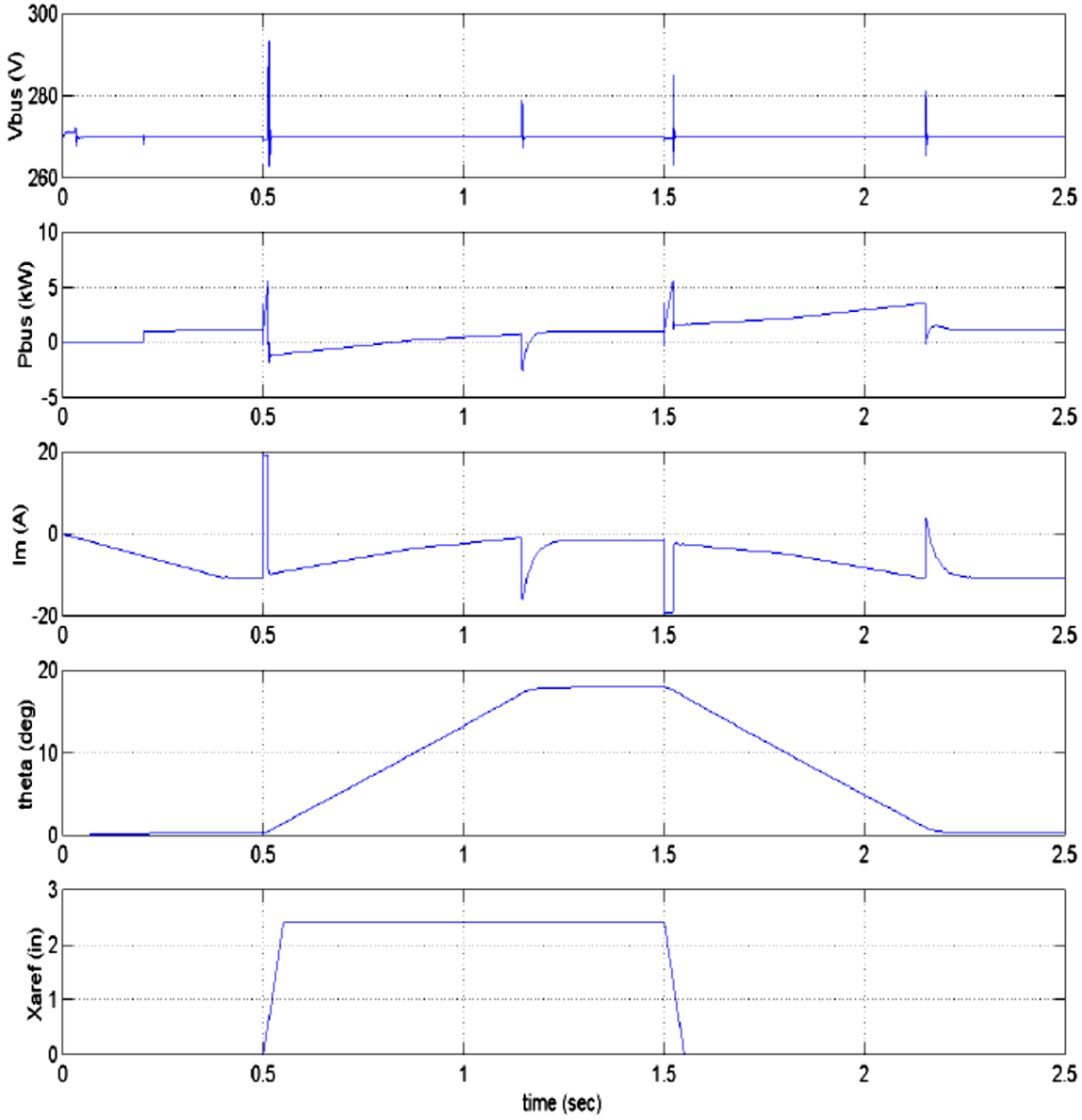

Figure 4.3 System operation with the wind load.

4.3 Overall System Performance Characteristics and Methodology of Bidirectional Power Flow Analysis

The distributed power quality may be characterized by the DC bus voltage disturbances. They are affected by the system damping, which is determined by parameters of both system elements and control structure. In this study of the DC bus power quality, magnitude of voltage spikes on the bus and settling time of the transients were used as performance measures. For the purpose of

this research, we defined a "voltage spike" as a voltage disturbance on the DC bus that exceeds an allowable limit $\pm\Delta V$. "Transients" are considered as a series of spikes. We define the "settling time of the transients" as a time interval during which the series of spikes occurs provided that the spikes in the series are separated by time intervals no more than an allowable time Δt. This concept is illustrated in Figure 4.4. The following values for these parameters were assumed:

$\Delta V = 2V$,

$\Delta t = 0.001s$.

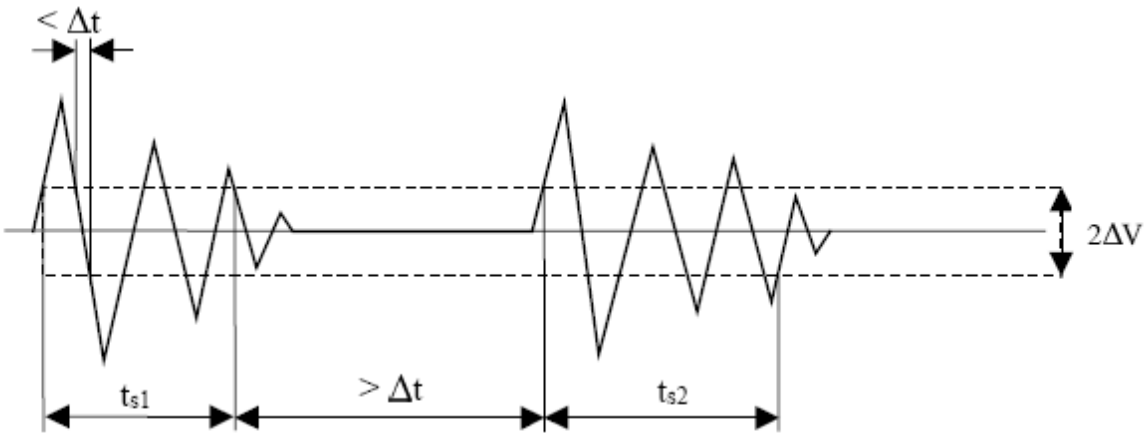

Figure 4.4 Settling time of the transients on the DC bus.

In order to characterize quantitatively the process of energy distribution and regeneration in the sample PDS (Figure 4.1), the complete energy flow analysis was performed. Energy flow in the system is described in terms of energy flow at subsystems boundaries (Figure 4.5). Energy is computed at each boundary by integrating the corresponding power as a function of time during the EMA operating cycle.

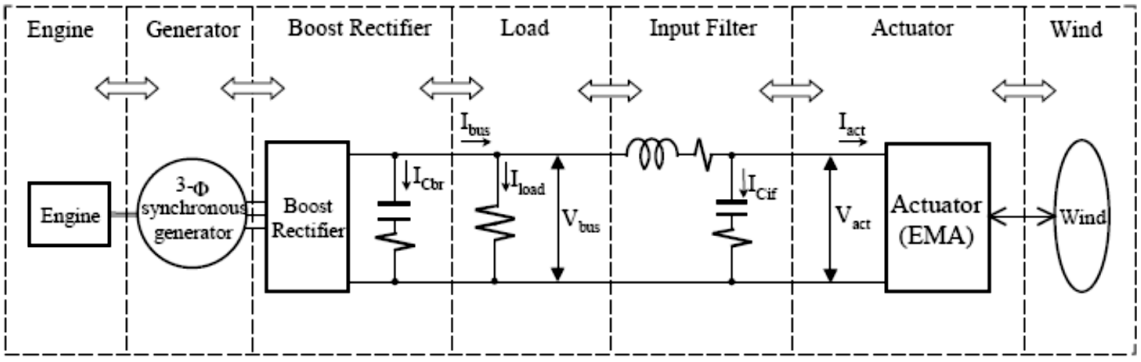

Figure 4.5 Bidirectional energy flow in the system.

The definitions used for energy flow analysis in the system are given below.

Mechanical power supplied by the engine to the generator:

$$\boldsymbol{P_{gm} = P_g + P_{gl}},$$

where P_g – power transferred from the generator to the boost rectifier,

P_{gl} – total power losses in the generator.

Power supplied by the generator to the boost rectifier:

$$\boldsymbol{P_g = 1.5\ (V_{gd}\, I_{gd} + V_{gq}\, I_{gq})},$$

where V_{gd}, V_{gq} – generator output voltages in *dq* coordinates,

I_{gd}, I_{gq} – generator output currents in *dq* coordinates.

Generator electrical losses are calculated as a sum of losses in phase windings, damper winding, and the excitation winding. Total generator losses are obtained by multiplying the electrical losses by two to account for magnetic and other types of losses. Total generator losses are used for calculating mechanical power supplied by the engine to the generator because no engine simulation is involved.

Losses in phase resistances:

$$P_{gls} = 1.5\ (I_{gd}^2 + I_{gq}^2)\, R_s,$$

where I_{gd}, I_{gq} – phase currents in *dq* coordinates,

R_s – resistance per phase in the equivalent circuit.

Losses in the damper winding:

$$P_{glk} = 1.5\ (I_{kd}^2\, R_{kd} + I_{kq}^2\, R_{kq}),$$

where I_{kd}, I_{kq} – damper winding currents in *dq* coordinates,

R_{kd}, R_{kq} – damper winding resistances in *dq* coordinates.

Losses in the field winding:

$$P_{glf} = I_{fd}^{2} R_{fd},$$

where I_{fd} – field winding current referenced to the stator,

R_{fd} – field winding resistance referenced to the stator.

Total generator losses:

$$P_{gl} = 2\,(P_{gls} + P_{glk} + P_{glf}),$$

Power transferred from the boost rectifier to the load:

$$P_{bus} = V_{bus}\, I_{bus},$$

where V_{bus} – DC bus voltage,

I_{bus} – DC bus current.

Power transferred from the load to the input filter:

$$P_{fi} = V_{bus}\,(I_{bus} - I_{load}),$$

where I_{load} – load current.

Power transferred from the input filter to the EMA:

$$P_{act} = V_{act}\, I_{act},$$

where V_{act}, I_{act} – input voltage and current of the EMA, respectively.

Power transferred from the actuator to the air:

$$P_{wind} = H_m\, \omega_{sur},$$

where H_m – external moment from the air flow,

ω_{sur} – actuation surface angular speed.

Energy flowing from the left to the right is considered positive, regenerative energy flowing in the opposite direction – negative. Based on energy flow analysis at subsystem interfaces shown in Figure 4.5, the energy balance for each subsystem is calculated. Energy balance for the engine, which is the net energy coming from the engine to the generator:

$$W_{eng} = W_{gmp} - W_{gmn},$$

where W_{gmp} – positive energy, coming from the engine,

W_{gmn} – negative (regenerative) energy, going back to the engine from the generator.

Energy balance for the generator, equal to the total losses in the generator:

$$W_{gen} = (W_{gmp} - W_{gmn}) - (W_{gp} - W_{gn}),$$

where W_{gp} – positive energy, transferred from the generator to the boost rectifier,

W_{gn} – negative (regenerative) energy, going back to the generator from the boost rectifier.

Energy balance for the boost rectifier, equal to its losses:

$$W_{brec} = (W_{gp} - W_{gn}) - (W_{busp} - W_{busn}),$$

W_{busn} – negative (regenerative) energy, going back to the boost rectifier from the bus.

Energy balance for the resistive load:

$$W_{load} = (W_{busp} - W_{busn}) - (W_{fip} - W_{fin}),$$

where W_{fip} – positive energy, transferred from the bus to the input filter,

W_{fin} – negative (regenerative) energy, going back from the input filter to the bus.

Energy balance for the input filter, equal to its losses:

$$W_{iflt} = (W_{fip} - W_{fin}) - (W_{actp} - W_{actn}),$$

where W_{actp} – positive energy, transferred from the input filter to the EMA,

W_{actn} – negative (regenerative) energy, going back from the EMA to the input filter.

Energy balance for the EMA, equal to its losses:

$$W_{actr} = (W_{actp} - W_{actn}) - (W_{windp} - W_{windn}),$$

where W_{windp} – positive energy, transferred from the EMA to the air,

W_{windn} – negative (regenerative) energy, going from the air flow to the EMA.

Energy balance for the air flow, equal to the net energy passed by the EMA to the air:

$$W_{wnd} = W_{windp} - W_{windn}.$$

Once the losses in the subsystems are calculated, the overall system efficiency is obtained as

$$\eta = \frac{W_{gmp} - (W_{gen} + W_{brec} + W_{iflt} + W_{actr})}{W_{gmp}}.$$

.

Efficiency is calculated for total energy coming from the engine. Total losses include the losses in the generator, boost rectifier, input filter, and the actuator. Energy dissipated in the resistive load, passed to the air by the actuator, and regenerative energy returned into the engine is considered to be usefully spent.

4.4 Effect of the Input Filter Capacitor on the System Characteristics under Bidirectional Power Flow Conditions

At the first stage of analysis, influence of the EMA input filter capacitor on the system performance was studied by using a parametric sweep technique. The system operation was simulated repeatedly for different values of the capacitance, with and without the wind load. The capacitance value range was chosen with the lowest value based on necessary switching ripple attenuation and the highest value approaching 1F. The system performance measures such as energy flow and voltage disturbance characteristics then were analyzed based on the simulation results.

The study showed that voltage spikes on the DC bus produced by the EMA cyclic operation are significantly reduced with the increase of the input filter capacitance C_{if}. For example, Figures 4.2 and 4.3 show the system operation with the lowest value of the capacitance, equal to 63μF. Figures 4.6 and 4.7 show the system waveforms for a capacitance value of 63mF, which is three orders of magnitude larger than the previous value. It is seen that voltage disturbances produced on the bus become lower in magnitude and longer in time with the increase of the capacitance. The EMA waveforms are preserved regardless of the capacitance value due to the EMA feedback control. Both positive (above 270V) and negative (below 270V) spikes reduce their magnitude almost to zero when the capacitance becomes extremely large. The figure shows that for low capacitance values, the settling time increases with the increase of the capacitance because the time constant of the circuit increases. At the same time, the magnitude of the disturbances decreases. When this magnitude falls below the allowable limit $\pm\Delta$V, the settling time becomes zero, according to the definition of the DC bus transients given above. The analysis showed that the same type of dependence is observed for all voltage disturbances on the bus, both regenerative and non regenerative, during the operating cycle.

The analysis of energy flow in the system shows that the amount of energy drawn by the system from the source (the engine) depends on the input filter capacitance. The total energy transferred from the engine to the system, the amount of regenerative energy passed back to the engine, and percentage of the regenerative energy in the total energy drawn by the system. It is seen that there is a global trend for the total energy to decrease when the capacitance becomes very large. At large capacitance values, the regenerative energy is almost fully absorbed by the capacitor without going back to the engine; the transients and associated with them losses are reduced. The

amount of regenerative energy going back to the engine at large values of the capacitance decreases to zero for operation without the wind load.

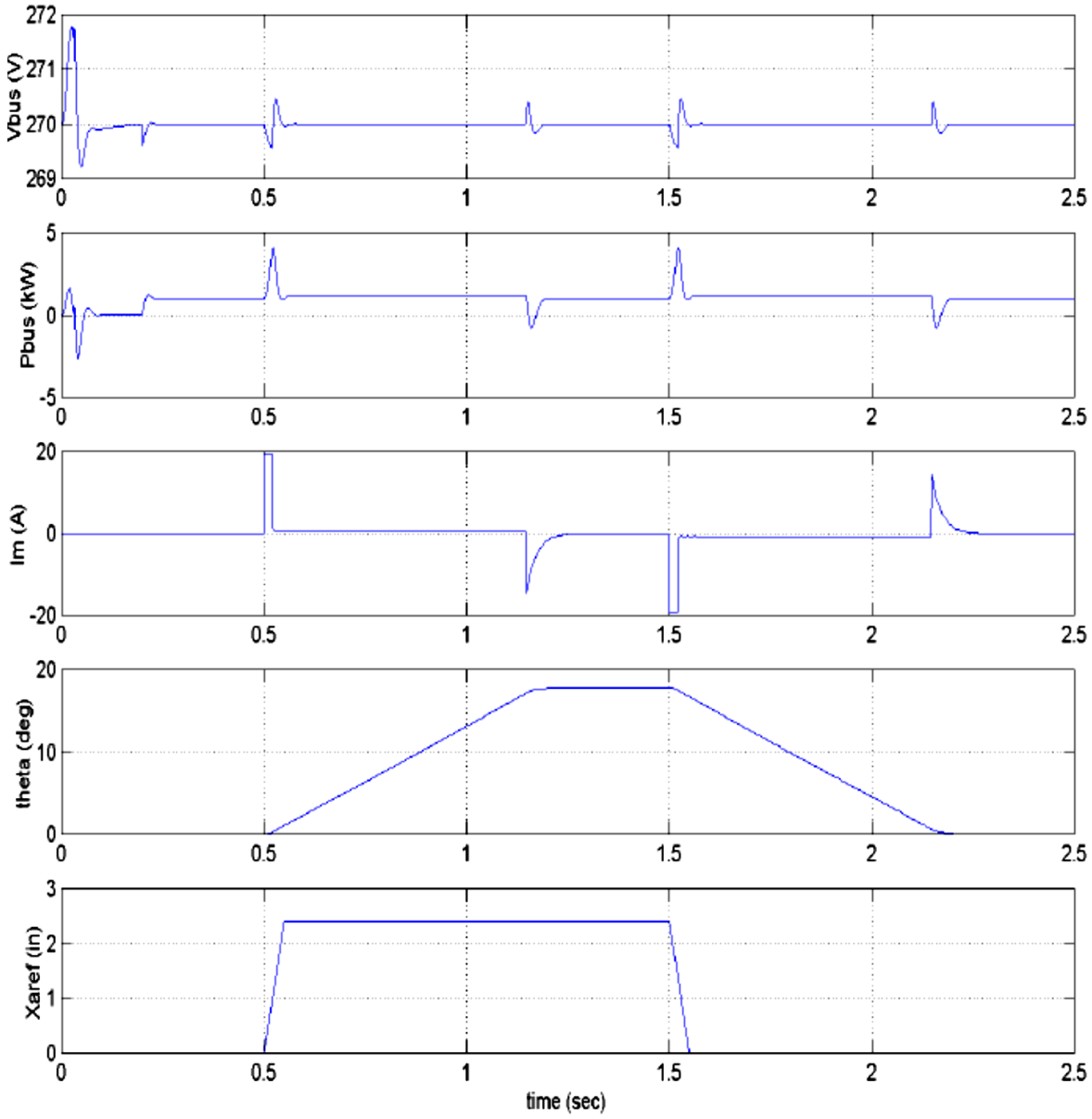

Figure 4.6 System operation without the wind load; C_{if} = 63mF.

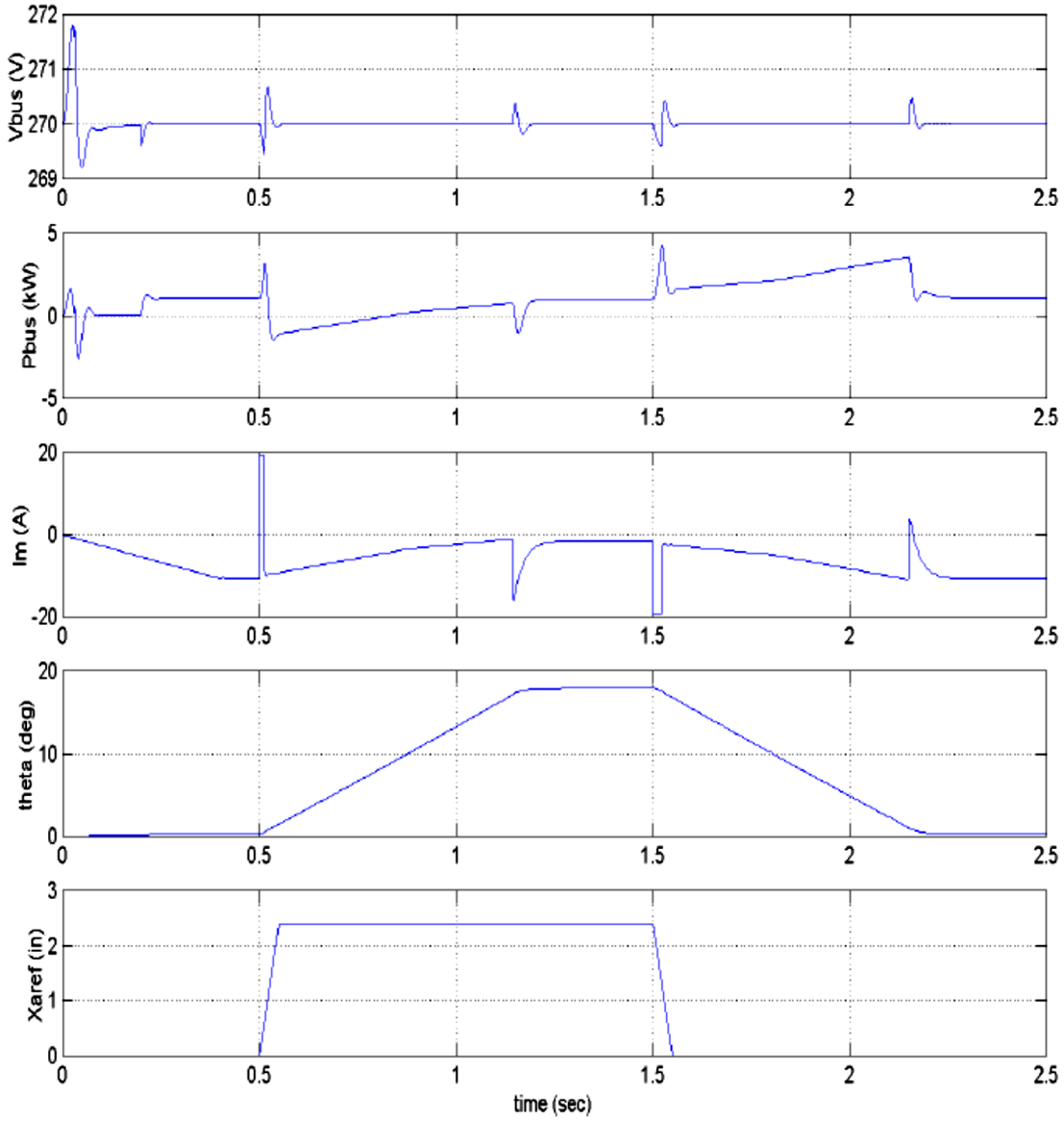

Figure 4.7 System operation with the wind load; C_{if} = 63mF.

In the case with the wind load, the amount of regenerative energy is much higher. This energy cannot be fully absorbed by the capacitor; however, its amount is reduced significantly. The air flow driving the actuator surface contributes significant amount of regenerative energy to the system. The figures show that the percentage of regenerative energy in the system operating with the wind load is six times higher than in the system operating without the wind load, where regenerative energy is contributed only by moving masses. For the generator, the boost rectifier, the input filter, and the actuator the energy balance represents losses in the respective subsystem.

It is seen that for the generator, the boost rectifier, and the input filter the losses tend to decrease at large capacitance values for operation both with and without the wind load. This phenomenon contributes to reduction of the total energy consumed by the system as was shown previously.

The actuator losses are not significantly affected by the capacitance value. Although the DC bus voltage transients are affected by the input filter capacitance, the actuator's feedback control makes its operation unaffected by the bus voltage variations. It is seen that losses in the generator, the boost rectifier, the input filter, and the actuator are noticeably higher in case with the wind load, because the extra energy processed by these subsystems is accompanied by extra losses.

The resistive load is considered a payload; its energy balance decreases due to the decrease in the bus voltage rms value when the transients become smaller at large capacitance values. The air flow energy balance represents the net energy passed to the air by the actuator flight control surface. This amount is equal to zero for operation without the wind load. When the system operates with the wind load, this amount is very small and independent of the input filter capacitance.

A special consideration was given to the generator losses, which demonstrate an increase in the middle of the capacitance range. Losses in the phase resistances and field winding are almost constant in the whole range of capacitance with a slight trend to decrease at large capacitance values because of a decrease in the amount of regenerative energy transferred back to the engine. However, losses in the damper winding experience an increase in the middle of the capacitance range. It is known that the damper winding does not carry current in steady-state operation of the generator. The purpose of the damper winding is to damp transients by dissipating their energy. For low values of the capacitance, the transients, although high in magnitude, are relatively short in duration, and do not produce much dissipation in the damper winding. For very large capacitance values, the transients become very small. It is in the middle of the capacitance range, when the transients are still relatively high and their duration is long because of the time constant increased by the large capacitance, the damper winding losses experience an increase. This phenomenon explains why the generator losses have an increase in the middle of the range. This

increase in losses produces an increase in energy drawn from the engine, and a corresponding decrease in the overall system efficiency.

The overall system efficiency is plotted in Figure 4.8. The variation of the efficiency as a function of the input filter capacitance is very small – within 1% of the initial value.

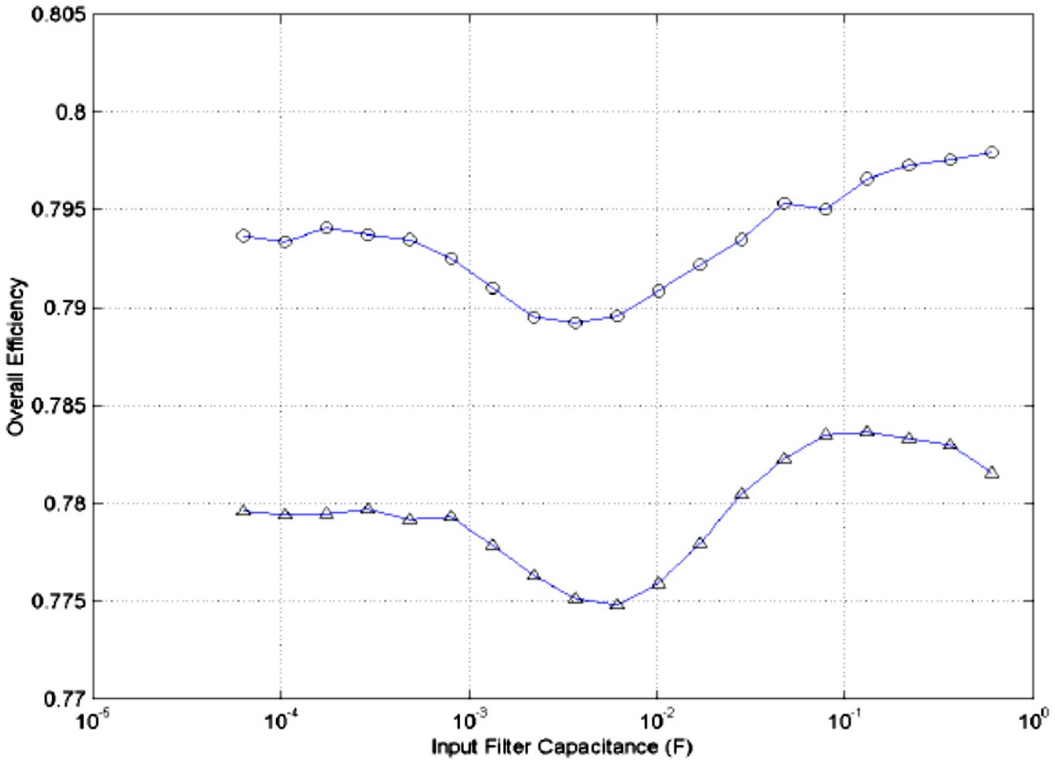

Figure 4.8 Overall efficiency of the system with (Δ) and without (o) the wind load.

The increase in the generator losses produces a decrease in the efficiency for operation both with and without the wind load. At the same time, a global trend in increase of the overall efficiency at very high capacitance values can be seen, especially for operation without the wind load. Efficiency of the system operating with the wind load is approximately 1% lower than without the wind load. The results show that there is no advantage in using large capacitors in the input filter in order to improve the overall system efficiency, although the DC bus power quality can be improved.

4.5 Effect of the Boost Rectifier Capacitor on the System Characteristics under Bidirectional Power Flow Conditions

The effect of the boost rectifier capacitor on the bidirectional power flow characteristics was studied by using the parametric sweep technique, similarly to the previous case with the input filter capacitor. The results obtained were similar as well. Figures 4.9 and 4.10 show waveforms of the system operating without and with the wind load, respectively, with the boost rectifier output capacitance C_{br} increased to 350mF. Compared with waveforms of the system

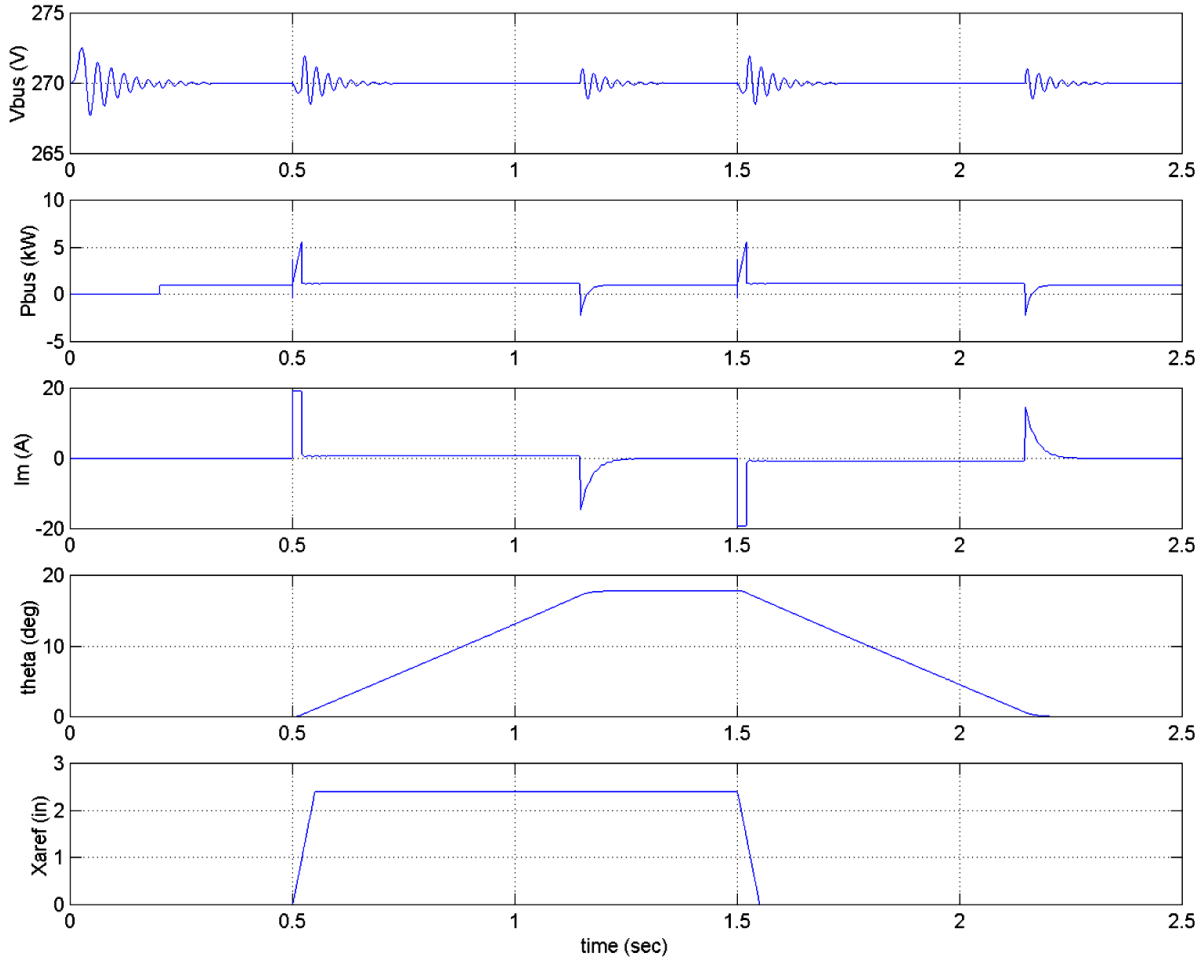

Figure 4.9 System operation without the wind load; C_{br} = 350mF.

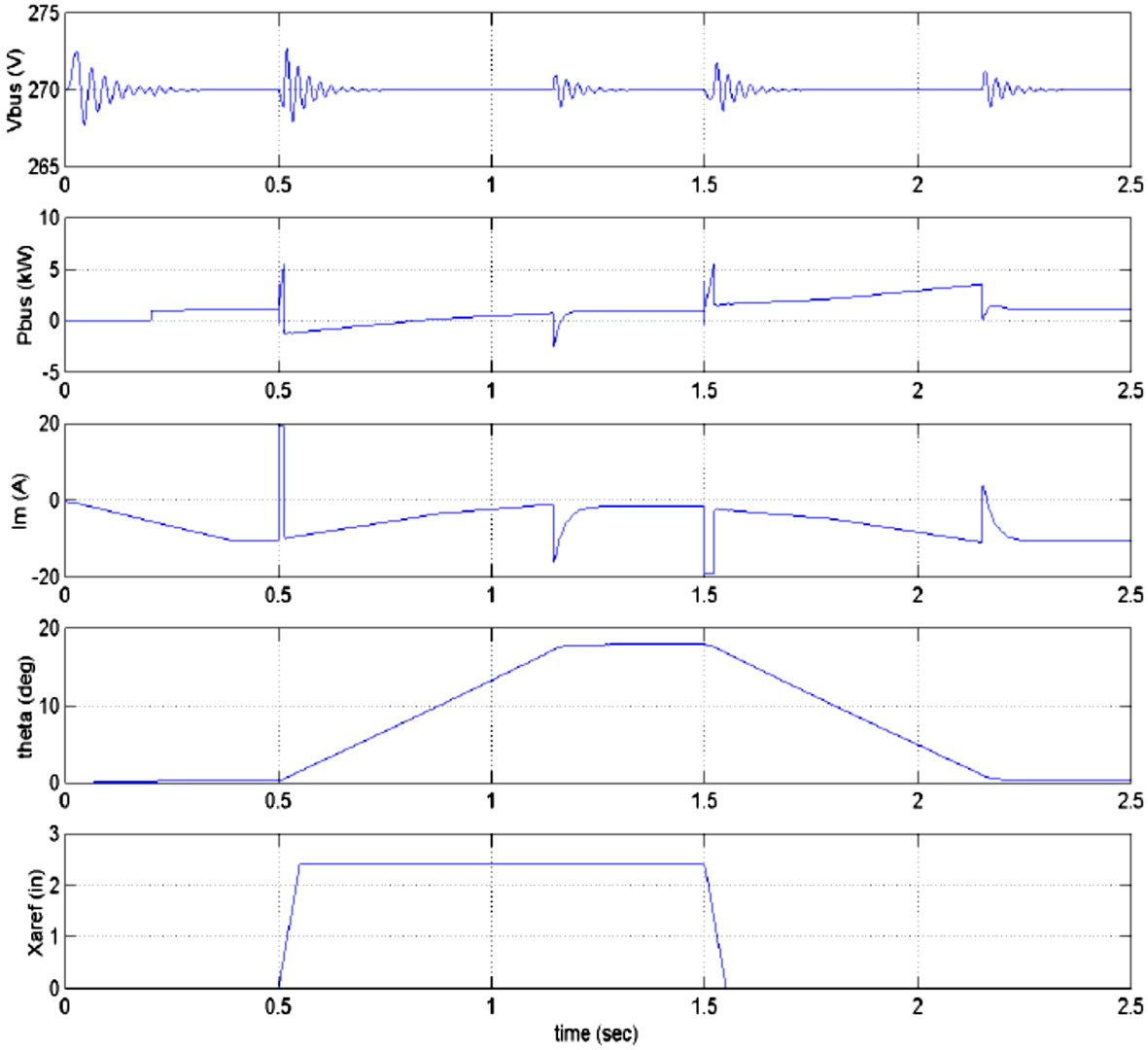

Figure 4.10 System operation with the wind load; C_{br} = 350mF.

with a nominal set of parameters (Figures 4.2 and 4.3), the results show that the DC bus voltage disturbances produced by both direct and regenerative power flow become lower in magnitude and longer in duration with the increase of the capacitance. This is because the boost rectifier capacitor is connected directly to the bus, without an intermediate inductor as in case of the input filter capacitor. The energy flow analysis yields the results very similar to the case with variation of the input filter capacitance and the DC bus transients are more oscillatory with 350mF boost rectifier capacitor than with 63mF input filter capacitor. In the latter case, the input filter inductance with its ESR provides an additional filtering and damping action when the regenerative power flow causes transients on the DC bus.

The long, poorly damped oscillations, which occur on the bus when a large boost rectifier capacitor is used, increase rms values of voltages and currents in the generator and the boost rectifier. This effect leads to increased losses in their phase resistances in addition to the increase in the damper winding losses as a result, the overall efficiency curves in Figure 4.11 experience a decrease in the middle of the capacitance range as much as three times larger than the corresponding curves.

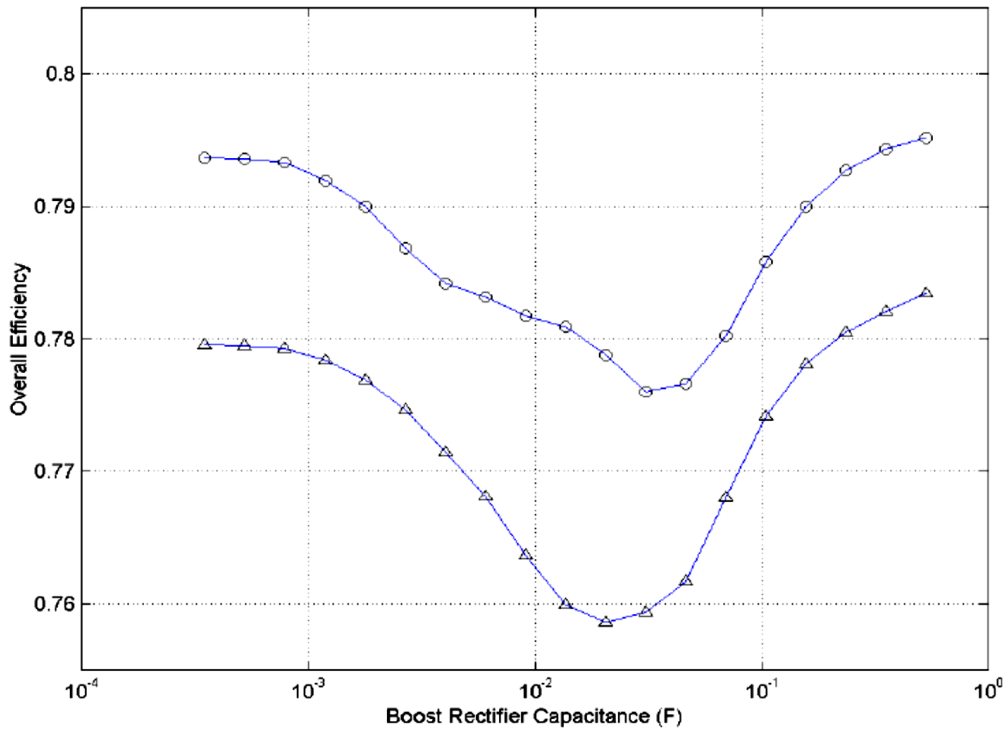

Figure 4.11 Overall efficiency of the system with (Δ) and without (o) the wind load.

The drop in efficiency is up to 1.5% in case with the wind load, and it is barely recovered with using of very large capacitance values at the end of the range. The results of bidirectional power flow analysis showed that large capacitors in the input filter and the boost rectifier can be effectively used to reduce the magnitude of voltage spikes on the DC bus. At the same time, the large capacitors do not provide any advantage in utilizing the regenerative power flow in the system. In fact, the overall system efficiency reduces insignificantly when the capacitance values are increased up to two orders of magnitude against their initial values. This is especially noticeable in case of using a large boost rectifier capacitor, which creates long, poorly damped,

low-frequency oscillations on the bus. For this reason, it is better to use a larger input filter capacitor than the boost rectifier capacitor in order to reduce the magnitude of voltage spikes on the DC bus.

Chapter 5

Conclusions

This work presents modeling and analysis of a typical DC power distribution system in a transport aircraft using a set of modeling and simulation tools developed in this research. MATLAB/Simulink was chosen as a software platform. The multi-level modeling concept was used as a modeling approach, which assumes building models of different levels of complexity for each subsystem within the PDS. Three types of models were built: a detailed model, a behavioral model, and a reduced order model. The subsystem models, implemented in Simulink, were combined into the whole PDS model following certain interconnection rules. Subsystem models of different levels were mixed for modeling of different scenarios of operation. Linearization techniques provided by MATLAB were used to obtain linearized models of nonlinear systems for stability analysis and control design. The subsystems modeled in this research included a three-phase synchronous generator, a three-phase boost rectifier, DC-DC converters, electromechanical and electro hydrostatic actuators, and different types of the DC bus loads.

The modeling tools were used to investigate different stability issues in the PDS. Dynamic properties of the boost rectifier were studied and then used for analysis of interactions between the boost rectifier and different types of loads. It was found that presence of a constant power load on the DC bus may cause instability in the system. This instability results in oscillations of the DC bus voltage and current, which exceed the allowable limits set by MILSTD- 704E. The DC bus stability diagram was proposed as a convenient tool for predicting stability of the PDS with different types of loads without performing an actual stability test based on regular stability analysis tools. It was shown that a potential for instability in the PDS exists under both direct and regenerative power flow conditions.

The PDS model developed in this research was used to study the effects of bidirectional power flow in the PDS, produced by regenerative action of flight actuators, on the DC bus power quality characteristics and energy efficiency of the PDS. The regenerative energy returned to the bus creates voltage disturbances, which may be beyond the allowable limits. The effect of using large energy storage capacitors located in the boost rectifier and the EMA on the voltage disturbances was investigated. It was found that increased values of these capacitors can significantly reduce voltage disturbances on the DC bus. A large input filter capacitor in the EMA was found more suitable for this purpose because a large boost rectifier output capacitor showed a tendency to create poorly damped low-frequency oscillations on the bus.

The analysis showed that large capacitors do not provide any energy savings in the PDS. The overall efficiency of the system remains nearly at the original level when very large capacitors are used. It even decreases up to 2% at intermediate capacitance values due to increased losses in the system produced by the DC bus transients. This effect is more prominent when using a large boost rectifier capacitor. Based on the analysis results, the following observations can be made:

- distribution of losses in the system is frequency-dependent and determined by all dynamic (filtering) components;
- additional capacitors at different places of the system not only redirect the transient energy flow, but also change the spectral characteristics of the disturbance.

As a result, the system efficiency should be determined and the system optimization should be performed taking into account its transient performance, not only the static operating conditions. The examples of analysis presented in this thesis show that the modeling and simulation tools developed in this research can be effectively used to study different aspects of the DC power distribution system including stability, transient response, and energy transfer issues. The concepts used in this research are versatile enough and can be used for building similar analysis tools for complex systems with closely interacting subsystems.

Figure 5.1 DC-DC Buck Converter Output

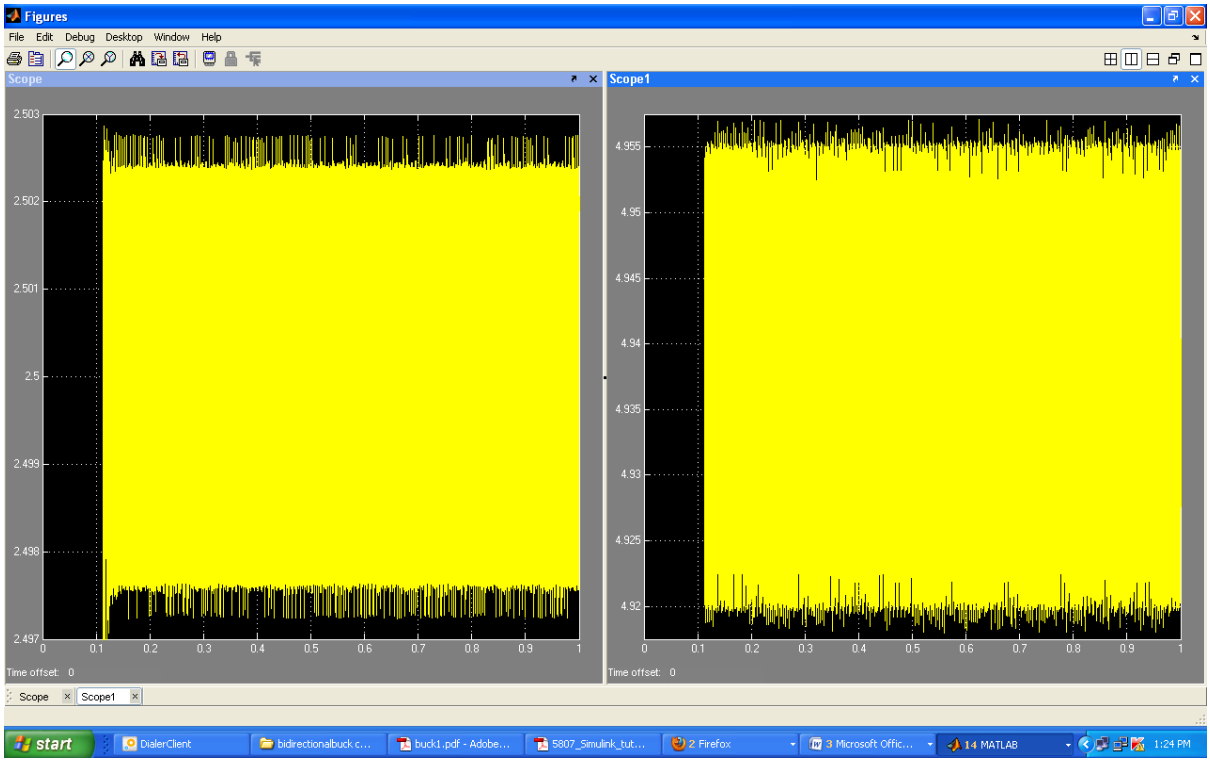

Figure 5.2 DC-DC Boost Converter Output

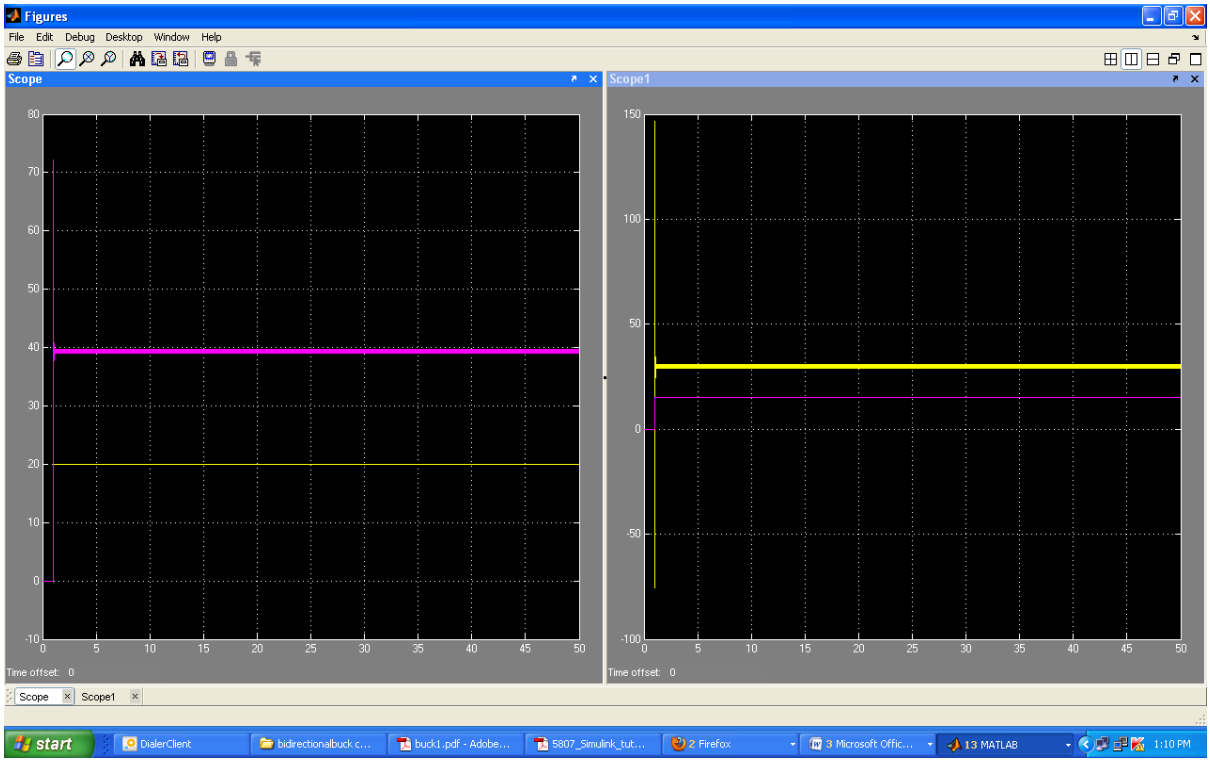

Figure 5.3 DC-DC Boost Converter Output with Feedback control system

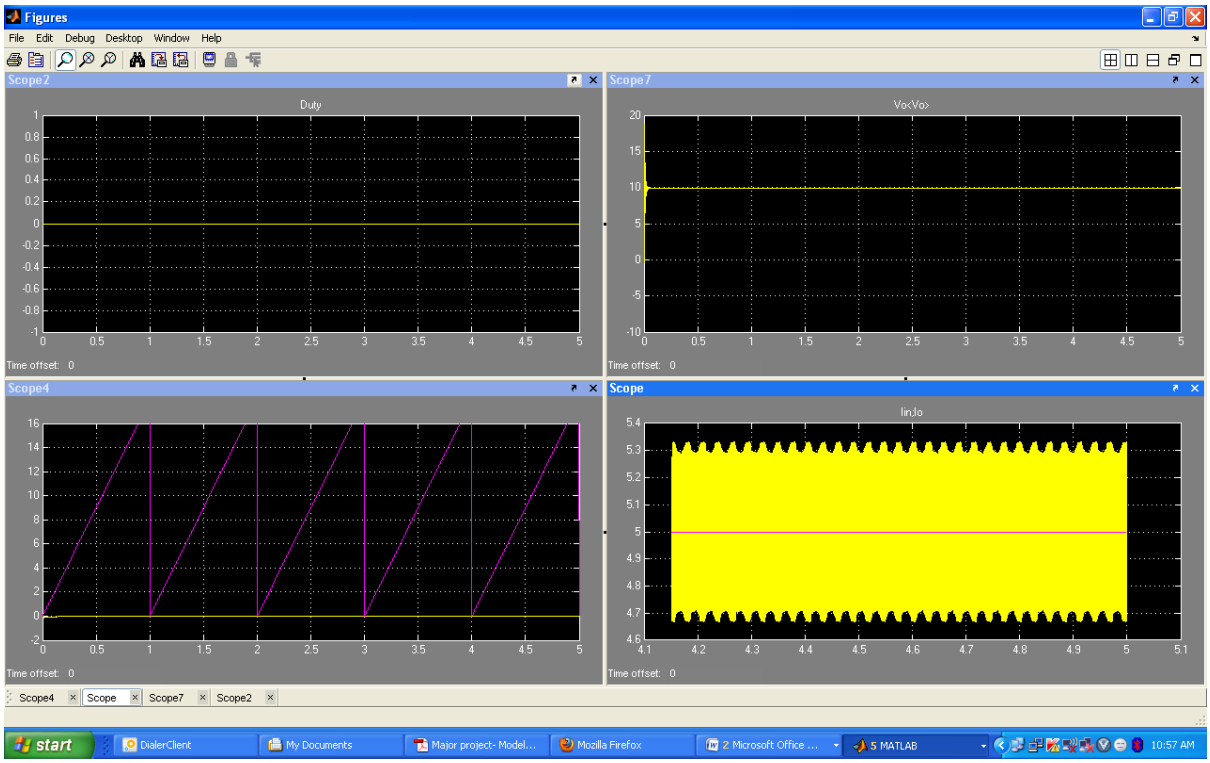

With duty cycle=0

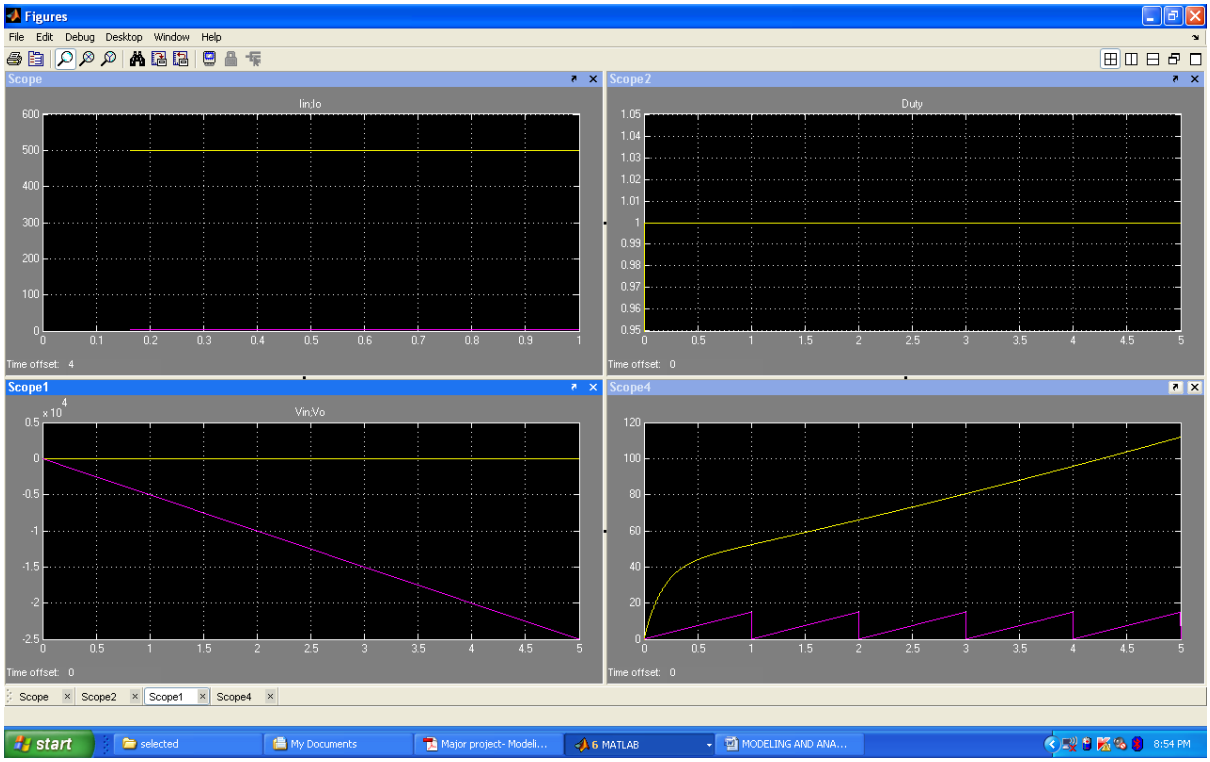

With duty cycle=1

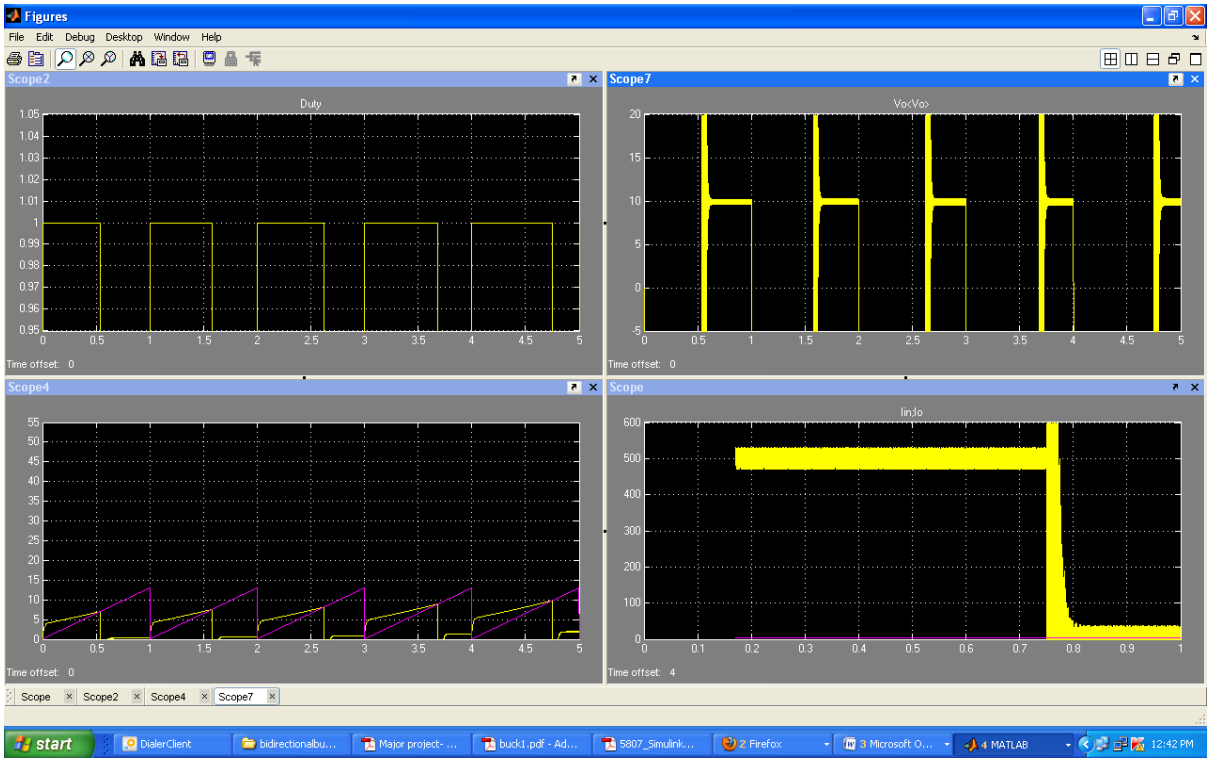

With duty cycle=0.55

Figure 5.4 Three-Phase Synchronous Generator Output

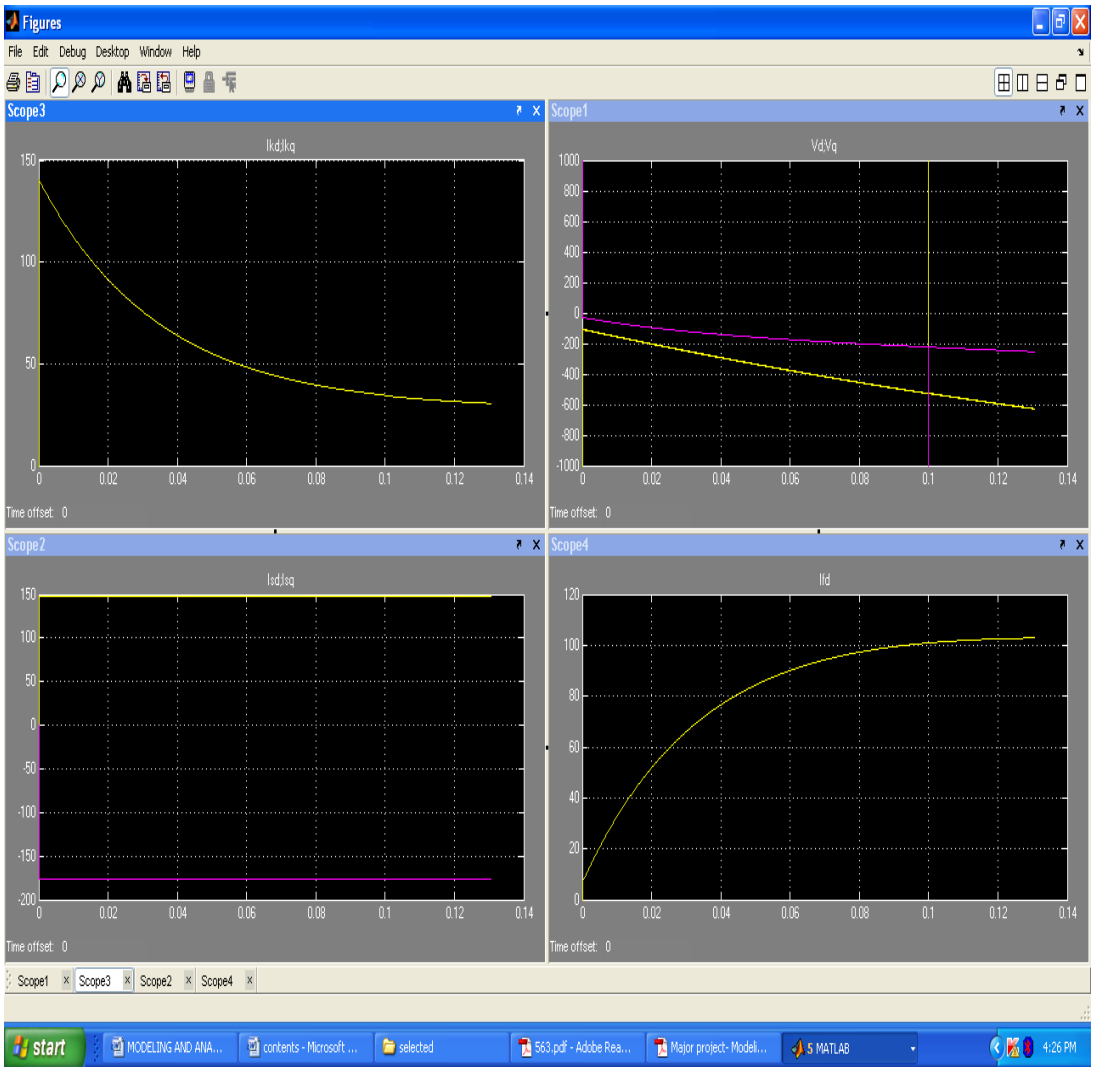

Figure 5.5 Bidirectional Power Flow Analysis in the DC Power Distribution System

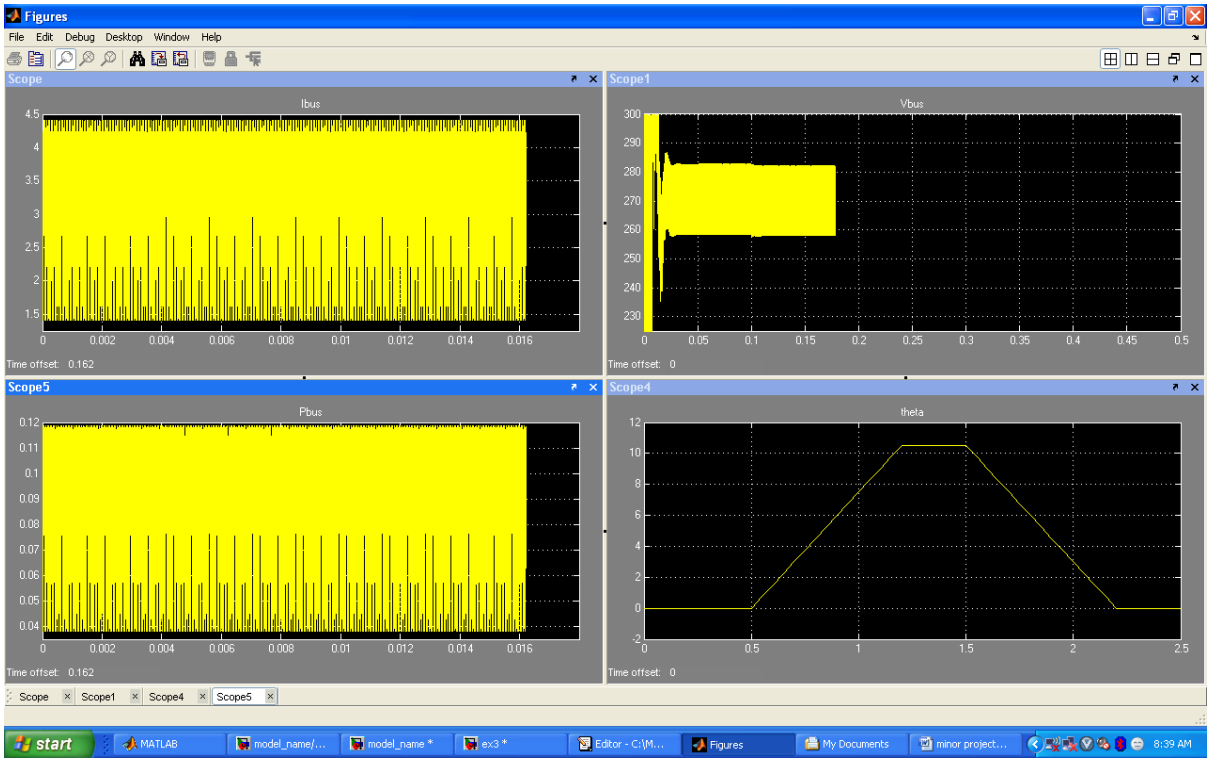

Appendix A

Parameters of the DC Power Distribution System Components

Table A.1 Synchronous generator parameters.

Parameter	Symbol	Unit	Nominal value
Armature phase resistance	R_s	Ohm	0.09113
Rotor speed	ω	rad/s	376.99
Armature phase leakage inductance	L_{ls}	H	0.9e-3
D axis coupling inductance	L_{md}	H	43e-3
Q axis coupling inductance	L_{mq}	H	21e-3
Field winding resistance (reflected to stator)	R_{fd}	Ohm	0.018
Field winding leakage inductance (refl. to stator)	L_{lfd}	H	3.4e-3
D axis damper winding resistance (refl. to stator)	R_{kd}	Ohm	0.08
Q axis damper winding resistance (refl. to stator)	R_{kq}	Ohm	0.08
D axis damper winding leakage inductance (reflected to stator)	L_{lkd}	H	0.16e-3
Q axis damper winding leakage inductance (reflected to stator)	L_{lkq}	H	0.35e-3
Additional resistance	R_a	Ohm	1e5
Field voltage (reflected to stator)	v_{fd}	V	1

Table A.2 Three-phase boost rectifier parameters.

Parameter	Symbol	Unit	Nominal value
One-phase inductance	L	H	18e-6
Output capacitance	C	F	350e-6
Output capacitor ESR	R_c	Ohm	0.01
Current feedback loops gain	K_{dq}	–	0.0126
Voltage loop proportional gain	K_{vp}	–	1
Voltage loop integral gain	K_{vi}	–	3300
Output voltage reference	$v_{o(ref)}$	V	270

Table A.3 DC bus cable parameters.

Parameter	Symbol	Unit	Nominal value
Resistance per foot	R	Ohm/ft	1.13e-3
Inductance per foot	L	H/ft	1e-9
Capacitance per foot	C	F/ft	1e-12
Capacitance ESR per foot	R_C	Ohm/ft	negligible
Cable length for Inboard Spoilers (EMA)	L_{EMA}	ft	10
Cable length for Elevators (EHA)	L_{EHA}	ft	40

Table A.4 EMA input filter parameters.

Parameter	Symbol	Unit	Nominal value
Inductance	L_i	H	1e-5
Inductor ESR	R_{li}	Ohm	0.1
Capacitance	C_i	F	1e-3
Capacitor ESR	R_{ci}	Ohm	0.01

Table A.5 DC motor parameters.

Parameter	Symbol	Unit	Nominal value
Armature inductance	L	H	4.5e-4
Armature resistance	R	Ohm	0.5
Back emf constant	K_e	V/(rad/s)	0.129
Torque constant	K_t	in-lb/A	1.141
Motor group inertia	J_m	in-lb-s^2	2.43e-4
Motor group damping	B_m	in-lb-s	3.125e-4

Table A.6 Actuator mechanical linkage parameters.

Parameter	Symbol	Unit	Nominal value
Motor to Actuator gear ratio	N	rad/in	249.6π
Actuator stiffness	K_{act}	lbf/in	9.0e5
Piston mass	M_p	lbf-s^2/in	5.43e-3
Piston damping	B_p	lbf-s/in	15
Surface load inertia	J_{sur}	in-lb-s^2	36.2
Surface load damping	B_{sur}	in-lb-s	1702
Horn radius	h	in	4.9
Horn stiffness	K_l	in-lb/rad	1.0e6
Structure stiffness	K_r	in-lb/rad	5.0e5
Gear efficiency	N_{mech}	–	0.85

Table A.7 EMA feedback controller parameters.

Parameter	Symbol	Unit	Nominal value
Motor current limit	–	A	19.3
Position forward gain	K_p	V/V	76
Velocity command limit	W_{lim}	V	+/–6.8
Velocity forward gain	K_v	V/V	122.5
Position feedback gain	H_p	V/in	1.6
Velocity feedback gain	H_v	V/(rad/s)	3.82e-3
Current feedback gain	H_i	V/A	0.25
Current forward gain	K_i	V/A	30

Simulink Model for Bidirectional Power Flow Analysis in the DC Power Distribution System

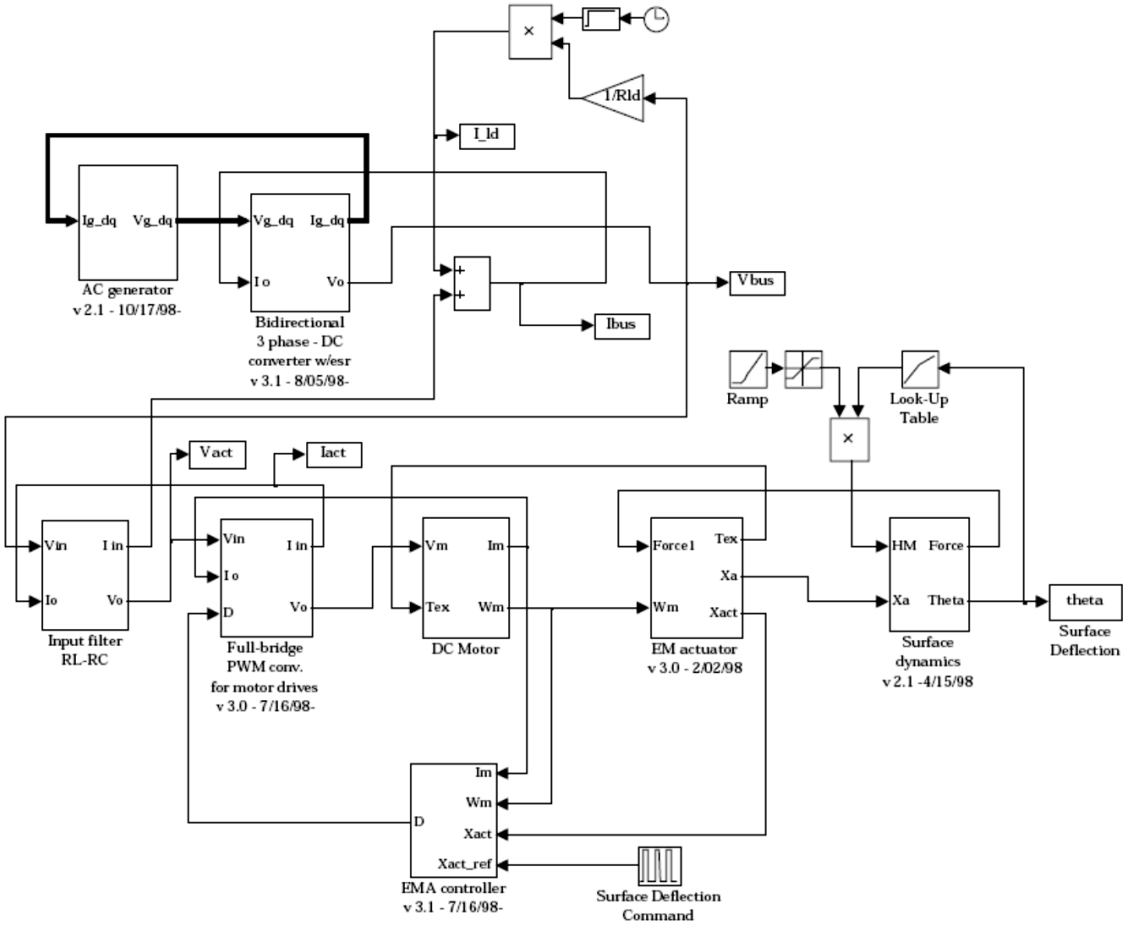

Figure A.1 Simulink model for bidirectional power flow analysis in the PDS.

"syngen_par.m" – Synchronous Generator Parameters

```
% State space matrices

Agtmp=zeros(5);

Agtmp(1,1) = -Lls-Lmd;

Agtmp(1,3) = Lmd;

Agtmp(1,5) = Lmd;

Agtmp(2,2) = -Lls-Lmq;

Agtmp(2,4) = Lmq;

Agtmp(3,1) = -Lmd;
```

```
Agtmp(3,3) = Lmd;
Agtmp(3,5) = Llfd+Lmd;
Agtmp(4,1) = -Lmd;
Agtmp(4,3) = Llkd+Lmd;
Agtmp(4,5) = Lmd;
Agtmp(5,2) = -Lmq;
Agtmp(5,4) = Llkq+Lmq;
Bg1 = zeros(5);
Bg1(1,1) = Ra+Rs;
Bg1(1,2) = -w*(Lls+Lmq);
Bg1(1,4) = w*Lmq;
Bg1(2,1) = w*(Lls+Lmd);
Bg1(2,2) = Ra+Rs;
Bg1(2,3) = -w*Lmd;
Bg1(2,5) = -w*Lmd;
Bg1(3,5) = -Rfd;
Bg1(4,3) = -Rkd;
Bg1(5,4) = -Rkq;
Bg2 = zeros(5,3);
Bg2(1,1) = -Ra;
Bg2(2,2) = -Ra;
Bg2(3,3) = 1;
Ag = inv(Agtmp)*Bg1;
Bg = inv(Agtmp)*Bg2;
Cg = zeros(7,5);
Cg(1,1) = Ra;
Cg(2,2) = Ra;
Cg(3:7,:) = eye(5);
Dg = zeros(7,3);
Dg(1,1) = -Ra;
Dg(2,2) = -Ra;
```

References

[1] Lester F. Faleiro," Trends towards a more electrical aircraft", Proc. 25th International Congress of the Aeronautical Sciences ICAS 2006.

[2] M. Howse, "All Electric Aircraft", Power Engineer, vol. 17, pp. 35-37, 2003.

[3] David Blanding, "Subsystem design and integration for the More Electric Aircraft". Proc. 25th International Congress of the Aeronautical Sciences ICAS 2006.

[4] Rosero, J.A.; Ortega, J.A.; Aldabas, E.; Romeral, L. "Moving towards a more electric aircraft" Aerospace and Electronic Systems Magazine, IEEE Volume 22, Issue 3, March 2007.

[5] M. David Kankam "A survey of Power Electronics applications in Aerospace Technologies". 36th Intersociety Energy Conversion Engineering Conference; Savannah, Georgia, July 29– August 2, 2001.

[6] Moir, Ian; Seabridge, Allan. "Aircraft Systems: Mechanical, Electrical and Avionics Subsystems Integration". 3rd ed. Chichester (West Sussex): Wiley, 2008. 546 p. Aerospace Series. ISBN: 978-0-470-05996 8.

[7] J. A. Weimer, "Power Management and Distribution for the More Electric Aircraft," Proceedings of the 30th Intersociety Energy Conversion Engineering Conference, 1995, pp. 273-277.

[8] M. L. Maldonado, N. M. Shah, K. J. Cleek, P. S. Walia, G. Korba, "Power Management and Distribution System for a More Electric Aircraft (MADMEL) – Program Status," Proceedings of the 31st Intersociety Energy Conversion Engineering Conference, 1996, pp. 148-153.

[9] B. H. Cho and B. Choi, "Analysis and Design of Multi-Stage Distributed Power Systems," Proceedings of the Virginia Power Electronics Conference, 1991, pp. 55-62.

[10] M. E. Elbuluk, M. D. Kankam, "Motor Drive Technologies for the Power-by-Wire (PBW) Program: Options, Trends, and Tradeoffs," Proceedings of the IEEE 1995 National Aerospace and Electronics Conference, NAECON'95, pp. 511-522.

[11] G. L. Fronista and G. Bradbury, "An Electromechanical Actuator for a Transport Aircraft Spoiler Surface," Proceedings of the 32nd Intersociety Energy Conversion Engineering Conference, 1997, pp.694-698.

[12] K.C. Reinhardt, M. A. Marciniak, “Wide-Bandgap Power Electronics for the More Electric Aircraft,” Proceedings of the 31st Intersociety Energy Conversion Engineering Conference, 1996, pp. 127-132.

[13] W. A. Tabisz, M. M. Jovanovic, F. C. Lee, “Present and Future of Distributed Power Systems,” Proceedings of the Applied Power Electronics Conference, 1992, pp. 11-18.

[14] T. L. Skvarenina, S. Pekarek, O. Wasynczuk, P. C. Krause, “Simulation of a More Electric Aircraft Power System Using an Automated State Model Approach,” Proceedings of the Intersociety Energy Conversion Engineering Conference, 1996, pp. 133-136.

[15] S. Hiti, D. Borojevic, “Small-Signal Modeling and Control of Three-Phase PWM Converters,” IEEE 1994 IAS Annual Meeting Proceedings.